STATE OF THE CLIMATE IN 2002

A. M. WAPLE AND J.H. LAWRIMORE, EDS.

TABLE OF CONTENTS

Affiliations (alphabetical by author)

1. Lisa Alexander and Briony Horton, Hadley Centre for Climate Prediction and Research, the Met Office, Bracknell, United Kingdom
2. Peter Ambenje and others, Drought Monitoring Centre, Nairobi, Kenya
3. Gerry Bell and Mike Halpert, NOAA/NWS/NCEP Climate Prediction Center, Washington, D.C.
4. O.N. Bulygina, N.N. Korshunova, and V.N. Razuvaev, All Russian Research Institute of Hydrometeorological Information, Obninsk, Russia
5. Suzana J. Camargo, Brad Lyon, and Anji Seth, International Research Institute for Climate Prediction (IRI), New York, New York
6. John Christy, University of Alabama, Huntsville, Alabama
7. Arthur Douglas, Creighton University, Nebraska
8. Karin Gleason, Jay H. Lawrimore, Matthew Menne, and Anne Waple (STG Inc.), NOAA, National Climatic Data Center, Asheville, North Carolina
9. Doug Hardy, Climate System Research Center, University of Massachusetts, Amherst, Massachusetts
10. Charlotte McBride, South African Weather Service, South Africa
11. David Phillips, Environment Canada, Ottawa, Canada
12. Roger Pielke Sr. and Christopher L. Castro, Colorado State University, Fort Collins, Colorado
13. David Robinson, Rutgers University, New Brunswick, New Jersey
14. Jim Salinger, National Institute of Water and Atmospheric Research, Newmarket, Auckland, New Zealand
15. Russell C. Schnell, NOAA/Climate Monitoring and Diagnostics Laboratory, Boulder, Colorado
16. Andrew Watkins, Australian Bureau of Meteorology, Melbourne, Australia

ABSTRACT

Neutral ENSO conditions at the beginning of 2002 gave way to a strengthening El Niño episode during boreal summer. Weather patterns in many areas of the world reflected the warm phase conditions.

The average global temperature in 2002 was 0.45°C above the 1961–1990 mean, which places 2002 as the second warmest year on record. Land temperatures were 0.78°C above average and ocean temperatures were 0.31°C above the 1961–1990 mean. This ranks both land and ocean as the second warmest on record.

Annual temperature anomalies in excess of 1.0°C were widespread across much of Russia, Eastern Europe, Alaska, and central South America, while significantly cooler than average conditions were confined to the eastern half of Canada, southern South America, and the eastern Pacific Ocean, near the coast of the United States.

Although 12 tropical storms developed in the Atlantic during the boreal summer of 2002, most of them were weak and short-lived, which resulted in a slightly below normal season in terms of overall activity. However, seven tropical storms made landfall in the United States, with an eighth brushing the coast of North Carolina. Hurricane Lili was the first hurricane to make landfall in the United States in three years.

Other notable aspects of the climate in 2002 include extreme drought in parts of the United States, Canada, and Australia; ongoing drought in portions of Central America; near-record flooding in central Europe; drought in West Africa; a failure of the Indian summer monsoon; flooding in China; the warmest year on record for Alaska; and the smallest Antarctic ozone hole in the last decade.

1. INTRODUCTION—A. M. Waple[8]

This is the 13th year that a summary of the state of the Earth's climate has been written. Formerly known as the Climate Assessment, this report has been renamed as the "State of the Climate in 2002" to better reflect its overall focus. It contains analyses of the global climate system for 2002 including significant events and their impacts, and atmospheric dynamics that have influenced weather and climate over the year. The report also seeks to place the climate of 2002 in historical perspective with analysis of trends and variability in temperature, precipitation, and climate forcing during the period of instrumental record. Proxy climate records are also included to aid in understanding the Earth's climate prior to the systematic collection of instrumental climate observations.

The analyses within this report rely on data from a number of different sources. These include, but are not limited to 1) land surface temperature and precipitation data from the Global Historical Climatology Network (Peterson and Vose 1997; Vose et al. 1992), and the U.S. Historical Climate Network (Easterling 1996); 2) surface temperature data from a land–sea blended dataset (Jones et al. 2001); 3) gridded analyses from the National Centers for Environmental Prediction–National Center for Atmospheric Research (NCEP–NCAR) Climate Data Assimilation System/50-Year Reanalysis (Kistler et al. 2001); 4) Satellite data; 5) ship reports; 6) paleoclimate data collected and stored by the National Oceanic and Atmospheric Administration (NOAA) Paleoclimatology Program. Due to the large number of data sources used throughout this report, it is not possible to refer to one standard base period.

Section 2 reviews global-scale climate in 2002. Surface temperature and upper-air temperatures are examined, as well as global precipitation and Northern Hemisphere snow cover. Section 3 addresses the global trends and impacts of trace gases, while sections 4 and 5 summarize conditions in the Tropics and polar regions, respectively. An assessment of ENSO, which transitioned to its warm phase in 2002 is included in section 4. The tropical storms of the Atlantic and Pacific are also summarized in this section. Section 5 reviews the climate of the Arctic and Antarctic including a summary of sea ice conditions and stratospheric ozone. In section 6 regional climate and weather events throughout 2002 are addressed including extreme drought, flooding, wind storms, and many other climate events around the world. The 2002 State of the Climate concludes with a section illustrating surface and upper-air temperatures for each season over the globe. While each section is essentially self-contained, frequent cross-referencing between sections occurs throughout the text.

It is the third year that the National Climatic Data Center has taken the lead in the preparation of this report, however, it is a cooperative effort that includes contributions from dozens of scientists around the United States and the world. To better link the authors with their respective expertise and contributed material, a change was made to the format this year. We have chosen to directly associate each section with its author(s), rather than listing everyone as general au-

thors. An appendix appears at the end of the article with the names and institutions of people who did not contribute written material but provided invaluable assistance with figures, data, or additional guidance.

Also as a new feature for the 2002 report, there are sidebar boxes in many sections illustrating the preinstrumental climate perspective or other additional information of interest.

2. GLOBAL CLIMATE

a. Global surface temperatures—M. Menne[8] and B. Horton[1]

According to surface temperature records maintained independently by institutions in the United Kingdom and in the United States, the global mean surface temperature in 2002 ranked as the second warmest in the observational period. Surface temperatures in 2002 averaged 0.48°C above the 1961–90 mean annual value according to the U.K. record (Jones et al. 1999; Parker et al. 1995) and 0.45°C above the annual mean calculated using the U.S. dataset (Peterson and Vose 1997; Quayle et al. 1999; Reynolds et al. 2002). Consequently, 2002 supplants 2001 as second warmest in the 1860 to 2002 (U.K.) and 1880 to 2002 (U.S.) periods of record. The record warm year, according to observations from both databases, is 1998 when surface temperatures averaged 0.07°C (U.K. value) or 0.06°C (U.S. value) higher than in 2002. Mean annual global temperature departures from the U.K. data source are shown in Fig. 1a, and by hemisphere in Figures 1b and 1c. Averaged separately, 2002 surface temperatures rank as second highest in both the Northern and Southern Hemispheres.

For land and ocean regions poleward of 30°N, the mean surface temperature ranked as highest on record, as shown in Fig. 2a. Average surface temperatures across the Northern Hemisphere mid- and high latitudes in the last five years are highest on record. In low latitudes (30°N–30°S), surface temperatures in 2002 rank as second highest in the period of record, the highest since 1998 (Fig. 2b). The 2002 average temperature in areas south of 30°S was approximately 0.22°C above the 1961–90 mean (U.K.) value, or eighth highest on record (Fig. 2c).

Global land and global sea surface temperatures (SSTs) from the U.S. data source are shown separately in Figs. 3 and 4. Both the global average land surface temperature and average SST during 2002 rank as second highest in the period of record (SSTs were tied with 1997 for the rank of second warmest). In Fig. 5, serial monthly temperature anomalies from the U.S. database are shown for the period 1961–2002 and with respect to a 1961–90 reference period. Two calendar-month record-high temperature departures occurred during 2002, in January and March, when the global surface temperature was 0.62° and 0.64°C, respectively, above the 1961–90 monthly mean value.

The geographic distribution of mean annual surface temperature differences from the 1961–90 average is shown in Fig. 6a, based on an analysis from U.K. surface temperature records. Widespread positive annual temperature anomalies are evident across much of the landmasses of Africa, Asia, and Europe, as well as across portions of the Indian Ocean and the central equatorial Pacific. In some of these locations, the mean annual temperature met or exceeded the estimated 90th percentile of the climatological occurrence, as shown in Fig. 6b.

b. Upper-air temperature—J. Christy[6]

Annual anomalies of the globally averaged, bulk atmospheric temperatures for the lower troposphere (LT), midtroposphere (MT), and lower stratosphere (LS) since 1979 are shown in Fig. 7. These temperatures are derived from the microwave emissions of atmospheric oxygen by the University of Alabama in Hunts-

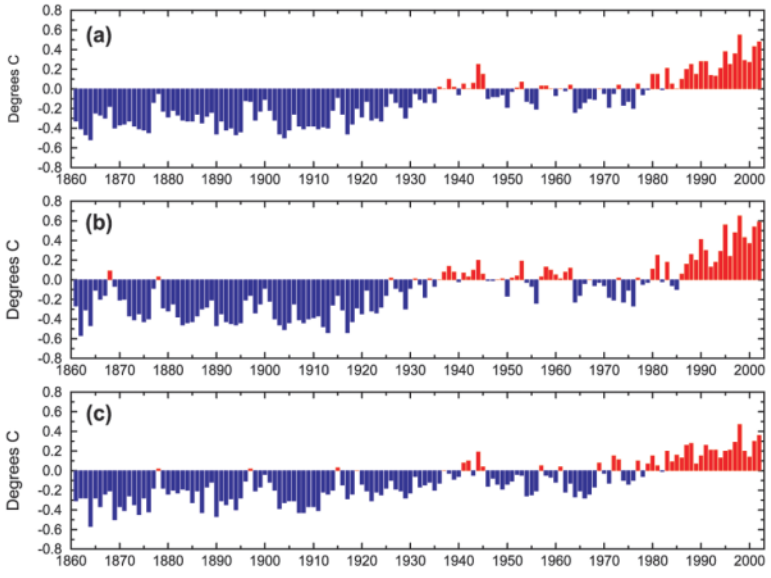

FIG. 1. Mean annual temperature anomalies (°C) 1860–2002. Anomalies are departures from a 1961–90 base period, and include both land and sea surface temperature observations (source: Climate Research Unit, University of East Anglia, and Hadley Centre, Met Office). (a) Global annual temperature anomalies; (b) Northern Hemisphere temperature anomalies; (c) Southern Hemisphere temperature anomalies.

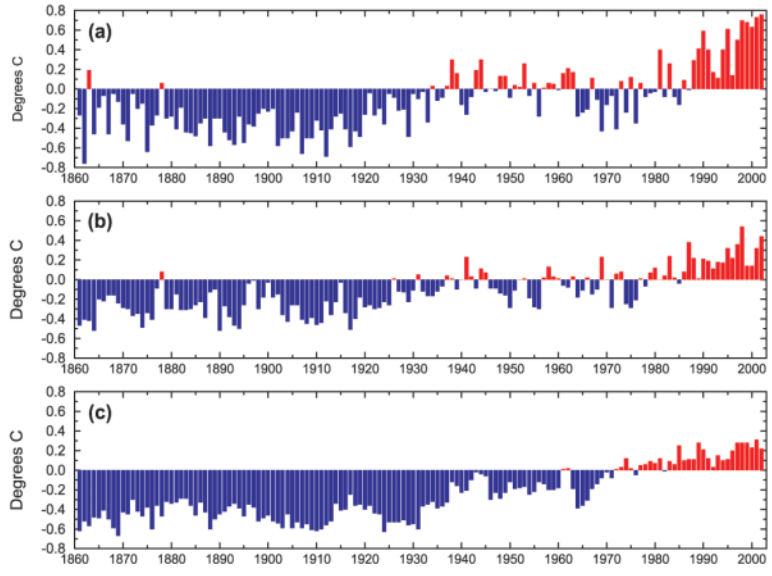

FIG. 2. As in Fig. 1, except by latitude band. (a) Mean annual temperature 30°–90°N; (b) same as (a) for 30°N–30°S; (c) same as (b) for 30°–90°S.

ville, Alabama (UAH), and monitored by microwave sounding units (MSUs) and the advanced MSUs (AMSUs since 1998) that are flown as part of the instrument suite on NOAA polar-orbiting satellites (Christy et al. 2000, 2003). Biases and errors due to spacecraft drift (both horizontal and vertical) and on-orbit calibration changes have been identified and removed. A new reconstruction of MSU MT temperatures has been completed by Remote Sensing Systems (RSS) in which differing methods for accounting for east–west drift and instrument calibration have been applied (Mears et al. 2003, manuscript submitted to *J. Climate*).

i) Lower Troposphere

The UAH 2002 global LT (roughly the mean temperature from the surface to 8-km altitude) annual anomaly relative to 1979–98 of +0.24°C was second warmest since 1979 (Fig. 7, top). The overall UAH LT trend since 1979 is +0.07°C decade^{-1}. Trends calculated from radiosondes (Met Office, Hadley Centre; Parker et al. 1997) and NCEP reanalyses (Stendel et al. 2000) are within 0.03°C decade^{-1}. The modest warm ENSO event of the second half of the year contributed to the warmth, though every month in 2002 exceeded the 1979–98 average. Only a few areas experienced cooler than average LT temperatures (central and eastern Canada, far eastern South Pacific, Africa, Urals area, and southeast Asia.) The trend discrepancy between surface and LT over the past 24 years has been supported by comparisons using other upper-air datasets based on radiosondes and meteorological analyses (Hurrell et al. 2000; Stendel et al. 2000) and by a radiosonde-based calculation of steepening lapse rates (Gaffen et al. 2000). However, trend differences between the troposphere and surface in some continental regions, such as North America and Europe, are virtually zero (Folland et al. 2001; Waple et al. 2002).

ii) Midtroposphere

Though the peak of the mass-weighted weighting function of the MT occurs near 400 hPa, this product senses emissions from a broad layer beginning at the surface and extending to the stratosphere. Both UAH (+0.23°C) and RSS (+0.48°) indicate 2002 was the second warmest year since 1979. However the global trends differ by 0.08°C decade^{-1} (+0.035° versus +0.115°, respectively), which is significant. Christy et al. 2003 estimate the 95% error range of UAH MT at ±0.05° while Mears et al. derive a value of ±0.02° for RSS. Because of the stratospheric influence on MT, radiosonde simulations of MT for comparison purposes are less reliable, but show trends less positive than either UAH or RSS.

iii) Lower stratosphere

Lower stratospheric temperatures, which represent the layer 16–23 km above the surface, have remained below average since 1993. However, 2002 was the warmest year since 1993 at –0.31°C. For the year as a whole, there were widespread negative anomalies northward of 50°S (Fig. 8) A split in the anticipated ozone depletion area over the South Pole in austral spring was associated with much warmer than expected annual anomalies, peaking at +4°C over eastern Antarctica relative to a mean of 1984–90. (Fig. 9). More information on Antarctic stratospheric ozone depletion in 2002 is available in section 5a. The tropical stratosphere began the year in the westerly or warm phase of the quasi-biennial oscillation (QBO) so the magnitude of negative anomalies compared with 2001 was diminished in that region.

c. *Global precipitation*—J. H. Lawrimore[8] and M. Halpert[3]

The development of warm phase ENSO conditions in mid-2002 had a notable influence on precipitation patterns during the latter half of the year. Traditional El Niño signatures are evident in the map of June–December 2002 accumulated precipitation anomalies

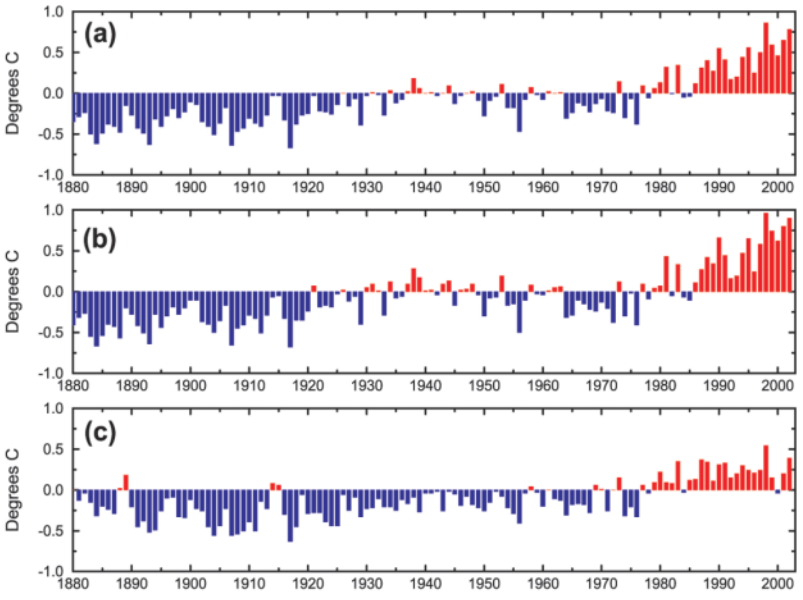

FIG. 3. Mean annual land surface air temperature anomalies (°C) 1880–2002. Anomalies are departures from a 1961–90 reference period (source: National Climatic Data Center, NOAA). (a) Global land surface air temperatures; (b) same as (a) for the Northern Hemisphere only; (c) same as (a) for the Southern Hemisphere only.

(Fig. 10). During this period, precipitation anomalies in the Tropics and sub-tropics from Indonesia eastward to South America, and along the Gulf Coast of the United States, were consistent with past warm episodes (Ropelewski and Halpert 1987). As shown in the accompanying monthly precipitation percentile graphs, above-average precipitation was evident over the central tropical Pacific beginning in May 2002, followed by considerably larger anomalies in that region during August–December.

Southeastern South America and the Gulf Coast of the United States both experienced significantly above-average rainfall during September–December 2002. However the above-average rains in the Gulf Coast were enhanced in September with rainfall from Tropical Storms Fay and Isidore, while rainfall during October was aided by landfalling Hurricane Lili (see section 4bi). In contrast, Indonesia, eastern Australia, the Amazon basin, and Central America all recorded below-average rainfall during their respective rainy seasons in association with El Niño.

Anomalies for the June–December period, based on measurements from land stations, are shown in Fig. 11b. Precipitation deficits for the 7-month period exceeded 200 mm throughout much of eastern Australia, where the lack of rainfall led to worsening drought conditions and destructive wildfires (see section 6gi). Much of India was affected by below-average rainfall, and the monsoon season (June–September) was 19% drier than normal, the first all-India drought since 1987 (see section 6fii). Scandinavia and much of North America also experienced widespread areas of below-average precipitation.

Conditions averaged throughout the first five months of the year were notably different than those during the last seven months in areas such as the Gulf Coast of the United States, much of Europe and the Mediterranean, as well as parts of southeastern China and Taiwan (see Fig. 11a). In other areas, such as Australia and the western United States, drier than average conditions persisted throughout the year. The persistently drier than normal conditions in the western

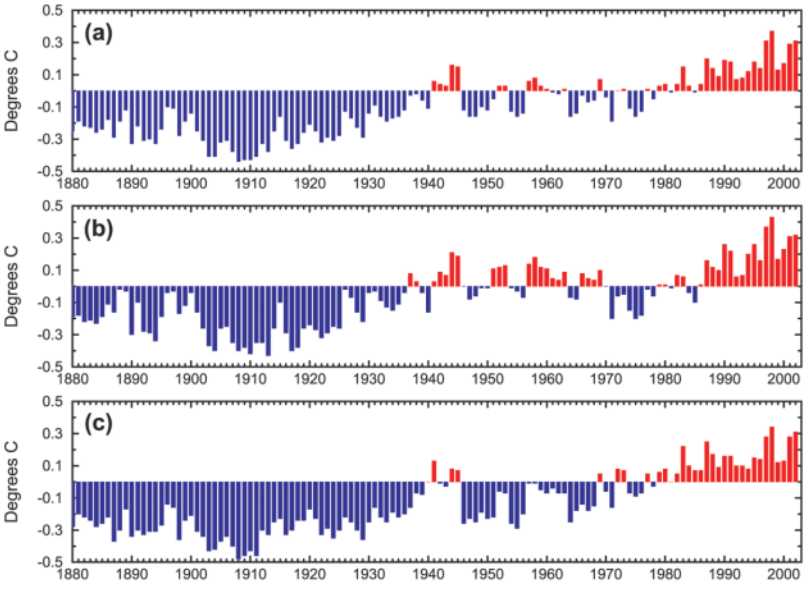

FIG. 4. Mean annual sea surface temperature anomalies (°C) 1880–2002. Anomalies are departures from a 1961–90 reference period (source: National Climatic Data Center, NOAA). (a) Global annual sea surface temperatures; (b) same as (a) for the Northern Hemisphere; (c) same as (a) for the Southern Hemisphere.

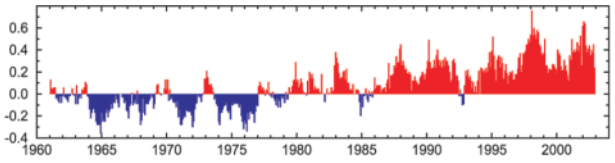

Fig. 5. Mean monthly temperature anomalies (°C) 1961–2002. Anomalies are departures from a 1961–90 reference period (source: NCDC, NOAA).

United States contributed to widespread severe and extreme drought and a very active wildfire season (see section 6aii). Throughout much of Argentina and other parts of southern South America, wetter than average conditions were prevalent during both periods.

On a global basis, land surface precipitation for the year was near the 1961–90 average. Average annual precipitation totals for the Northern Hemisphere extratropics (90°–20°N), Tropics (20°N–20°S), and Southern Hemisphere extratropics (20°–90°S) all deviated less than 1% from average. Over the past century, increases in precipitation in many areas have coincided with the increases in temperature that have been observed (see section 2a), most notably in the mid- and high latitudes of the Northern Hemisphere. The century-scale rate of increase is greater than 10% in the 55°–85°N latitude band and is near 5% in the region from 30°N to 55°N. This increase may be partly due to an increase in the water-holding capacity of the atmosphere (Houghton et al. 2001).

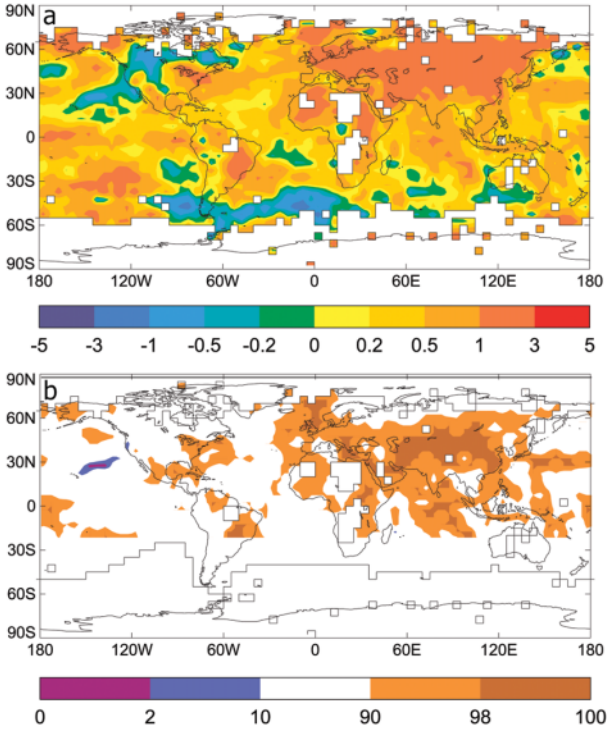

Fig. 6. (a) Global surface temperature anomalies (°C) for 2002. Areas with insufficient data are shown as empty grid boxes. Anomalies are departures from 1961–90 reference period means. (b) Global annual temperature anomaly percentiles for 2002 based on gamma distribution for the 1961–90 reference period, in 5° grid boxes. Shading in orange and red indicate regions where the temperature anomalies were estimated to be with the warmest 10% and 2%, respectively, of climatological occurrence (source: Climate Research Unit, University of East Anglia, and Hadley Centre, Met Office).

d. Northern Hemisphere snow cover—D. Robinson[13]

While the annual snow extent over Northern Hemisphere lands was close to average in 2002, most individual months were anything but average. The mean annual Northern Hemisphere snow cover extent in 2002 was 25.4 million km^2, just 0.2 million km^2 below the over three decade-long average (Table 1). This includes snow over the continents, including the Greenland ice sheet. The area covered by snow in 2002 ranged from 46.9 million km^2 in January to 2.7 million km^2 in August. Monthly snow extent values are calculated at Rutgers from weekly maps of snow cover produced by NOAA meteorologists, who rely primarily on visible satellite imagery to construct the maps.

Near-record-low snow extents were observed in February and March 2002, and a record low was reached in July. The former two months ranked third and second lowest, respectively, based on 36 yr of observations dating back to 1967 (Fig. 12). A completely different picture emerged late in 2002, with October, November, and December each ranking among the top 5 highest extent. The October positive anomaly of 5.2 million km^2, 28% above average, is the second largest anomaly in terms of absolute snow area on record for any month since observations began in November 1966. The widely different picture from winter to fall is illustrated in Figs. 13 and 14, which show anomaly maps for February and October 2002.

Anomalies of Eurasian and North American snow extents were not always in synch during 2002 (Figs. 15 and 16). January cover was extensive in Eurasia but low in North America. Both were low in February, but the January pattern was reversed in March. The fall snow season began early in Eurasia but late in North America, as witnessed by September anomalies. Both continents had extensive October and November covers, while the December 2001 snow cover was a record maximum in Eurasia and the sixth lowest on record over North America. December 2002 conditions were quite similar, though more extreme than those observed in December 2001.

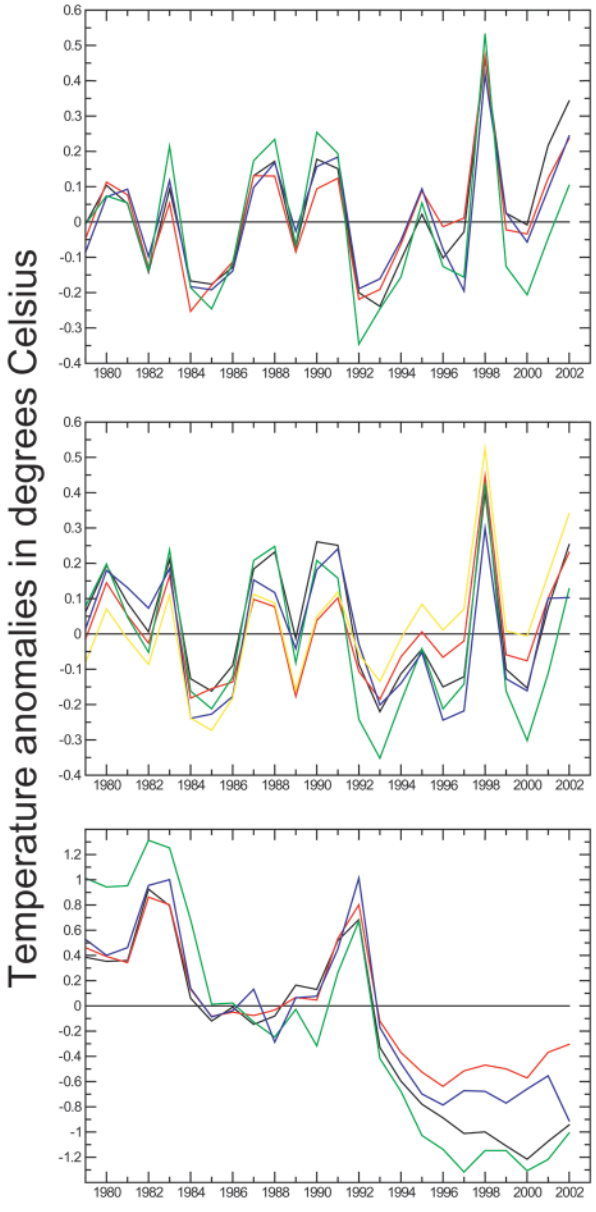

FIG. 7. Annual global temperature anomalies derived from MSU and AMSU for A—the lower troposphere, B—the middle troposphere and C—the lower stratosphere. For panels A and B, anomalies are from a 1979–1998 base period and for panel C, the base period is 1984–1990. Lines are black = NCEP, red = UAH, green = ANGELL, blue = HADRT and yellow = RSS. (Data provided by the University of Alabama in Huntsville and Remote Sensing Systems).

Maps depicting weekly and monthly conditions, monthly anomalies, and monthly climatologies for the entire period of record may be viewed at the Rutgers Climate Lab snow Web site (http://climate.rutgers.edu/snowcover). Monthly areas for the hemisphere and for Eurasia and North America are also posted, along with

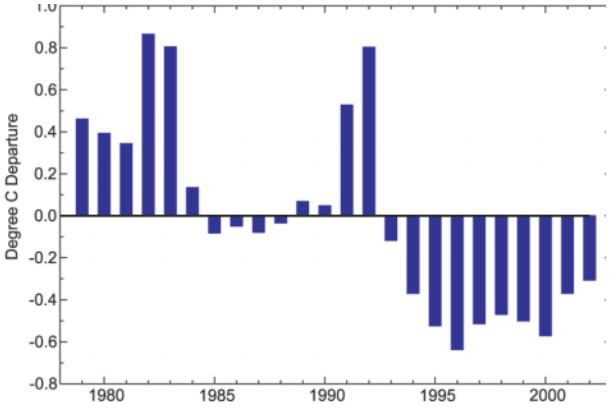

FIG. 8. Mean lower stratospheric temperature anomalies (°C) for 2002. Anomalies are departures from the 1984–90 base period means. (Data provided by the University of Alabama in Huntsville.)

information on how to ftp weekly areas and the weekly and monthly gridded products.

3. TRENDS IN TRACE GASES—R. C. Schnell[15]

a. Stratospheric water vapor

Water vapor concentrations in the stratosphere are much smaller than those in the troposphere, but water vapor concentration changes may play a significant role in altering the temperature in both the stratosphere and troposphere (Forster and Shine 2002). Increasing water vapor in the stratosphere can lead to a cooling while these same increases in the troposphere can lead to a warming near the surface (Forster and Shine 2002). The 22-yr record of water vapor observations at Boulder, Colorado, is characterized by a significant increase through the upper troposphere and stratosphere as

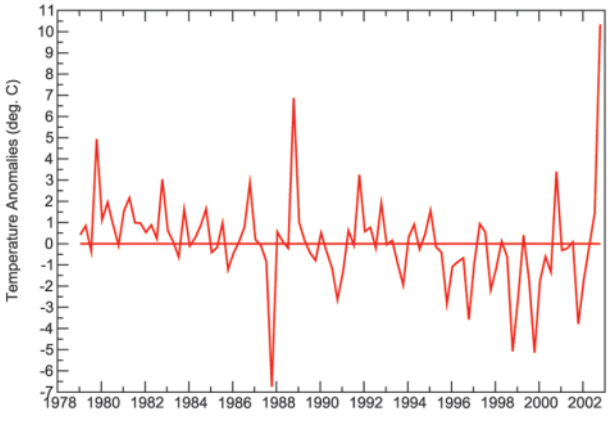

FIG. 9. Time series of seasonal lower stratospheric temperature anomalies over Antarctica (70°–90°S). The last entry is SON 2002 at 10.3°C, the warmest anomaly of the 24-yr time series.

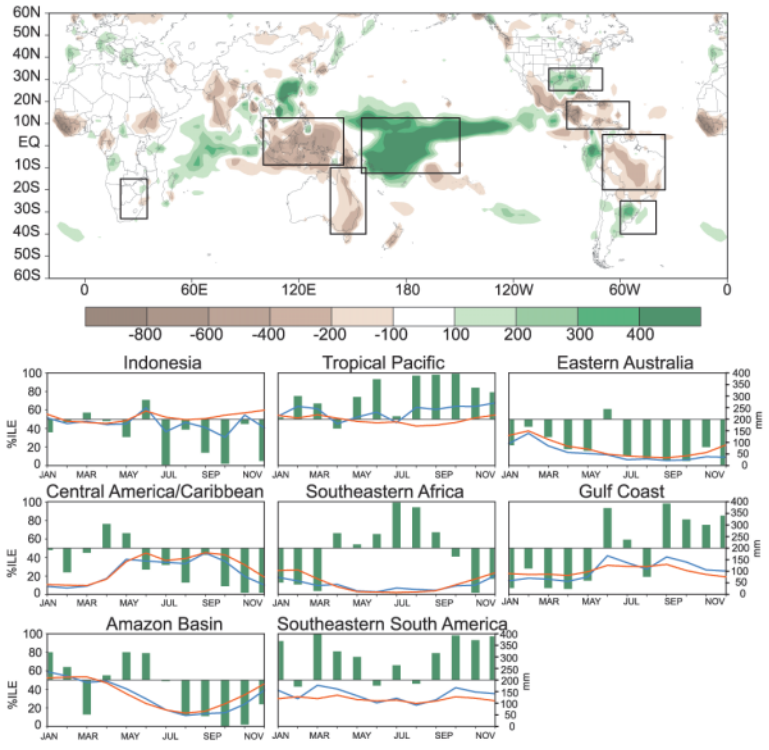

Fig. 10. (top) Jun–Dec 2002 accumulated precipitation anomaly, and regional area-averaged estimates of monthly mean precipitation amounts (mm, blue lines) and precipitation percentiles (%, bars) during 2002 for the boxed regions shown in top panel. The monthly precipitation climatology (mm, dashed, red lines) is the 1979–95 base period monthly means. The percentiles are labeled on the left-hand vertical axis and totals are labeled on the right-hand vertical axis. Precipitation amounts are obtained by merging rain gauge observations and satellite-derived precipitation estimates (Janowiak and Xie 1999).

shown in Fig. 17. The observations are obtained from monthly balloon soundings using a cryogenic, chilled-mirror hygrometer. Approximately 30% of the increase can be accounted for by the increase in atmospheric methane, but the source of the remainder of the increase is not well established. The rate of increase has shown significant year-to-year variations, and during 2002 smaller mixing ratios were seen in the lower stratosphere over Boulder. Over the longer term, however, the 1% yr^{-1} increase through the entire stratosphere sampled by the balloon measurements is statistically significant.

b. Decreases in ozone depleting halogens in the troposphere

During 2002, the tropospheric burden of ozone-depleting halogen, expressed as effective equivalent chlorine (EECl) from anthropogenic gases, continued to decrease. Although tropospheric trends are indicated in Figs. 18 and 19, the EECl derived from tropospheric measurements provides an estimate of the stratospheric burden of ozone-depleting halogen in future years as tropospheric air becomes mixed into the stratosphere.

The tropospheric burden of EECl during 2002 was down about 6% from the peak observed in 1993–94 (Fig. 18). The change in EECl continues to be driven primarily by the rapid decline in atmospheric methyl chloroform (CH_3CCl_3). The rate of decline in EECl is becoming smaller, however, as the atmospheric burden of methyl chloroform approaches zero. Mixing ratios of methyl chloroform approached 30 parts per trillion (ppt) by the end of 2002 compared with the peak mixing ratios of about 140 ppt in the early 1990s.

Further declines in EECl hinge on the balance of changes for gases other than methyl chloroform. EECl from chloroflorocarbons (CFCs) has been decreasing since about 1997 despite the absence of a decreasing growth rate for CFC-12. Based upon declining production, one expects mixing ratios of this CFC to begin decreasing over the next decade. Growth rates for the potent ozone-depleting halons have declined slowly over the years so that by 2002 the contribution to the annual increase in EECl from halons was comparable to that contributed by hydrochloroflorocarbons (HCFCs). HCFCs are chemicals used as substitutes for CFCs and other potent ozone-depleting gases. The data through 2002 suggest that the contribution to EECl from HCFCs is not increasing exponentially; HCFCs have caused the tropospheric burden of EECl to increase by a constant amount during the past 5–6 yr.

Declines in EECl also hinge on the influence of methyl bromide, a gas that is emitted to the atmosphere from both regulated industrial production and natural processes. Global mixing ratios of methyl bromide, however, are not well documented in recent years so they have not been considered in Figs. 18 and 19. Nevertheless, some additional declines in EECl in recent years arising from changes in methyl bromide are expected due to global production restrictions since 1999 attributed to the Montreal Protocol on Substances that Destroy the Ozone Layer.

c. Global carbon dioxide in 2002

After water vapor, CO_2 is the most important infrared absorbing gas (i.e., greenhouse gas) in the at-

mosphere. For about 10,000 years prior to the industrial revolution, the atmospheric abundance of CO_2 was nearly constant at ~280 ppm (ppm = parts in 106 by mole fraction). This abundance represented a balance among large seasonal fluxes (on the order of 100 Gt C yr^{-1}, where 1Gt = 1015 g) between the atmosphere and biosphere (photosynthesis and respiration) and between the atmosphere and the ocean (physical exchange of CO_2). Since the late 1800s, atmospheric CO_2 has increased by ~30%, primarily because of emissions from combustion of fossil fuels (currently about 7 Gt C yr^{-1}) and, to a lesser extent, deforestation (0–2 Gt C yr^{-1}). High-precision measurements of atmospheric CO_2, beginning in 1958, show that the average increase of CO_2 in the atmosphere corresponds to ~55% of the CO_2 emitted by fossil fuel combustion (Keeling et al. 1995), but this fraction varies from ~20% to ~90% (Conway et al. 1994; Ciais et al. 1995). The remaining fossil fuel–CO_2 is removed from the atmosphere by the oceans and the terrestrial biosphere.

The net annual increase in atmospheric CO_2, determined from a globally distributed network of air sampling sites, is plotted for 1980–2001 in Fig. 20 (red line). Global emissions of carbon resulting from fossil fuel combustion (available from the Carbon Dioxide Information and Analysis Center, Oak Ridge, Tennessee, Web site: http://cdiac.esd.ornl.gov/trends/emis/em_cont.htm) are also plotted (black line). Note the variability in the atmospheric increase in carbon during the 20-yr period. The increase was a relatively small fraction of fossil fuel emissions in 1992, but nearly 90% of the fossil fuel emissions of carbon remained in the atmosphere during 1998. The difference between fossil fuel emissions and the atmospheric increase is the net global sink. Clearly, the variations in the atmospheric increase are much larger than the variations in fossil fuel emissions. However, these variations arise from relatively small imbalances between the large one-way atmosphere–ocean and atmosphere–terrestrial biosphere fluxes. Most attempts to explain the interannual variability of the atmospheric CO_2 increase have focused on short-term climate fluctuations (e.g., ENSO and post-Pinatubo cooling), but the mechanisms, especially the role of the terrestrial biosphere, are not well understood. For example, it has been speculated that the high CO_2 growth rate in 1998 was related to unusually warm temperatures. Analysis of 1999 CO_2 measurements indicates a return to average or a lower than average growth rate in 1999, although 1999 was only slightly cooler than 1998.

Understanding the relative contributions of the ocean and biosphere to the net global carbon sink has important environmental policy implications.

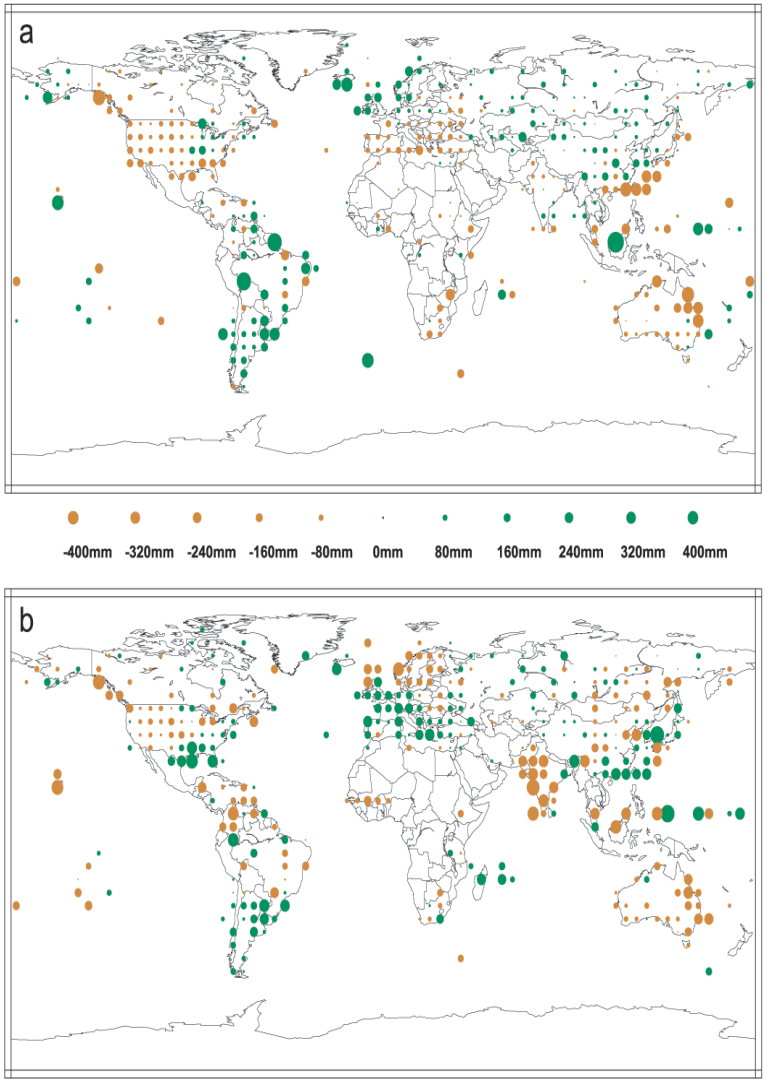

Fig. 11. (a) Jan–May 2002 and (b) Jun–Dec 2002. Anomalies are for five-degree grid squares based on the 1961–90 base period and are expressed in millimeters. The magnitude of the anomalies are depicted by the areas of the circles. Green indicates normal or above normal, while brown indicates below-normal precipitation. Areas without circles reflect insufficient data for calculating anomalies (source: NCDC's Global Historical Climatology Network).

Table 1. Monthly and annual climatological information on Northern Hemisphere and continental snow extent between Nov 1966 and Dec 2002. Included are the numbers of years with data used in the calculations, means, standard deviations, Dec 2001 and Jan–Dec 2002 values and rankings. Areas are in millions of square kilometers. The years 1968, 1969, and 1971 have 1, 5, and 3 missing months, respectively, thus are not included in the annual (Ann) calculations (annual only applies to Jan–Dec 2002). North America (N. Am.) includes Greenland.

	Yrs	Mean	Std dev	Area	H. Hem. rank	Eurasia rank	N. Am. rank
Dec 01	37	43.4	1.9	45.0	5	3	25
Jan 02	36	46.8	1.5	46.9	16	9	30
Feb 02	36	45.8	1.9	42.9	35	36	23
Mar 02	36	41.0	1.9	37.9	34	36	12
Apr 02	36	31.5	1.8	30.8	25	24	16
May 02	36	20.6	1.9	19.7	20	29	14
Jun 02	35	11.1	2.1	9.5	26	32	19
Jul 02	33	5.0	1.4	3.2	33	31	31
Aug 02	34	3.6	1.0	2.7	27	30	25
Sep 02	34	5.7	1.0	5.6	20	7	33
Oct 02	35	18.3	2.7	23.5	2	2	2
Nov 02	37	34.1	2.1	35.8	5	10	12
Dec 02	37	43.4	1.9	45.9	3	1	32
Ann 02	33	25.6	1.0	25.4	19	18	17

High-precision measurements of atmospheric CO_2 abundance alone are insufficient to calculate this partitioning. Researchers use measurements of the carbon-isotopic composition of CO_2 and atmospheric O_2 to constrain understanding of this partitioning. Average uptake for the 1990s has been estimated using these methods to be 1.7±0.5 Gt C yr^{-1} by the oceans and 1.4±0.7 Gt C yr^{-1} by the terrestrial biosphere.

d. Global methane in 2002

Methane's contribution to anthropogenic radiative forcing, including direct and indirect effects, is about 0.7 W m^{-2}, half that of CO_2. Changes in the burden of methane feed back into atmospheric chemistry, affecting the concentrations of hydroxide (OH) and O_3. The increase in methane since the pre-industrial era is responsible for about one-half the estimated increase in background tropospheric O_3 during that time. Changes in OH concentration affect the lifetimes of other greenhouse gases such as the replacement refrigerants [hydroflorocarbons (HFCs) and HCFCs].

High-precision measurements of atmospheric methane (CH_4) provide climate modelers with current and past rates of CH_4 increase, and they are also useful in constraining the CH_4 budget. In Fig. 21 smoothed, globally averaged CH_4 mole fractions from the NOAA/CMDL air sampling network are plotted as a function of time. During nearly 20 yr of measurements, CH_4 has increased, but the rate of increase has slowed and is near zero during 2000 and 2001, consistent with the measurements of Simpson et al. (2002).

An example of an important budget constraint, total global annual emissions, is plotted as a function of time in Fig. 21b. Global CH_4 emissions were calculated from the mass balance equation:

$$Q = d[CH_4]/dt + [CH_4]/\zeta,$$

where the rate of CH_4 increase, $d[CH_4]/dt$, and the atmospheric CH_4 burden, $[CH_4]$, are determined from the observations, and the lifetime, t, is assumed constant at 8.9 yr. There is certainly unaccounted-for interannual variability in the CH_4 lifetime. For example, the CH_4 growth rate increased during 1991 immediately after the eruption of Mt. Pinatubo. Dlugokencky et al. (1996) attributed this to the effects of SO_2 and ash injected during the eruption on CH_4 chemical loss rates. Such changes in CH_4 lifetime would manifest themselves as changes in emissions in this analysis. Positive (Krol et al. 1998; Karlsdóttir and Isaksen 2000) and negative (Prinn et al. 2001) trends in (OH) have been reported but have not been verified. Decreases in (OH) during the 1990s of the magnitude reported by Prinn et al. (2001) would require more than a 10% decrease in CH_4 emissions during the past decade (Cunnold et al. 2002), which is not consistent with our understanding of the CH_4 budget. The observa-

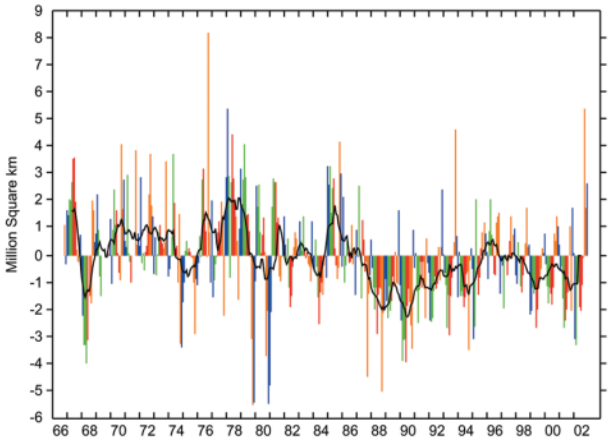

FIG. 12. Anomalies of monthly snow cover extent over Northern Hemisphere lands (including Greenland) between Nov 1966 and Dec 2002. Also shown are twelve-month running anomalies of hemispheric snow extent, plotted on the seventh month of a given interval. Anomalies are calculated from NOAA snow maps. Mean hemispheric snow extent is 25.6 million sq. km. for the full period of record. Monthly means for the period of record are used for 9 missing months between 1968 and 1971 in order to create a continuous series of running means. Missing months fall between Jun and Oct, no winter months are missing

tions are consistent with small rates of increase in (OH); however, for simplicity, we assume that the CH_4 lifetime has been constant.

This analysis suggests that total global CH_4 emissions averaged 540 Tg CH_4 yr^{-1} during 1984–2001 with no significant trend. As mentioned previously, the increased "emission" rate during 1991 was actually because of a temporarily longer lifetime (less chemical sink). The significant increase in emissions during 1998 was because of wetter and warmer than average conditions resulting in increased emissions from wetlands (Dlugokencky et al. 2001).

e. *Global carbon monoxide in 2002*

Unlike CO_2 and CH_4, carbon monoxide (CO) does not strongly absorb terrestrial IR radiation, but it still impacts climate through its chemistry. The chemistry of CO affects OH (which influences the lifetimes of CH_4 and HFCs) and tropospheric O_3 (itself a greenhouse gas), so emissions of CO can be considered equivalent to emissions of CH_4 (Prather 1996). Current emissions of CO may contribute more to radiative forcing over decadal timescales than emissions of anthropogenic N_2O (Daniel and Solomon 1998).

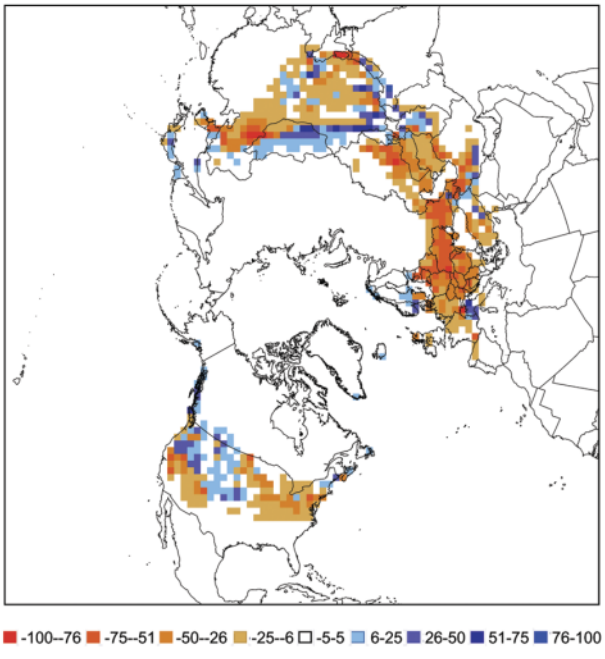

FIG. 13. Feb 2002 monthly snow extent anomalies with respect to climatology maps covering the period Nov 1966–May 1999. Departures show differences in the percent frequency of cover between 2002 and the long term mean. Feb 2002 and Feb climatology may be viewed online at http://climate.rutgers.edu/snowcover.

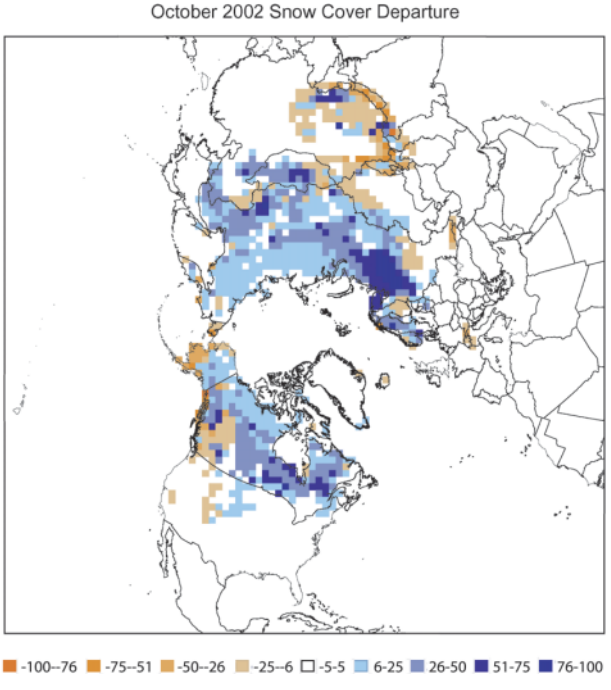

FIG. 14. Oct 2002 monthly snow extent anomalies with respect to climatology maps covering the period Nov 1966–May 1999. Departures show differences in the percent frequency of cover between 2002 and the long-term mean. Oct 2002 and Oct climatology may be viewed online at http://climate.rutgers.edu/snowcover.

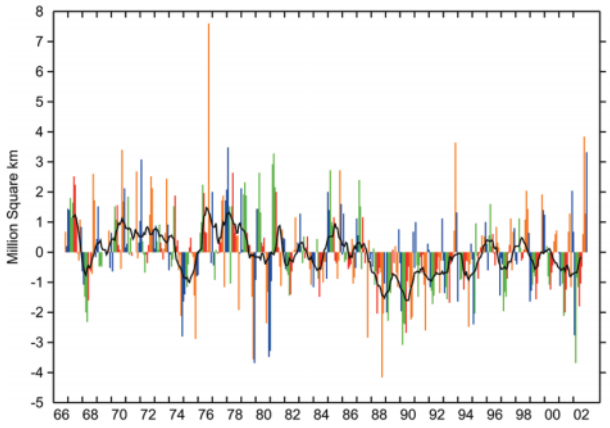

Fig. 15. Same as Fig. 12, except for Eurasia.

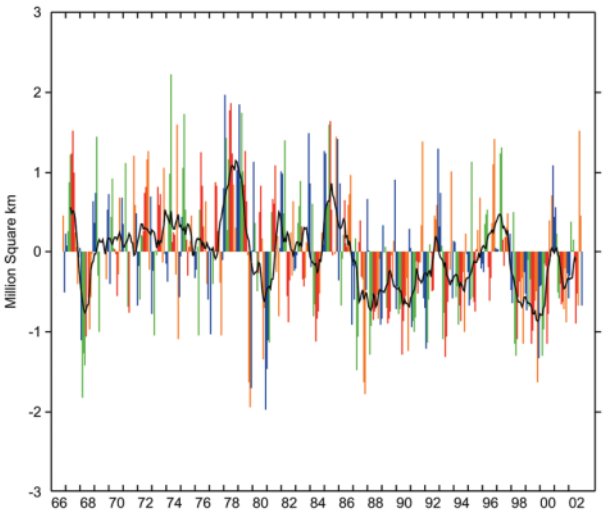

Fig. 16. Same as Fig. 15, except for North America (including Greenland).

Zonally averaged, deseasonalized CO mole fractions (lines) are plotted as a function of time in Fig. 22. The shading in this figure represents 1 sigma uncertainty in these trend lines. There is a long-term trend in globally averaged CO, driven by a trend in the Northern Hemisphere (Novelli et al. 2003). In the Southern Hemisphere, no long-term trend exists. Superimposed on the trends are significant interannual variations, most notably during the late 1990s. The CO bump starting in 1997 in the Tropics is likely the result of tropical biomass burning (Langenfelds et al. 2002). Note also the significant feature at high northern latitudes during 1998. Bruhwiler et al. (2000) and Kasischke et al. (2000) have studied the potential causes of this anomaly in CO during 1998. They found that large forest and peatland fires in North America and Siberia during late summer and early autumn released an estimated 164 Tg CO, and that these emissions are responsible for the anomalous CO observed during 1998.

f. Mauna Loa solar transmission

Apparent direct solar transmission has been measured continuously from the Mauna Loa Observatory, Hawaii, from 1958 through 2002 as shown in Fig. 23. The dark blue line in Fig. 23 is a 6-month running weighted mean of monthly average clear-sky solar transmission values. The straight red line in Fig. 23 is a subjective estimate of the linear upper limit (cleanest times) of the observed data through the end of 1999 with an anticipation of continued recovery from the Mt. Pinatubo eruption in 1991 as presented by Dutton and Bodhaine (2001). Dutton and Bodhaine concluded that very little or no long-term change in the transmission had occurred through the end of 1999 based on the expectation that the then indicated recovery from the eruption of Mt. Pinatubo would continue a few more years. However, a distinct break from that recovery occurred in 2000 and continued through 2002.

The black straight line is for the same type of estimate as before except using data through the end of 2002. The

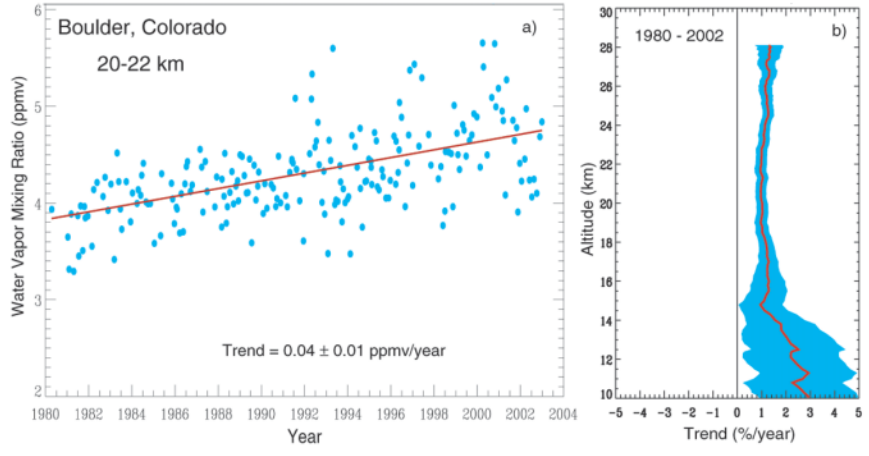

Fig. 17. (a) The record of monthly water vapor mixing ratio in parts per million by volume (ppmv) over Boulder, CO, in the 20–22 km layer. The straight line is a linear trend fit to the data. (b) The trend in water vapor with altitude over Boulder in percent per year. The shading represents the 95% confidence interval. (Courtesy S. Oltmans, H. Vomel, and Z. Sherman, NOAA/CMDL.)

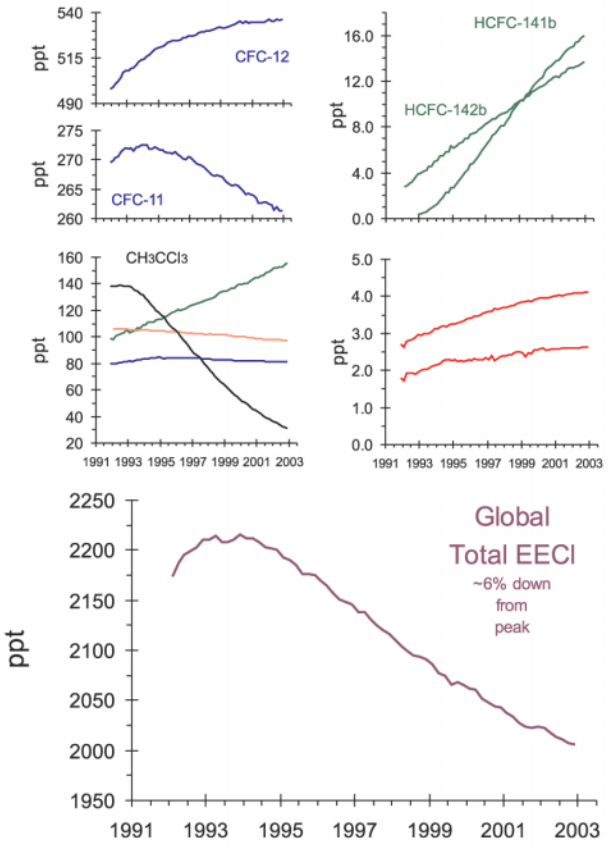

FIG. 18. Trends of global tropospheric mixing ratios of CFC-12, CFC-11, methyl chloroform, and carbon tetrachloride from in situ EC-GC, and CFC-113, HCFC-22, HCFC-141b, HCFC-142b, halon-1211, and halon-1301 from flask analyses of samples collected from the NOAA/CMDL network. Total EECl (effective equivalent chlorine) is an expression of the total burden of ozone-depleting halogen in the atmosphere and is derived from the surface measurements weighted by each individual compound's efficiency for releasing reactive chlorine and bromine in the stratosphere, and a relative efficiency factor for bromine that is 45 times that of chlorine. (Courtesy S. Montzka, J.H. Butler, T. Thompson, D. Mondeel, and J. Elkins, NOAA/CMDL.)

2002 data are consistent with the previous two years and, those three years in combination, change the earlier conclusion based on data through the end of 1999. Applying the sensitivity analysis of Dutton and Bodhaine (2001), the suggested overall change in measured direct solar transmission of 0.005 from 1958 to January 2003 translates into a decrease in total net (24-h average) solar irradiance of nearly 3 W m^{-2} over the Mauna Loa Observatory at the 3.4-km altitude of the observations.

The study by Dutton and Bodhaine (2001) concludes that through the end of 1999, a maximum decrease of only 0.4 W m^{-2} was observed.

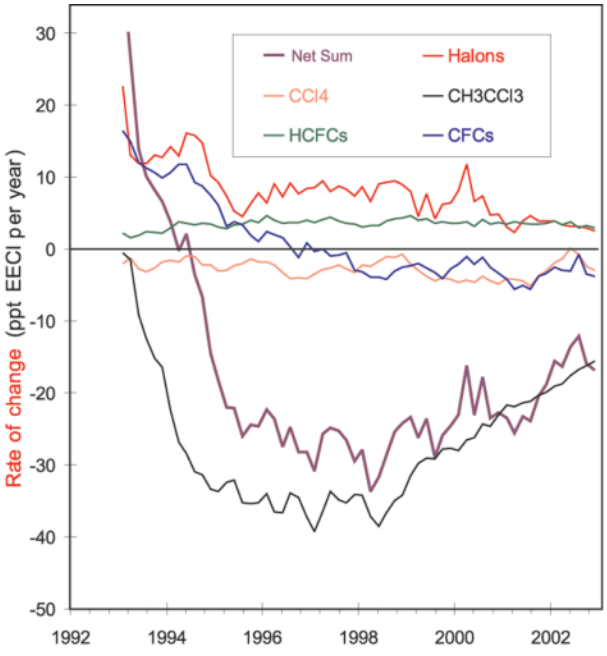

FIG. 19. The net rate of change of EECl in recent years (thick purple line) from the measured trends of the ozone-depleting gases included in Fig. 1. Also shown are the contributions of other gases and groups of gases on the observed net rate of change. [Courtesy S. Montzka, J. H. Butler, T. Thompson, D. Mondeel, and J. Elkins: updated from Montzka et al. (1999).]

Another approach to estimating change in background transmission from 1958 to 2003 is to contrast multiyear averages at the beginning and end of the record. Doing this for the first and last three years, 1958–60 and 2000–02, also indicates a transmission dif-

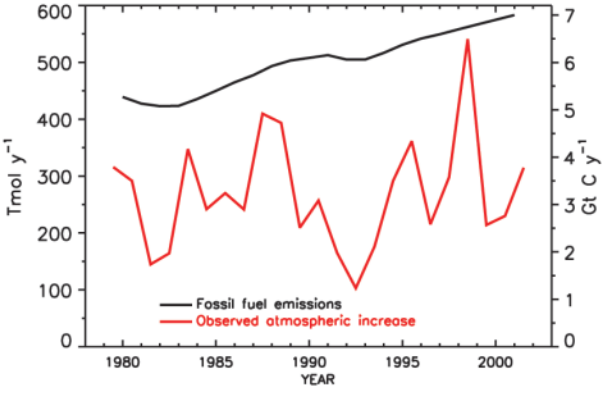

FIG. 20. Global CO_2 emissions due to fossil fuel use (black line) from the Carbon Dioxide Information and Analysis Center (Oak Ridge National Laboratory, Oak Ridge, TN 37831) and observed global atmospheric CO_2 increase (red line) determined from NOAA /CMDL cooperative air sampling network measurements. (Courtesy T. Conway, NOAA/CMDL.)

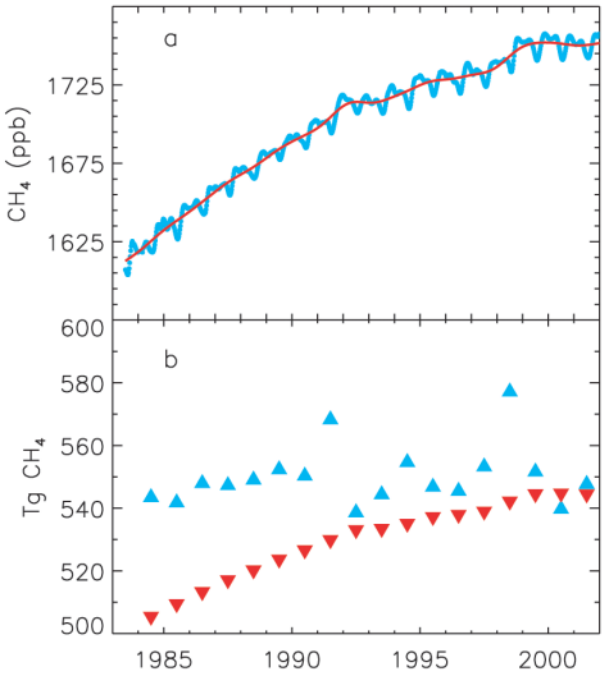

FIG. 21. (top) Globally averaged methane mole fractions. The solid line is the deseasonalized trend. (bottom) Total global CH_4 emissions (blue) and sink (red). (Courtesy E. Dlugokencky, NOAA/CMDL.)

ference of 0.005. We suggest that the sudden sustained decrease in solar transmission measured at Mauna Loa that occurred beginning in 1999 may be related to increased transport of Asian aerosols and air pollution observed in other measurements at Mauna Loa.

4. THE TROPICS

a. ENSO and the tropical Pacific—M. Halpert[3] and G. Bell[3]

i) Overview

Pacific warm episode (El Niño) conditions developed during May–August 2002, and strengthened during September–December. An important precursor to this warm episode was the development of anomalously warm waters at approximately 100–200-m depth across most of the central equatorial Pacific, which began in May 2001 in association with a deepening of the oceanic thermocline. Increased depths of the thermocline are indicated by positive depth anomalies of the 20°C isotherm, which approximates the center of the thermocline across the eastern equatorial Pacific (Fig. 24a).

By February 2002 area-average SSTs had become slightly warmer than normal over the eastern half of the equatorial Pacific (Fig. 24c). During late May 2002 the oceanic thermocline deepened further and sea surface temperature departures increased, as the low-level equatorial easterly winds weakened across the central and east-central equatorial Pacific (Fig. 24b). This more rapid evolution toward El Niño was partly linked to strong westerly wind anomalies associated with the MJO (section 4e).

El Niño conditions developed during May–August as sea surface temperatures warmed to almost 1°C above average across the east-central equatorial Pacific, and the equatorial easterly winds remained weaker than normal. The well-known El Niño–related pattern of tropical convection also became more evident during this period, as enhanced convection overspread the central equatorial Pacific and suppressed convection developed across Indonesia. The appearance of above-normal heights at 200-hPa reflected the increase in deep tropospheric heating over the central equatorial Pacific associated with the enhanced convection (Fig. 24d).

Further strengthening of the El Niño occurred during October–December as the thermocline continued to deepen, area-averaged SST departures increased to +1.75°C, and tropical convection strengthened across the central and east-central equatorial Pacific. This strengthening of the El Niño conditions also appears to be partly associated with the MJO.

ii) Equatorial Pacific Ocean sea surface and subsurface temperature evolution

During the pre–El Niño period December 2001/May 2002 the axis of warmest SSTs over the central tropical Pacific was located south of the equator, and equatorial temperatures greater than 28°C (the temperature representing the approximate threshold for

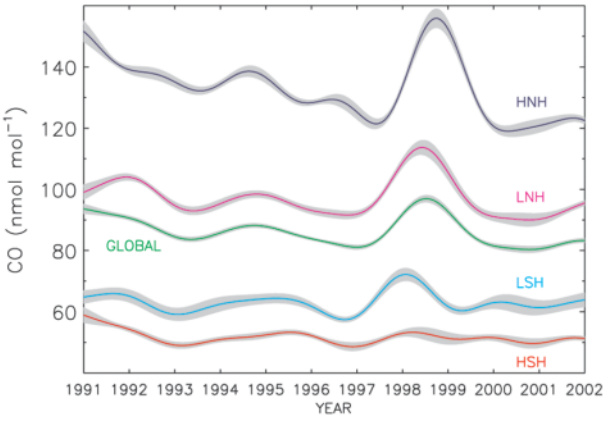

FIG. 22. Globally and zonally averaged (deseasonalized) trends for surface tropospheric CO (solid lines) determined from the CMDL cooperative air sampling network. Shading is ±1s uncertainty. Zonal averages are as follows: HSH = 30°–90°S, LSH = equator–30°S, LNH = equator–30°N, and HNH = 30°–90°N. (Courtesy P. Novelli, NOAA /CMDL.)

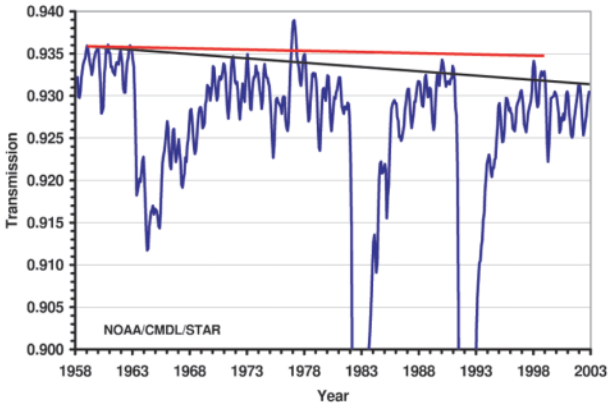

FIG. 23. Plot of the running weighted means (1,2,4,2,1) of the monthly average apparent direct solar transmission from the Mauna Loa Observatory, Hawaii from 1958 through 2002. The two straight lines indicate the potential change in the general level of the transmission based on different assumptions. The red line was suggested by Dutton and Bodhaine (2001) for data through 1999 with the expectation of continued recovery of atmospheric transmission following the most recent volcanic events. The black line is what is now considered a better estimate of that change given the additional years of data beyond 1999. [Courtesy of E. Dutton, NOAA/CMDL, updated from Dutton and Bodhaine (2001).]

deep tropical convection over the central equatorial Pacific; Gadgil et al. 1984), were confined to the area west of the date line (Figs. 25a,c). However, the equatorial cold tongue was already exhibiting signs of weakening along its western boundary during this period as indicated by warmer than average SSTs near the date line (Figs. 25b,d).

During June–July–August (JJA, hereafter all 3-month periods will be denoted by the first letter of each month) equatorial SSTs warmed to greater than 28°C over the central and east-central equatorial Pacific, and exceeded 29°C near the date line (Fig. 25e). These temperatures were more than 1°C above average across most of the eastern Pacific, and reflected a further anomalous weakening of the equatorial cold tongue (Fig. 25f). The increase in SSTs to beyond 28°C during JJA is consistent with development of El Niño, and with the onset of enhanced convective activity and above-average precipitation over the central equatorial Pacific. Warm episode ENSO conditions then intensified during SON (Figs. 25g,h) as SSTs reached more than 2°C above average over the central equatorial Pacific, and departures greater than 1°C covered the entire eastern half of the equatorial Pacific.

The subsurface thermal structure is a fundamental component of the ENSO cycle. During DJF and MAM anomalously warm waters were evident between 100- and 200-m depth across the central and east-central equatorial Pacific (Figs. 26a,b). This warmth is consistent with an increased depth of the oceanic thermocline, and with a decreased west–east slope of the thermocline across the tropical Pacific. The El Niño onset and subsequent strengthening occurred in association with an intensification, eastward expansion, and upward extension of the anomalous warm pool to the ocean surface (Figs. 26c,d).

iii) Atmospheric circulation—Pacific basin

Many of the prominent atmospheric circulation features typical of past Pacific warm episodes were observed during JJA and SON 2002. In the Tropics the El Niño–related anomaly features during these seasons included 1) lower-level westerly wind anomalies across the central and eastern Pacific in association with a reduced strength of the tropical easterlies (Figs. 27c,d), 2) enhanced ascending motion and convective activity over the central equatorial Pacific, and 3) anomalous descending motion and suppressed convective activity over Indonesia. These conditions reflect a weaker-than-average strength of the equatorial Walker circulation across the Pacific basin, which is a well-known characteristic of Pacific warm episodes.

In the meridional direction the circulation during SON featured anomalous poleward flow in the upper troposphere over the central tropical Pacific just west of the date line (Fig. 28a), along with anomalous upper-tropospheric divergence and lower-level convergence, as indicated by the anomalous outgoing longwave radiation (OLR) pattern. These conditions reflect an enhanced Hadley circulation, which is another well-known feature of Pacific warm episodes.

Also SON anticyclonic streamfunction anomalies [indicated by positive (negative) anomalies in the Northern (Southern) Hemisphere] were evident at upper levels in the subtropics of both hemispheres (Fig. 28b) flanking the region of enhanced tropical convection over the central and east-central Pacific. These anticyclonic anomalies are also typical of El Niño (Mo and Kousky 1993). They reflect a strengthening and eastward extension of the subtropical ridges in both hemispheres, along with an overall weakening of the mid-Pacific troughs farther east.

Enhanced westerlies and anomalous upper-level confluent flow across the central extratropical Pacific was evident along the poleward flanks of the anomalous subtropical ridges in both hemispheres (Fig. 28a). These anomalies reflect an eastward extension of the midlatitude jet streams in both hemispheres, and an eastward shift in the areas of strong upper-level diffluence that define these jet exit regions.

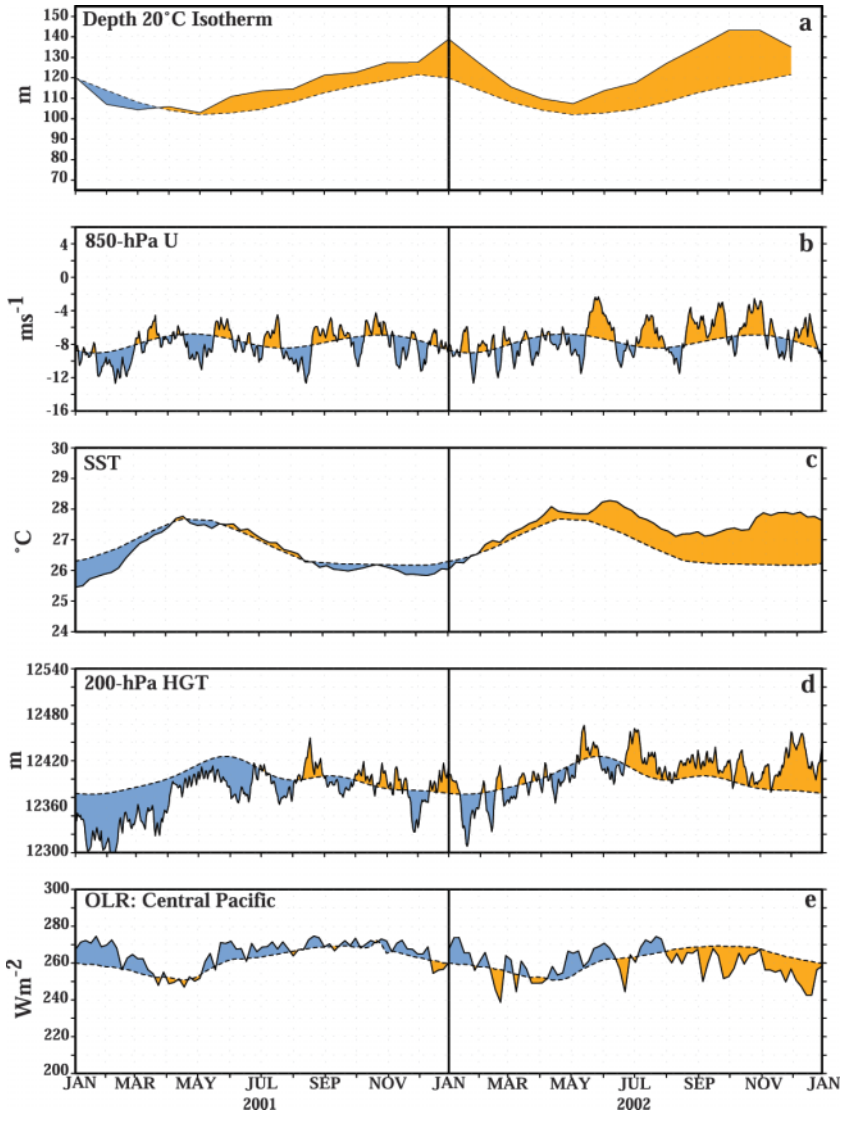

FIG. 24. 24 monthly time series of (a) the depth of the 20°C isotherm (m), (b) 850-hPa zonal wind speed (m s^{-1}), (c) SST (°C), (d) 200-hPa height (m), and (e) outgoing longwave radiation (OLR, W m^{-2}) over the central Pacific. Values are determined by averaging over the region bounded by 5°N–5°S and 180°–100°W in (a)–(d), and 20°N–20°S and 180°–100°W in (e). The solid curve in all panels shows the monthly mean values and the dashed curved shows the climatological mean. The anomalies are shown shaded, with orange (blue) shading indicating positive (negative) anomalies, except for in (e) where the shading convention is reversed. The climatology and anomalies are computed with respect to the 1979–95 base period.

iv) The Madden–Julian oscillation and Kelvin wave activity

Low-frequency variability in the Tropics is strongly influenced by the MJO (e.g., Madden and Julian 1971, 1972, 1994). The MJO is an atmospheric disturbance that modulates the patterns of tropical convection and atmospheric circulation with a typical period of 30–60 days. It tends to be most active during ENSO-neutral years (Kousky and Kayano 1994), especially just prior to El Niño (Higgins et al. 2000).

There was considerable MJO activity beginning in late April 2002, with the upper-level velocity potential anomalies showing continuous propagation of this activity around the global Tropics (shading, Fig. 29). This MJO activity contributed to alternating periods of enhanced and suppressed convection (shading), and to alternating periods of low-level easterly and westerly wind anomalies across the tropical Pacific (contours). Of particular interest is the strong MJO activity during both May and late June/early July, which coincided with the development of El Niño. During both late-May and late June/early July the ascending phase of the MJO (indicated by negative velocity potential anomalies) overspread the central and east-central equatorial Pacific, and strong low-level westerly wind anomalies extended to well east of the date line. Another MJO in late October also contributed to a marked increase in the strength of the low-level westerly anomalies across the east-central equatorial Pacific.

While the MJO does not cause El Niño, the associated periods of strong low-level westerly wind anomalies are thought to contribute to the speed of development, and possibly the intensity of El Niño episodes via the generation of oceanic Kelvin waves (Zhang et al. 2001). Kelvin waves are eastward propagating oceanic gravity waves that feature downwelling at their leading edge and upwelling behind. A typical eastward propagation rate for these waves is roughly 10° of longitude per week. As a Kelvin wave passes a given location the thermocline deepens, resulting in increased ocean temperatures at thermocline depth. This is followed some time later by a shoaling of the thermocline and cooling temperatures. Successive waves, combined with an overall weakening of the equatorial low-level

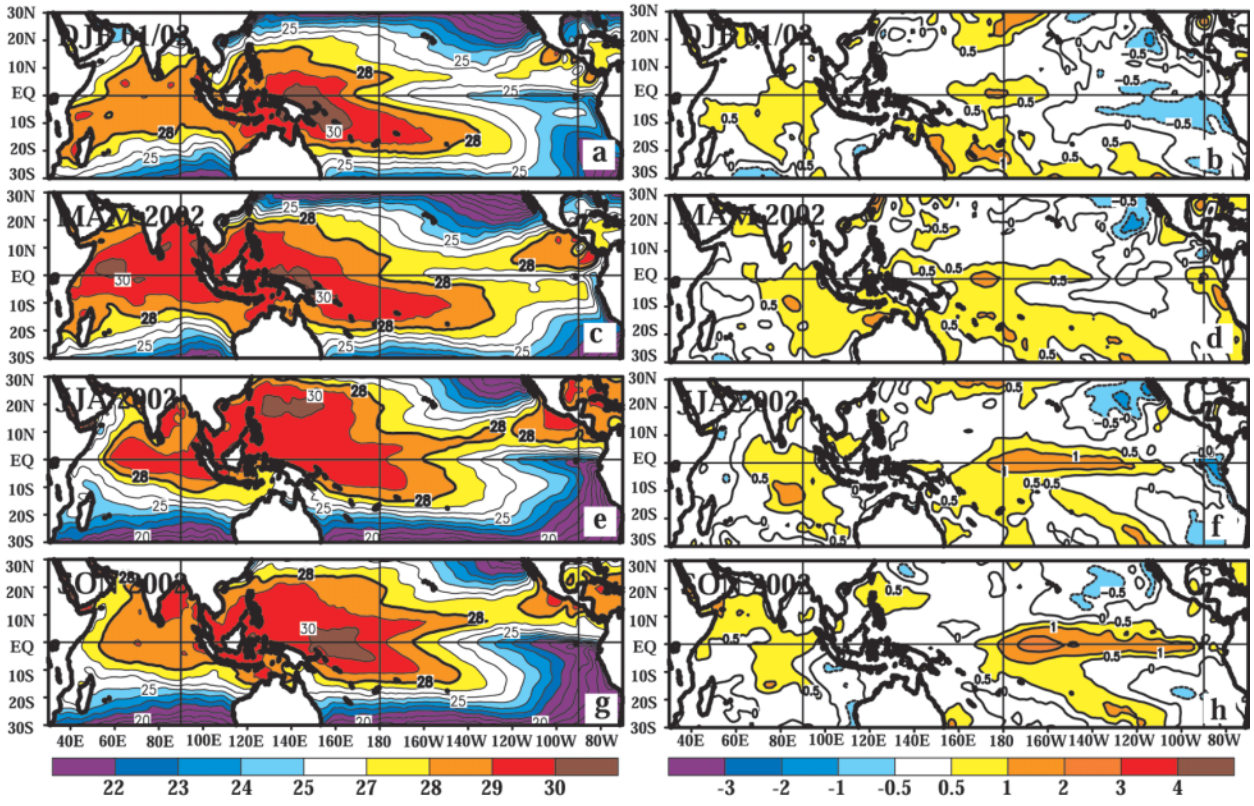

Fig. 25. (left) Seasonal SST and (right) anomaly for (a), (b) DJF 2001/2002, (c), (d) MAM 2002, (e), (f) JJA 2002, and (g), (h) SON 2002. Contour interval is 1°C, with the 0.5°C anomaly contour included. Anomalies are departures from the 1971–2000 adjusted optimal interpolation (OI) climatology (Smith and Reynolds 1998).

easterlies, can maintain the thermocline at a deeper-than-normal level, even after initial waves have passed.

There are three distinct periods when the MJO and its associated Kelvin wave activity appear to have influenced the developing El Niño during 2002. The first was in May when the low-level westerly wind anomalies associated with the MJO generated an eastward-propagating Kelvin wave that contributed to increased depths of the 20°C isotherm (Fig. 24a), and to a sharp increase in SST anomalies over the central and east-central equatorial Pacific (Fig. 24c). This evolution immediately preceded the onset of El Niño. The second period was during July after the onset of El Niño, when strong westerly wind anomalies triggered a further deepening of the oceanic thermocline. The third period occurred during the second half of October, when the westerly wind anomalies contributed to a sharp increase in SSTs that led to a further strengthening of the El Niño.

b. Tropical Storms

1) Atlantic hurricane season—G. J. Bell[3]

(i) Overview

The 2002 Atlantic hurricane season featured 12 named storms, 4 hurricanes, and 2 major hurricanes.

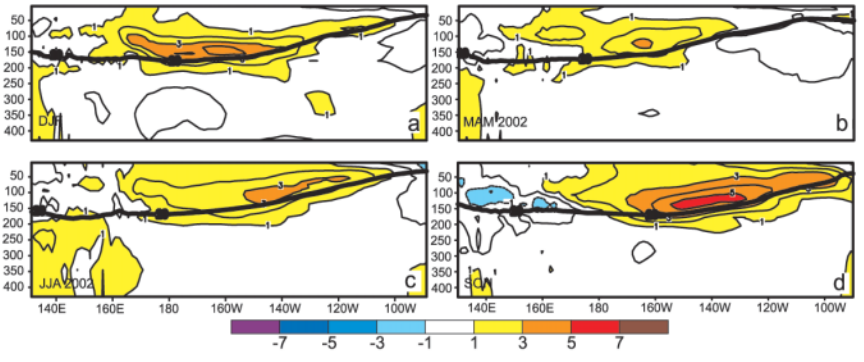

Fig. 26. Equatorial depth–longitude sections of ocean temperature anomalies for (a) DJF 2001/2002, (b) MAM 2002, (c) JJA 2002, and (d) SON 2002. Shading interval is 1°C. The dark line is the 20°C isotherm. Data are derived from an analysis system that assimilates oceanic observations into an oceanic GCM (Behringer et al. 1998). Anomalies are departures from the 1981–2000 base period means.

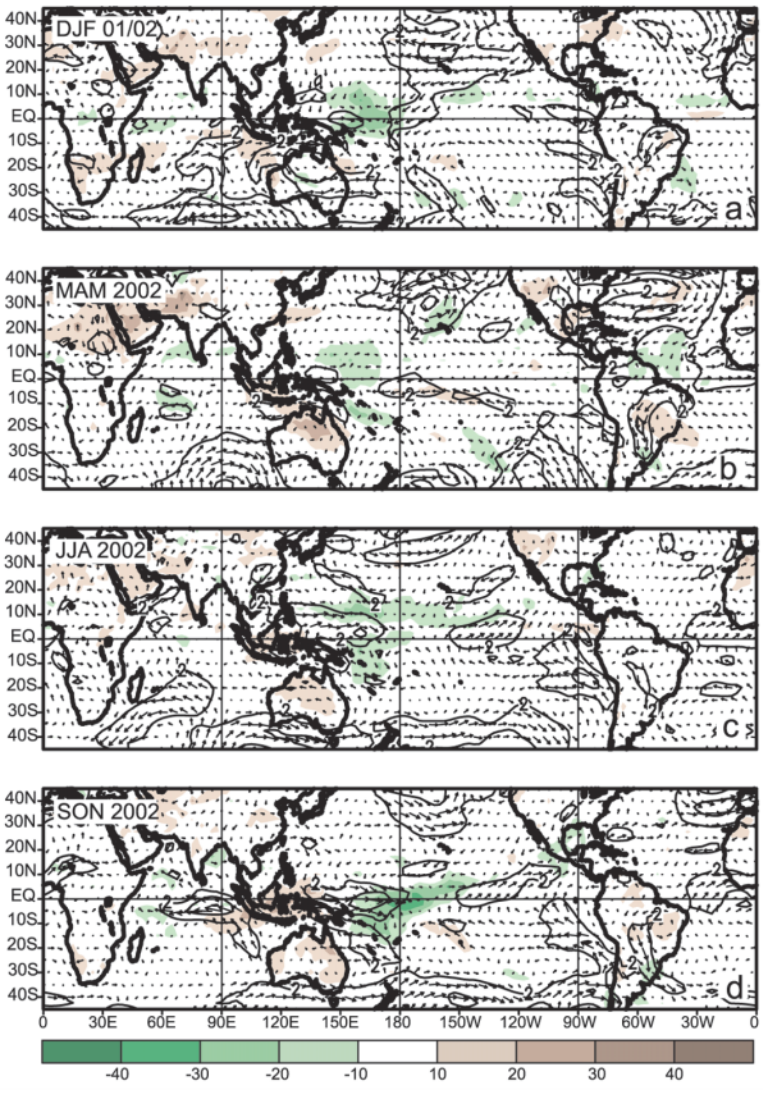

Fig. 27. Outgoing longwave radiation (OLR) anomalies (shaded) and 850-hPa vector wind anomalies and isotachs for (a) DJF 2001/2002, (b) MAM 2002, (c) JJA 2002, and (d) SON 2002. Contour interval for isotachs is 2 m s^{-1}. Shading interval for OLR anomalies is 10 W m^{-2}. Anomalies are departures from the 1979–95 base period monthly means.

This is one-half the average seasonal number of hurricanes measured since a marked upturn in hurricane activity began in 1995 (Goldenberg et al. 2001). The climatological peak in Atlantic hurricane activity occurs between mid-August and mid-October from an increased number of hurricanes and major hurricanes forming in the main development region (MDR; defined as the tropical North Atlantic south of 21°N and the Caribbean Sea). During 2002 9 of the 12 named storms and all four hurricanes formed during this 2-month period, but only three of these systems formed in the MDR.

The 2002 seasonal activity reflected the competing influences of three leading climate factors: El Niño, the active multi-decadal signal, and the MJO. The decreased activity in the MDR was related to El Niño [see section 4bi(iv)(a): El Niño]. However, key aspects of the atmospheric circulation over the tropical Atlantic continued to reflect the ongoing active multidecadal signal, which moderated the "apparent" El Niño signal in portions of the MDR [see section 4bi(iv)(b): The active multidecadal signal]. A "window of opportunity" for hurricane activity in late September and early October developed in response to the westerly phase of the MJO, which temporarily offset the high vertical wind shear associated with El Niño during a period when conditions are climatologically most conducive to hurricane development [see section 4bi(v)].

(ii) Seasonal activity

NOAA defines the total seasonal activity based on the combined strength, duration, and number of named storms and hurricanes (Bell et al. 2000). One measure of this seasonal activity is the accumulated cyclone energy (ACE) index (Fig. 30), which is essentially a wind energy index calculated by summing the squares of the estimated 6-hourly maximum sustained wind speed in knots (V_{max}^2) for all periods while the system is either a tropical storm or hurricane. For the 2002 season the total ACE index was 62.5 $\times 10^5$ kt^2 (Fig. 30), or 73% of the long-term median value. NOAA defines near-normal seasons as having a total ACE value in the range of 65–103 $\times 10^5$ kt^2. Therefore the 2002 season activity falls into the below-normal range.

Almost 75% of the total 2002 seasonal activity was associated with three hurricanes that formed during a brief 6-day window of 18–23 September (Fig. 31). Two of these systems became hurricanes over the Caribbean Sea (Isidore and Lili) and eventually became major hurricanes, and the third (Kyle) persisted over the extratropical North Atlantic for 20 days between 23 September and 12 October.

Three tropical storms, two of which became hurricanes (Isidore and Lili), formed in the MDR during 2002. This is only one-third the average number of

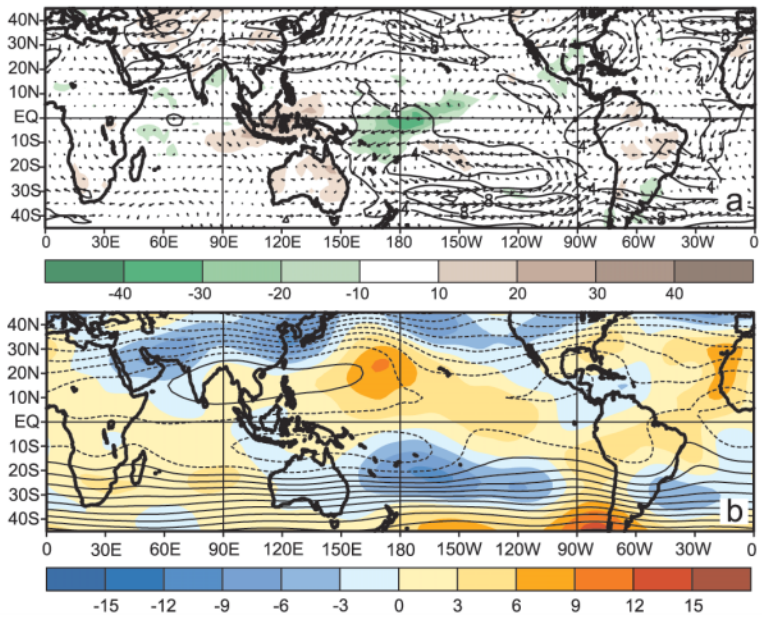

FIG. 28. (a) SON 2002 vector wind and isotachs and (b) streamfunction anomalies at 200 hPa. Contour interval for isotachs is 4 m s^{-1}. Shading interval for streamfunction anomalies is 3 x 106 m2 s^{-1}. In the Northern Hemisphere positive (negative) streamfunction anomalies indicate an anticyclonic (cyclonic) circulation. In the Southern Hemisphere, negative (positive) values indicate a cyclonic (anticyclonic) circulation. Anomalies are departures from the 1979–95 base period monthly means.

hurricanes forming in the MDR since the 1995 upturn in hurricane activity, and is consistent with the El Niño–related suppression of hurricane formation in this region. These three named storms accounted for 37.1 × 10^5 kt^2 (or 59.4%) of the seasonal ACE value, which amounts to 55% of the 1950–2001 period mean for the region (Fig. 30). This deficit in activity within the MDR accounts for 90% of the 2002 seasonal ACE anomaly of −31.5 × 10^5 kt^2.

Six tropical storms, two of which became hurricanes (Gustav and Kyle), formed over the extratropical North Atlantic during 2002, and accounted for 22.7 × 10^5 kt^2 (or 36.3%) of the seasonal ACE value. Long-lived Hurricane Kyle contributed to more than one half of this regional total (Fig. 31). Three tropical storms also formed over the Gulf of Mexico during the season, but accounted for only 2.7 × 10^5 kt^2 (or 4.3%) of the seasonal ACE value.

(iii) Landfalling U.S. tropical storms and hurricanes

Seven named storms made landfall in the United States during the 2002 hurricane season, six as tropical storms and one as a hurricane (Lili). Five of these systems made landfall along the Gulf Coast. The first of these Gulf Coast systems was Tropical Storm (TS) Bertha (Fig. 32a), which produced local precipitation amounts of 25–50 mm in southern Mississippi and Alabama. The second was TS Fay and its remnant low pressure center during 6–10 September (Fig. 32c), which produced on average more than 175 mm of rain over southeastern Texas. The third was TS Hanna, which brought 75–125 mm of precipitation to the Florida panhandle (Fig. 32d). In late September Hurricane Isidore brought extremely heavy rains (200–300 mm) to the Yucatan Peninsula (Fig. 33a) prior to making landfall along the Gulf Coast as a tropical storm. In the United States rainfall from TS Isidore during 25–26 Sep-

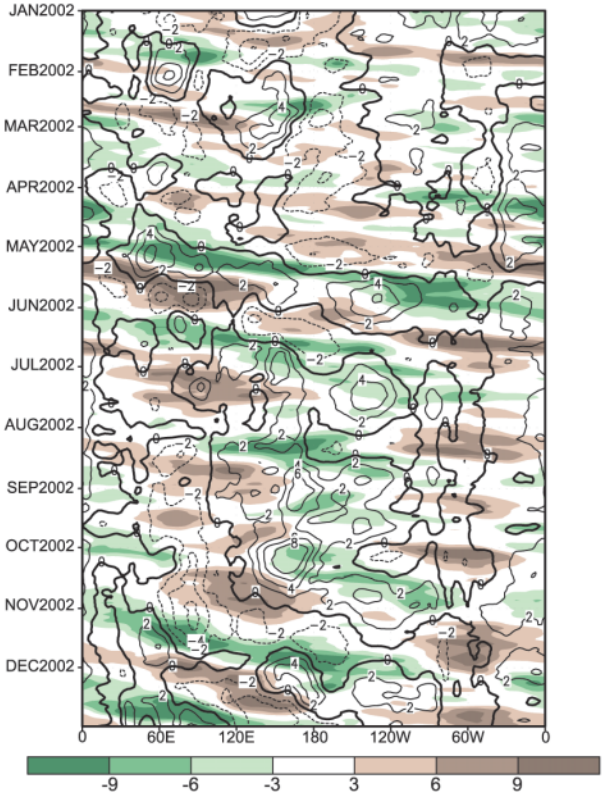

FIG. 29. Time–longitude section (5°N–5°S) of anomalous 200-hPa velocity potential (shading) and 850-hPa zonal wind (contours). Shading interval for velocity potential is 3 × 106 m^2 s^{-1}. Contour interval for winds is 2 m s^{-1}. The velocity potential (zonal wind) data are smoothed using a 5-day (15-day) running average. Anomalies are departures from the 1979–1995 base period daily means.

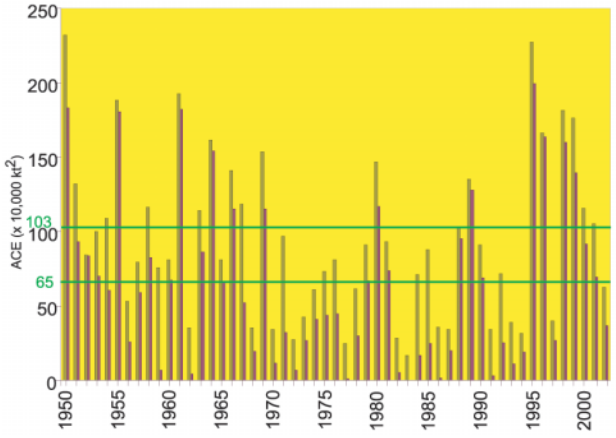

FIG. 30. Seasonal values of the accumulated cyclone energy (ACE) index for the total Atlantic basin (blue) and the main development region (MDR) (red). The ACE index for the MDR is based only on systems that first become named storms within the MDR, which includes the tropical North Atlantic south of 21°N and the Caribbean Sea. NOAA defines near-normal seasons as having a total ACE value in the range of 65–103 x 10^5 kt^2 (green lines).

tember exceeded 200 mm from eastern Louisiana to the western Florida panhandle, and also extended northward across Mississippi and Alabama (Fig. 33b). Hurricane Lili then followed with 100–150 mm of precipitation between 2 and 5 October across central and eastern Louisiana (Fig. 32f).

Tropical Storm Edouard was the only system to directly hit Florida during the 2002 season. Edouard came onshore along the northeastern coast on 4 September before moving across the state and dissipating over the Gulf of Mexico (Fig. 32b). The final named storm to impact the United States during the season was Hurricane Kyle, which moved along the South Carolina and North Carolina coasts on 11–12 October after being downgraded to a tropical storm.

August–October 2002 rainfall totals exceeded 600 mm along the Gulf Coast from eastern Texas to western Florida, and reached 500 mm across most of Mississippi extending northward into western Tennessee (Fig. 34a). These amounts are more than twice the long-term average (Fig. 34b) and are attributed to the landfalling tropical systems (Fig. 34c), which generally accounted for 40%–50% of the seasonal total in these areas (Fig. 34d).

New Orleans, Louisiana, situated within the seasonal rainfall maximum, experienced heavy rains from four named storms. A time series of daily rainfall totals at New Orleans indicates approximately 35 mm of rain from both TS Bertha and Fay, and nearly 300 mm from Isidore, which completely eliminated the precipitation deficits that had accumulated during the preceding 3.5 months (Fig. 35a). Hurricane Lili then produced an additional 80 mm of rain, resulting in a total station accumulation from these four storms of almost 450 mm.

(iv) Dominant climate factors influencing the 2002 Atlantic hurricane season

The Atlantic basin seasonal activity during 2002 reflected the competing influences of three leading climate factors: El Niño, the active multidecadal signal [section 4bi(iv)(b)], and the MJO [section 4bi(v)].

(a) El Niño

The ENSO cycle is a major factor influencing interannual variations in Atlantic hurricane activity (Gray 1984). During 2002 El Niño was the primary contributor to the seasonal downturn in activity by causing a sharp reduction in the number of hurricanes forming within the MDR during August–October. El Niño was also thought to be responsible for the shortened period of tropical activity, with no named storms forming after 23 September and no tropical storm or hurricane activity evident after 12 October.

The El Niño contributed to suppressed hurricane activity in the MDR in three characteristic and interrelated ways. First, it contributed to an enhanced tropical upper-level trough (TUTT) across the North Atlantic and to an overall weaker than average subtropical ridge across the heart of the MDR (Fig. 36). Second, it was associated with enhanced westerly winds at 200 hPa in the Tropics extending from the Pacific Ocean eastward across the MDR (vectors in Fig. 37). Third, these winds resulted in anomalous westerly vertical wind shear across the eastern tropical North Pacific, northern South America, and most of the MDR (blue

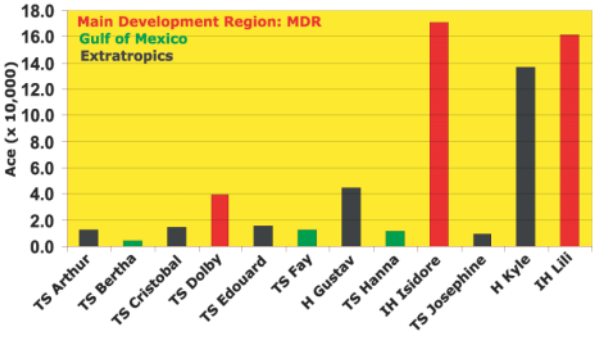

FIG. 31. The ACE index calculated for each of the twelve Atlantic tropical storms during 2002, determined by summing the squares of the estimated 6-hourly maximum sustained wind speed in knots (V_{max}^2) for all periods while the particular system is either a tropical storm or hurricane.

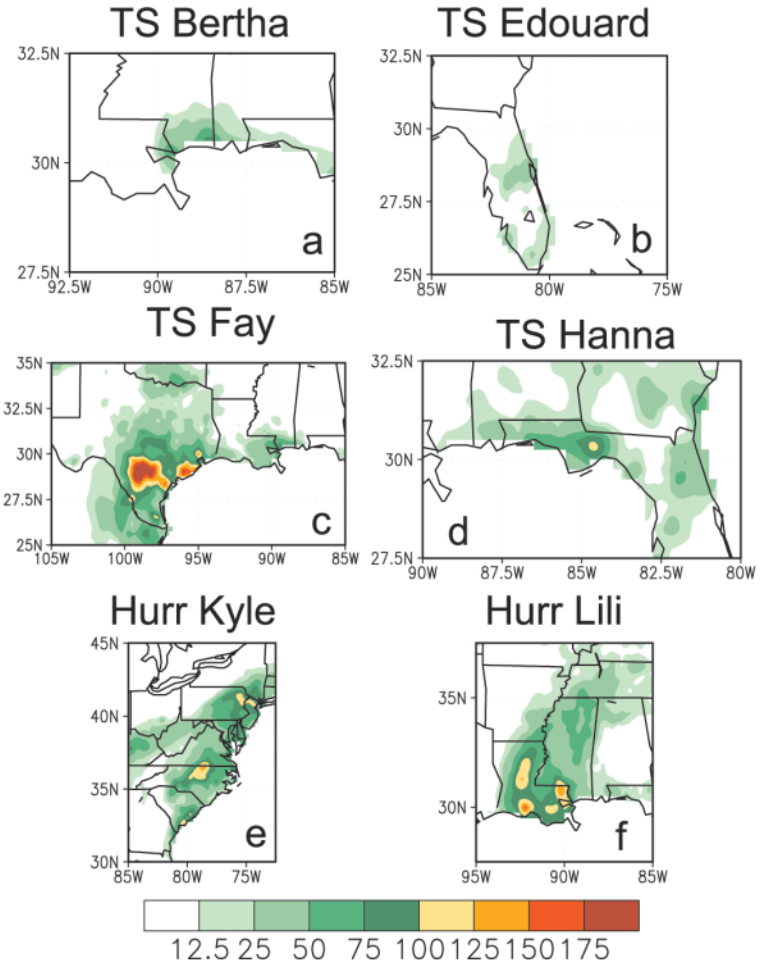

Fig. 32. Total rainfall (mm) associated with (a) TS Bertha during 4–5 Aug 2002, (b) TS Edouard during 4–5 Sep, (c) TS Fay during 6–10 Sep, (d) TS Hanna during 13–14 Sep, (e) Hurricane Kyle during 11–12 Oct, and (f) Hurricane Lili during 2–5 Oct 2002.

shading in Fig. 37). The resulting increase in the magnitude of the vertical wind shear within the MDR suppressed Atlantic hurricane formation similar to that discussed by Goldenberg and Shapiro (1986).

(b) The active multidecadal signal

Large multidecadal variations in seasonal Atlantic basin activity are evident in the ACE index time series (Fig. 30, also Landsea 1993; Landsea et al. 1999). Above-normal activity occurred during 1950–69 and 1995–2002, while below-average activity occurred during 1970–94. For the 1995–2002 period the average seasonal ACE index and the average seasonal number of hurricanes and major hurricanes (Goldenberg et al. 2001) were larger than any consecutive 8-yr period in the record.

These fluctuations in activity have been linked to multidecadal variations in several key atmospheric circulation features within the MDR, including the vertical wind shear (Fig. 38a; Goldenberg et al. 2001), the tropical easterly trade winds (Fig. 38b), and the structure of the African easterly jet (Fig. 38c). For the first half of the 1980s anomalous westerly (i.e., increased) vertical wind shear is evident over the central tropical North Atlantic (Figs. 38a,b), the tropical easterly trade winds are stronger than average between 5° and 10°N (Figs. 38c,d), and anomalous anticyclonic relative vorticity occupies the tropical eastern North Atlantic along the equatorward flank of the mean African easterly jet (Figs. 38e,f). This combination of conditions is known to be unfavorable for Atlantic hurricane formation.

Since the mid-1990s the circulation has featured more easterly (i.e., lower) vertical wind shear over the central tropical Atlantic, along with weaker tropical easterly trade winds and anomalous cyclonic relative vorticity along the equatorward flank of the African easterly jet. This combination of conditions is known to favor tropical cyclone formation from African easterly wave disturbances during the climatological peak in the season, and has prevailed during the past four above-normal hurricane seasons (Bell et al. 2000; Waple et al. 2002). The continuing presence of these active-decade circulation features during August–October 2002 (Figs. 37, 39) suggests a moderating influence of the El Niño signal by the multidecadal signal.

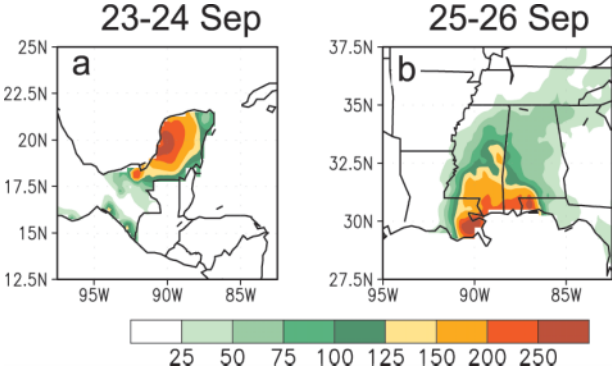

Fig. 33. Total rainfall (mm) associated with Hurricane Isidore during (a) 23–24 Sep and (b) 25–26 Sep 2002.

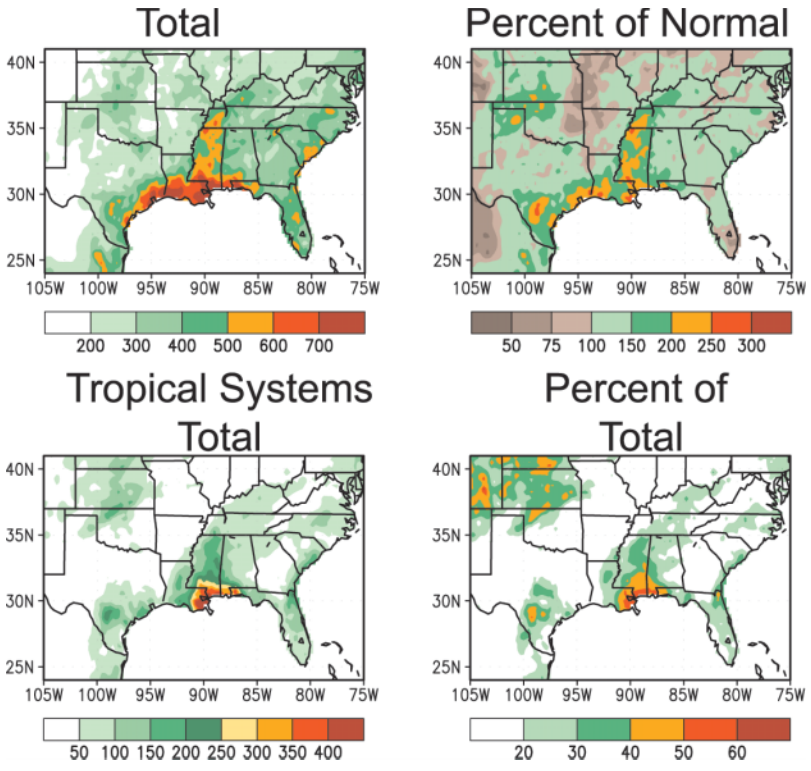

Fig. 34. August–October 2002 precipitation (a) total (mm) and (b) percent of normal. (c) Total rainfall (mm) and (d) percent of the total ASO rainfall associated with the seven landfalling tropical systems shown in Figs. 2 and 3. Normals in panel (b) are based on the 1971–2000 base period daily means.

This multidecadal variability has been related to three climate factors: 1) the Atlantic multidecadal mode (Mestas-Nuñez and Enfield 1999; Goldenberg et al. 2001), 2) the leading unrotated multidecadal EOF global SST anomalies (e.g., Mo et al. 2001), and 3) West African monsoon variability (Hastenrath 1990; Landsea and Gray 1992; Goldenberg and Shapiro 1996).

More recently Chelliah and Bell (2003, submitted to *J. Climate*) showed that the leading tropical multidecadal atmospheric mode in the NCEP–NCAR reanalysis system (Kalnay et al. 1996) not only accounts for the multidecadal variations seen in Fig. 38, but also captures low-frequency fluctuations in the above three climate factors themselves. This tropical multidecadal mode is related to coherent fluctuations in convective activity occurring throughout the global Tropics between the 1950s–60s and the 1980s–90s, including the West African monsoon region, the central equatorial Pacific, and tropical South America.

(v) Intraseasonal hurricane variability associated with the Madden–Julian oscillation

Anomalous intraseasonal variability in hurricane activity has been linked to the MJO, which influences both the rotational and divergent components of the wind in the MDR (Maloney and Hartmann 2000; Mo 2000). The easterly and westerly phases of the MJO derive their names from the sign of the low-level zonal wind anomalies over the eastern tropical Pacific. The easterly phase is associated with enhanced convection over the central tropical Pacific, and with negative (i.e., cyclonic) 200-hPa streamfunction anomalies, westerly 200-hPa zonal wind anomalies, and increased (i.e., anomalous westerly) vertical wind shear in the MDR. These conditions are "El Niño–like" and act to inhibit Atlantic hurricane formation in the MDR (Mo 2000). Opposite circulation anomalies during the westerly MJO phase are "La Niña–like," and are associated with increased hurricane activity in the MDR. Maloney and Hartmann (2000) suggest a nearly four-fold increase in hurricane

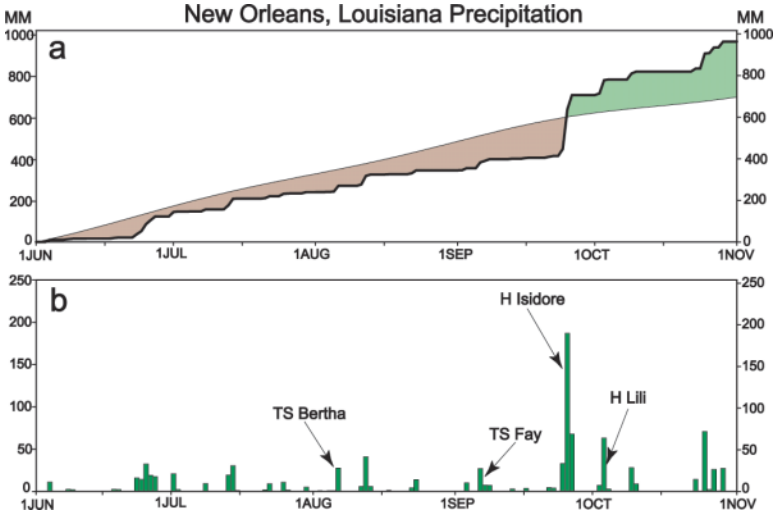

Fig. 35. (a) Accumulated precipitation (thick curve) and (b) daily rainfall totals (mm) at New Orleans, LA, during Jun–Oct 2002. Panel (a) also shows accumulation of climatological precipitation (thin line) and accumulated departures from normal (shading) beginning 1 Jun 2002. Green (brown) shading denoted an accumulated precipitation surplus (deficit).

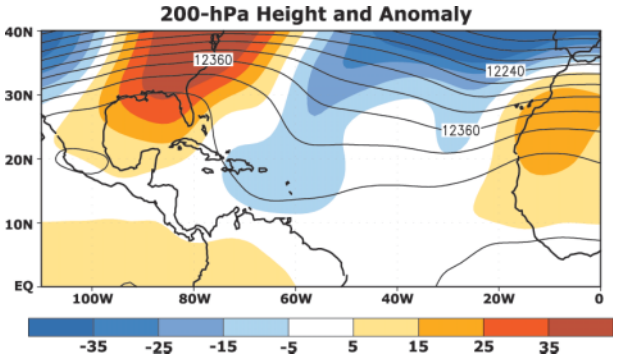

Fig. 36. Aug–Oct 2002 mean (contours) and anomalous (shaded) 200-hPa heights. Contour interval for heights is 30 m. Shading interval for anomalies is 10 m. Anomalies are departures from the 1971–2000 base daily means.

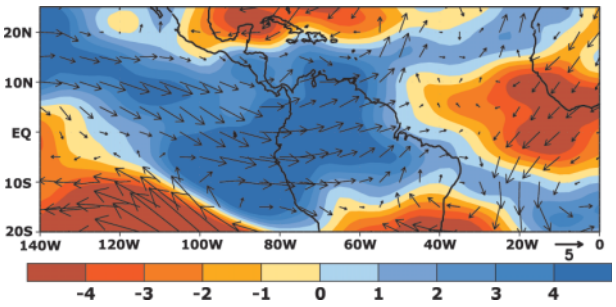

Fig. 37. Aug–Oct 2002 anomalous 200–850-hPa vertical shear of zonal wind (shaded) and 200-hPa vector wind. Shading interval for vertical shear is 1.0 m s^{-1}. Anomalies are departures from the 1971–2000 base daily means.

activity within the MDR during the westerly phase of the MJO compared to the easterly phase.

Time–longitude sections of 200-hPa velocity potential anomalies between 5°N–5°S (Fig. 29) and 10°–20°N (Fig. 40) are used to identify both the El Niño–related and MJO-related variability during the 2002 hurricane season. The El Niño–related anomalous upper-level divergence and enhanced convective activity over the central equatorial Pacific are associated with negative velocity potential anomalies beginning early July 2002. Over the western tropical North Atlantic Ocean and Caribbean Sea, positive velocity potential anomalies during much of the season are associated with anomalous upper-level convergence and descending motion/suppressed convective activity. These conditions were most pronounced during the first halves of August and September and most of October, in association with the combination of El Niño and the easterly MJO phase. Over the western MDR and the Gulf of Mexico the cyclonic streamfunction anomalies (Fig. 41), the upper-level trough (Fig. 42a), and the westerly (i.e., higher) vertical wind shear, are also stronger during these periods relative to the background El Niño signal.

In contrast, the westerly MJO phase during both late July and late September is associated with a temporary disappearance of the El Niño–related enhanced convection from the central equatorial Pacific, and with a shift of the negative velocity potential anomalies and associated anomalous ascending motion to the eastern tropical Pacific and MDR. Anticyclonic streamfunction anomalies (Fig. 41) and an amplified subtropical ridge are also evident during both periods over the Caribbean Sea and Gulf of Mexico. Importantly, the stronger MJO in late Sep-

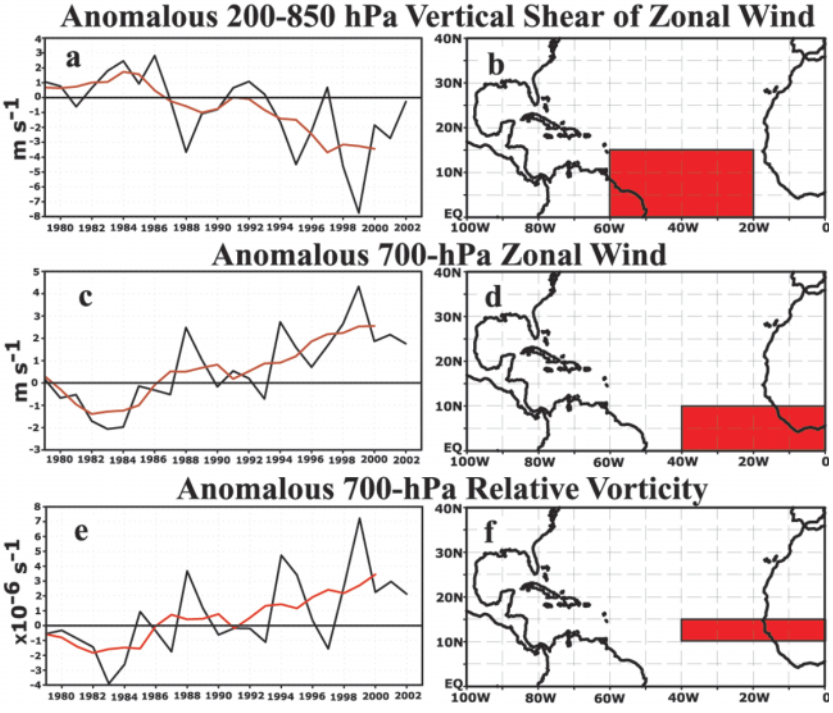

Fig. 38. Area-averaged anomaly time series for each Aug–Sep period between 1979 and 2002: (a) 200–850-hPa vertical shear of zonal wind (m s^{-1}), (c) 700-hPa zonal wind (m s^{-1}), and (e) 700-hPa relative vorticity (x 10^{-6} s^{-1}). In each panel the black curve shows the unsmoothed 2-month anomalies and the red curve shows a 5-point running mean smoother applied to the Aug–Sep 2-month anomalies. Averaging regions are highlighted in red in panels (b, d, f), respectively. Anomalies are departures from the 1979–95 base period monthly means.

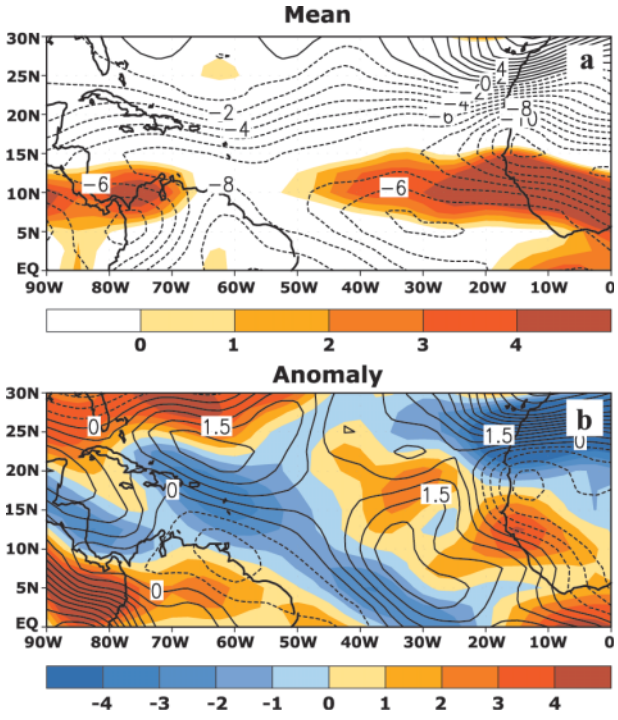

Fig. 39. Aug–Sep 2002 (a) mean and (b) anomalous 700-hPa zonal wind (contours) and relative vorticity (shading). Contour interval for zonal wind is 2 m s^{-1} and for anomalies is 0.5 m s^{-1}. Shading interval for relative vorticity and anomalies is 1 x 10^{-6} s^{-1}, with cyclonic relative vorticity shaded red in both panels. In (a) anticyclonic relative vorticity is unshaded.

tember contributed to larger anomalies at a time when conditions are normally most conducive to hurricane development (Fig. 42b).

Consistent with these conditions a broad area of anomalous easterly (i.e., lower) vertical shear is evident over most of the MDR and across the western extratropical North Atlantic during late September. Two major hurricanes, including long-lived Hurricane Kyle, and almost 75% of the total seasonal activity, occurred in this period. Waple et al. (2002) also note several periods of substantially increased activity during the 2001 Atlantic hurricane season in association with the westerly phase of the MJO.

ii) Pacific tropical storms—B. Lyon[14] and A. M. Waple,[24]

(i) Western North Pacific typhoon season

Typhoons can develop throughout the year in the western North Pacific with climatological peak activity between July and November. In 2002 there were 33 tropical cyclones in the region, counting typhoons, tropical storms, and tropical depressions, close to the 1982–2001 average of 31.6 (data from Joint Typhoon Warning Center best-track data). Two of these (Ele and Huko) developed in the central Pacific region (140°W to 180°), while the others had genesis west of the date line. The number of tropical cyclones reaching typhoon intensity, 17, was close to the 1982–2001 average of 17.6. However, eight typhoons reached supertyphoon intensity (tropical cyclones with a maximum sustained 1 min wind exceeding 130 kt), twice the 1982–2001 average. The only years on record with more supertyphoons were 1997 and 1965, both El Niño years (defined by the July–October Nino-3.4 index), with 11 supertyphoons, and 1958, a neutral ENSO year, with nine supertyphoons. In addition to 2002 (an El Niño year), eight supertyphoons also occurred in 1957, 1963 (both El Niño years) and 1961 (a neutral ENSO year), as seen in Fig. 43.

The peak of the 2002 tropical Pacific cyclone season occurred in the months of June–August. There were three typhoons in June surpassing the 1982–2001 average of 0.9 and matching the maximum in the histori-

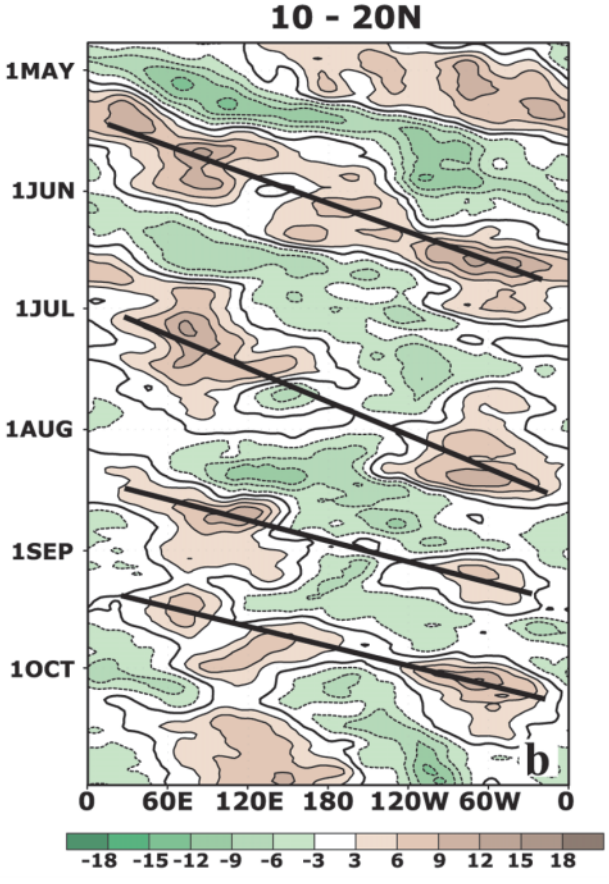

Fig. 40. Time–longitude sections of 5-day running mean 200-hPa velocity potential anomalies averaged over the latitude band 10°–20°N. Contour interval is 3 x 10^6 m^2 s^{-1}. Anomalies are departures from the 1979–95 base period daily means

cal record for that month. The month with the most typhoons was August, with four typhoons (1982–2001 average is 3.7). The only two typhoons in September–October were Higos in September and Bavi in October, while the 1982–2001 means for these months are 3.6 and 3.1, respectively. Therefore the 2002 tropical cyclone season started earlier and diminished earlier than usual, as shown in Fig. 44. This early peak is also seen in the number of tropical cyclones (tropical depressions, tropical storms, and typhoons) and in the number of named tropical storms (no tropical depressions included). The early seasonal peak of tropical cyclone frequency in El Niño years has been noted in the literature (see, e.g., Lander 1994).

For the first time since records began in 1950, a supertyphoon (Mitag) occurred in February, historically the month with the lowest minimum typhoon activity in the western North Pacific. For the second consecutive year, a typhoon (Pongsona) reached supertyphoon intensity in the month of December. Prior to the occurrence of supertyphoon Faxai in December 2001, the last December supertyphoons were Susan and Opal in 1963 and 1964, respectively.

The monthly and seasonal values of the ACE for the western North Pacific during the June–November 2002 season were near normal (see Fig. 45a), while the ACE index for the whole year was slightly above normal (not shown). There was unusually high cyclone activity in the month of March 2002, and the ACE index was the highest on record for March (see Fig. 45b), due to Supertyphoon Mitag, which lasted from 26 February to 8 March. The ACE index in the month of July was the second highest on record. Only 1972, also an El Niño year, was higher. In contrast, the ACE index in the month of October, was the second smallest on record, indicating again a season with both an early peak and an early fall in activity. Only the El Niño year of 1976 had a smaller ACE index in the month of October.

In El Niño years, there is usually a southeastward displacement of the tropical storm and typhoon genesis region (Chan 1985; Chia and Ropelewski 2002; Wang and Chang 2002). Tropical storms and typhoons in 2002 had an average genesis position of (15°N, 149°E), slightly east of the historical average near (15°N, 143°E; Chia and Ropelewski 2002). Another characteristic of El Niño years is the enhanced tendency of tropical cyclones that form in the southeastern quadrant of the western North Pacific (0°–17°N, 140°E–180°) to recurve northeastward to around 28°N and reach north of 35°N, compared to strong La Niña years, when fewer tropical cyclones reach such northern latitudes (Wang and Chang 2002). These characteristic El Niño tracks were observed in 2002, with a large number of typhoon and

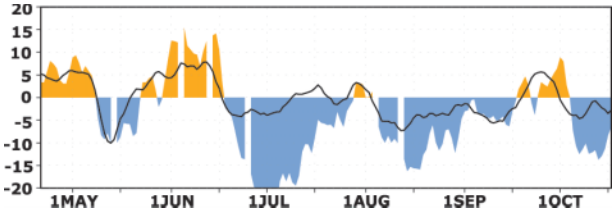

Fig. 41. Daily time series during 22 Apr–16 Oct 2002 of area-averaged anomalous 200-hPa velocity potential (solid curve) and streamfunction (shading). Velocity potential anomalies are calculated for the central tropical Pacific region bounded by (160°E–170°W) (10°–20°N). Streamfunction anomalies are calculated for the Gulf of Mexico and Caribbean Sea bounded by (100°–60°W) (10°–30°N). Anomalies are departures from the 1979–95 base period daily means.

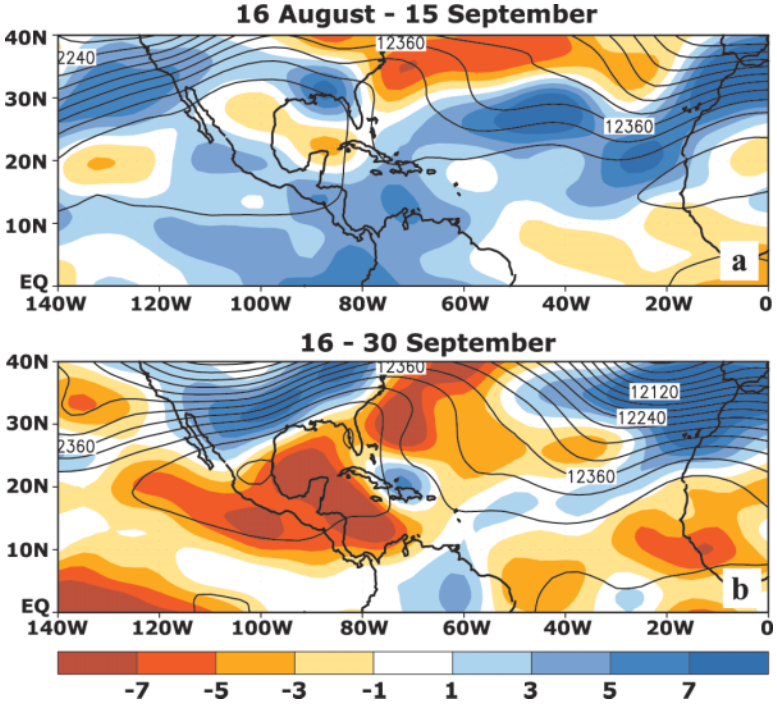

Fig. 42. Mean 200-hPa heights (contours) overlaid with anomalous 200–850-hPa vertical shear of zonal wind (shading) during (a) 16 Aug–15 Sep 2002 and (b) 16–30 Sep 2002. Contour interval for heights is 30 m. Shading interval for anomalous vertical shear is 2.0 m s^{-1}, with easterly shear anomalies shaded red and westerly shear anomalies shaded blue. Anomalies are departures from the 1979–95 base period daily means.

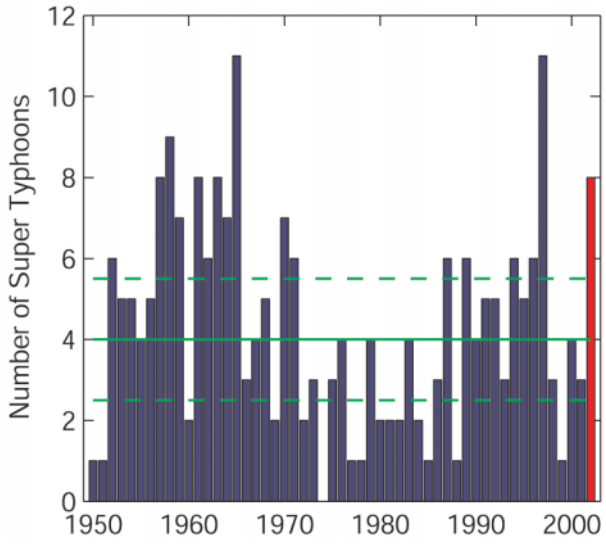

FIG. 43. Number of supertyphoons per year in the western North Pacific for the years 1950–2002. The solid green line indicates the median for 1982–2001 and the dashed green lines show the 25 and 75 percentiles. Data obtained from the Joint Typhoon Warning Center (JTWC).

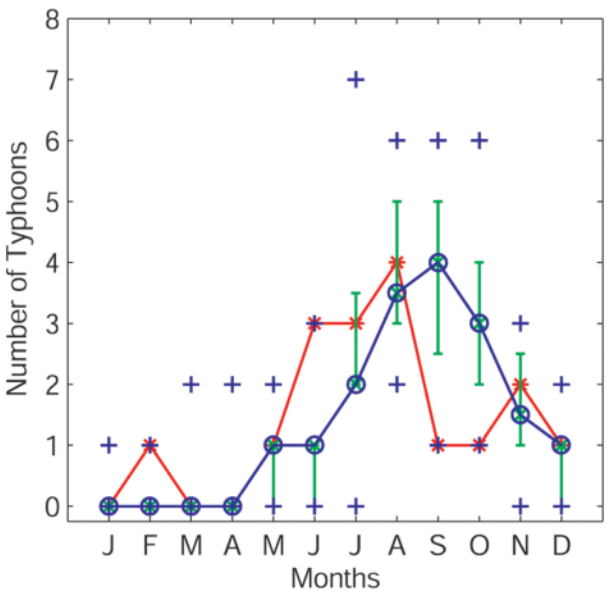

FIG. 44. Number of typhoons per month in the western North Pacific in 2002 (red line) and median in the years 1982–2001 (blue line). The error bars indicate the 75 percentile (upper) and 25 percentile (lower) for that month in the years 1982–2001. In the cases with no error bars, the upper and/or lower percentiles coincide with the median. The blue cross marks show the maximum and minimum values in each month during the period 1982–2001. Data obtained from the Joint Typhoon Warning Center (JTWC).

tropical storms beginning in the southeast part of the basin with a recurvature from northwest to northeast and reaching beyond 35°N. Another characteristic of El Niño years is a greater number of tropical cyclones forming in the central Pacific region (Chu and Wang 1997; Clark and Chu 2002). Some of these cyclones then propagate into the western North Pacific, as was the case of Ele and Huko in the 2002 season.

The 2002 typhoon season had a significant impact in many countries of the region. In a very active period of three weeks at the end of June and beginning of July, four tropical cyclones affected the region: Supertyphoons Chataan and Halong, Typhoon Rammasun, and Tropical Storms Nakri. Chataan and Rammasun triggered flash floods and landslides which affected the Phillipines causing at least 22 deaths. Chataan also flooded hundreds of homes in Japan killing at least 5 people. Hardest hit by Chataan was Micronesia, where dozens of people were buried in mudslides triggered by the torrential rain. Effects of Typhoon Rammasun were also felt in China and South Korea.

Typhoon Rusa hit South Korea at the end of August, causing considerable damage [estimates $4,500 million (U.S.)]. Rusa was the most powerful typhoon to hit South Korea sinceTyphoon Sarah in 1959 and Supertyphoon Thelma in 1987, with official reports of at least 124 people dead and 70 missing due to flash floods and landslides. Rusa dumped up to 890 mm of rain within 30 h in eastern and southern South Korea. Strong winds knocked down trees and electricity poles, causing a blackout for more than 1 million households. More than 36,000 houses and buildings in low-lying areas were submerged and the floods also inundated tens of thousands of acres of farmland, while high waves swept away more than 200 ships.

Typhoon Sinlaku battered Japan's Okinawa Island in September causing widespread damage, while also affecting Taiwan. Typhoon Sinlaku made landfall in eastern China near the industrial city of Zhejiang, leaving 28 people dead or missing, after about 300,000 residents were evacuated. Typhoon Higos was the third strongest typhoon to hit Tokyo since World War II and the heavy rains and high winds caused at least 4 deaths, but the destructive power of the typhoon was diminished because it moved quickly through the region (around 80 km h^{-1}).

In December, Supertyphoon Pongsona caused severe damage on the U.S. territory of Guam. Although no deaths were reported, the impact of the supertyphoon on the island infrastructure was tremendous. This was the second typhoon that affected Guam during the season following Typhoon Chataan, which also caused some material damage on the island in July.

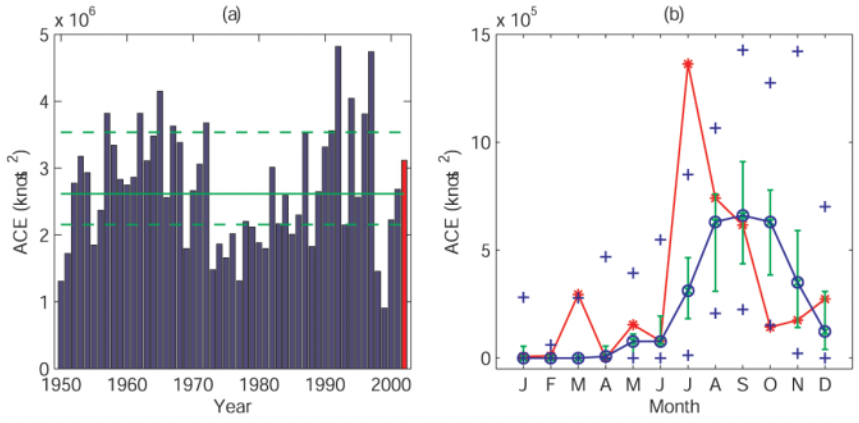

FIG. 45. (a) Jun–Nov ACE index for the western North Pacific for the years 1950–2002. The solid green line indicates the median for the years 1982–2001 and the dashed green lines show the 25 and 75 percentiles. (b) ACE index per month in the western North Pacific in 2002 (red line) and median in the years 1982–2001 (blue line). The green error bars indicate the 25 and 75 percentiles for that month in the years 1982–2001. In the cases with no error bars, the upper and/or lower percentiles coincide with the median. The blue cross marks show the maximum and minimum values in each month during the period 1982–2001. Data obtained from the Joint Typhoon Warning Center (JTWC).

(ii) Eastern North Pacific hurricane season

The hurricane season in the eastern tropical Pacific runs from 15 May to 30 November and on average there are 16 named storms, including 9 hurricanes, 4 of which are major (category 3 or higher on the Saffir–Simpson scale). Five of the 12 named storms that formed in 2002 reached category-3 strength on the Saffir–Simpson scale. The east Pacific season was less active than average, though there were several notable storms.

For the second consecutive year, the season got underway very early. Hurricane Alma reached hurricane status on 28 May, and eventually reached category 3 (100 kt) two days later on the 30 May but never threatened land.

The three storms that reached category-5 strength in the eastern Pacific in 2002 were Elida, which developed rapidly in late July, Hernan in early September ,and Kenna from 22–26 October.

As a category four storm, Kenna was the third strongest hurricane on record to landfall in Mexico. Kenna reached hurricane status about 740 km south of Cabo Corrientes, Mexico on 23 October and strengthened to wind speeds of approximately 140 kt and a central pressure 917 hPa on 24 October. After strengthening to a peak wind speed of 145 kt, Kenna slowly weakened under conditions of increased shear and by landfall, near San Blas, Mexico, on 25 October, peak wind speed was around 120 kt. Kenna weakened extremely rapidly as it moved inland over the mountains of Mexico and only four deaths were attributed to the storm. However the storm surge associated with the storm caused around $5 million (U.S.) of damage in Puerto Vallarta, Mexico.

The only other tropical storm to make landfall during the 2002 eastern tropical Pacific hurricane season was Tropical Storm Julio, which made landfall with a maximum intensity of 40 kt on the coast of Mexico just west-northwest of Lazaro Cardenas around 0000 UTC 26 September. The storm then moved over the mountains of southwestern Mexico, where it dissipated north of Manzanillo later that day.

5. THE POLES—A. M. Waple[8] and R. C. Schnell[15]

a. The Antarctic

1) South Pole ozonesondes and the 2002 ozone hole

The NOAA/Climate Monitoring and Diagnostics Laboratory (CMDL) summary for 2002 ozonesonde measurements at the South Pole station is shown in Fig. 46. The total column ozone in Dobson Units (DU) (blue line) and temperature in the 20–24-km layer of the stratosphaere (red line) indicate a highly perturbed stratosphere beginning near the middle of September.

Three selected ozonesonde profiles illustrate the rapid change in ozone above 15-km altitude. From 1 September to 19 September, total column ozone dropped from 263 to 166 DU, which represents a typical chemical destruction process during the development of the Antarctic ozone hole. The minimum usually occurs at the end of September and by simple extrapolation would have reached approximately 110 DU, slightly above the 100 DU minimum observed in 2001 (dashed blue line).

However, by 25 September 2002 total ozone was up to 378 DU, far above the 1986–2002 average for that date. The increase also coincides with a stratospheric temperature increase in the 20–24-km layer of over 50°C, rising from –80° to over –30°C.

NOAA and National Aeronautics and Space Administration (NASA) satellite observations showed that the Antarctic polar vortex split in two at the time large in-

creases in stratospheric ozone and temperature were occurring and both vortices were displaced away from the South Pole station. One of the vortices appeared to regain its position over the South Pole in early October and a minimum total ozone of 152 DU was observed on 21 October before increasing rapidly again to more than 300 DU on 27 October. Since ozonesonde observations began at the South Pole in 1986, only 1988 is comparable to 2002 when an early breakup of the polar vortex resulted in a minimum total ozone of 190 DU on 10 October 1988.

ii) Temperature and sea ice

Antarctic climate is crucial to the global climate system in several respects. Most of the continent remains snow covered throughout the year. This is extremely reflective to incoming solar energy and is an important component in the global radiation budget. In particular, if snow and ice began to melt on the continent, the darker, ice-free areas would absorb more incoming solar energy and warm more easily, leading to further icemelt and additional warming.

If substantial amounts of the Antarctic ice and snow were to melt, the world's sea level would rise, leading to the inundation of many coastal regions. In addition, ocean water is cold and dense in the area surrounding the Antarctic continent. It is in these regions that water sinks and moves equatorward helping to drive ocean currents around the world.

Sea ice extent (Fig. 47) was lower than average for almost the entire year in 2002, reaching a minimum negative anomaly of approximately 1 million km^2 in June 2002, and then increasing to near average at the end of the year. The sea ice extent was below average by mid-2001 (July) and did not rise above average again until December 2002.

The temperature trends over the last 30 years (1973–2002) over the continent of Antarctica are shown in Fig. 48. While the annual trend is mostly negative, marked seasonal and spatial differences in trends are evident. The reasons for the variability are a complex mix of atmospheric dynamics and sea ice conditions, but reliable surface observations are difficult to obtain because of harsh climatic extremes and the transitive nature of Antarctic scientists, among others. However, from the limited data available, the last decade has been predominantly colder than average, in contrast to the general increasing temperature trend from 1959 to the early 1990s. In 1991, the Mount Pinatubo (Philippines) and Mount Hudson (Chile) volcanoes erupted, and it is possible that these eruptions had a significant influence on the general lowering of temperatures after that year (Jacka and Budd 1998).

b. The Arctic

Snow cover in the Northern Hemisphere, including land regions extending into the Arctic is described in section 2d.

Annual sea ice extent was less than average in 2002 for all 12 months over the Northern Hemisphere (Fig. 50). Negative departures from the 1973–2000 mean have occurred in all months since September 2001, and a maximum negative anomaly of approximately –0.78 million km^2 was reached in September 2002. This continues a general trend toward reduced sea ice since the early 1980s. When broken down by season, the Northern Hemisphere sea ice extent reached record minima for both spring and summer as well as the annual extent (Fig. 51). It is likely that a combination of unusual warmth and storminess in the Arctic summer contributed to the extensive melt and breakup of the icepack in 2002. NOAA's Snow and Ice Data Center reported that it is also likely that the 2002 minimum sea ice record in the Arctic is the lowest since the early 1950s and possibly the lowest in several centuries.

The reduced Arctic sea ice extent is combined with extensive melt on the Greenland Ice Sheet in 2002. Preliminary measurements from the Greenland Ice Sheet

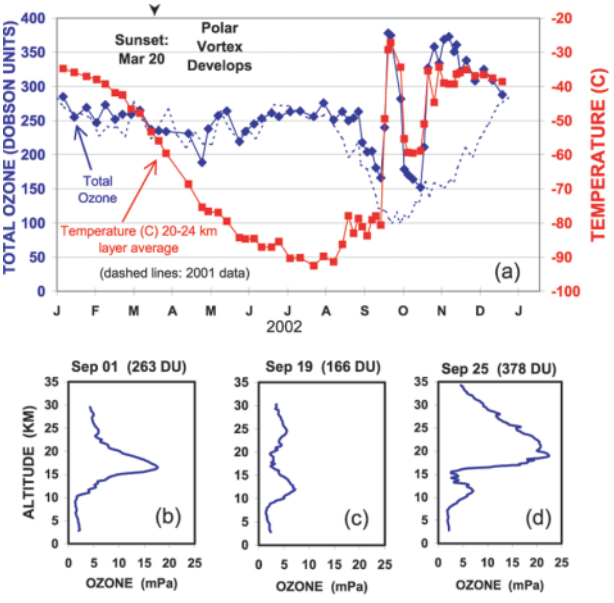

Fig. 46. (a) Summary of South Pole total ozone in Dobson Units (DU) and stratospheric temperatures measured by ozonesondes during 2002. Three selected profiles of altitude vs ozone partial pressure (millipascals) are shown in the lower panels. (b) Prior to the 2002 ozone hole, (c) mid September (about 10 days before the expected minimum would occur) and (d) during the split of the polar vortex. (Courtesy B. Johnson and S. Oltmans, NOAA/CMDL.)

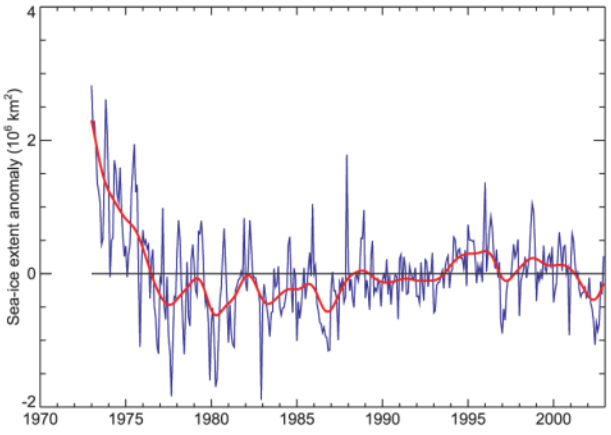

FIG. 47. Monthly sea ice extent anomalies for the Southern Hemisphere (source: Hadley Centre, Met Office; updated with help from NOAA/NCEP).

by K. Steffen and colleagues at the University of Colorado (http://cires.colorado.edu/steffen/melt/index.html) show a melt extent of 265,000 mi^2, a new record, underscoring the unusual warming there and surpassing the maximum melt extent from the past 24 years by more than 9%. Steffen and colleagues also describe a dramatically higher melting trend since 1979 that appears only to have been interrupted once, when the Philippines' Mt. Pinatubo erupted in 1991. The trend of melt-area increase over the 1979–2002 period is approximately 16% (http://cires.colorado.edu/steffen/melt/index.html). Both sea ice and glacier ice help regulate atmospheric temperature by reflecting about 80% of springtime solar radiation and 40%–50% during summer snowmelt. In winter, ice cover slows heat loss from relatively warm ocean water to the cold atmosphere.

ADVANCING BARROW, ALASKA, SNOW-MELT DATE

A record early date of spring snowmelt (25 May 2002) occurred at Barrow, Alaska, both over the tundra at the remote Barrow CMDL Atmospheric Baseline Station and within the urban confines of Barrow town at the National Weather Service (NWS) station as shown in Fig. 52. The 25 May 2002 tundra melt date was four days earlier than the previous record of 21 May 1989. Quantitative snowmelt data have been recorded in the Barrow area since 1942.

The 2002 melt date for the tundra area adjacent to the Barrow Baseline Station had been predicted to within two days of actual occurrence two months in advance by CMDL scientists using an empirical methodology developed by Stone et al. (2002). Their model primarily accounts for seasonal variations in synoptic meteorological conditions over the immediate preceding winter, which dominated the prediction for 2002, and to a lesser degree, the indicated downward (advancing) linear trend in the snowmelt date.

Before the regional snowmelt predictive model could be established, two different and partially contradictory data series had to be examined with respect to the effects of the development and growth of the town of Barrow on urban snowmelt. In Fig. 52 the data series identified as "NWS" is acquired within the town

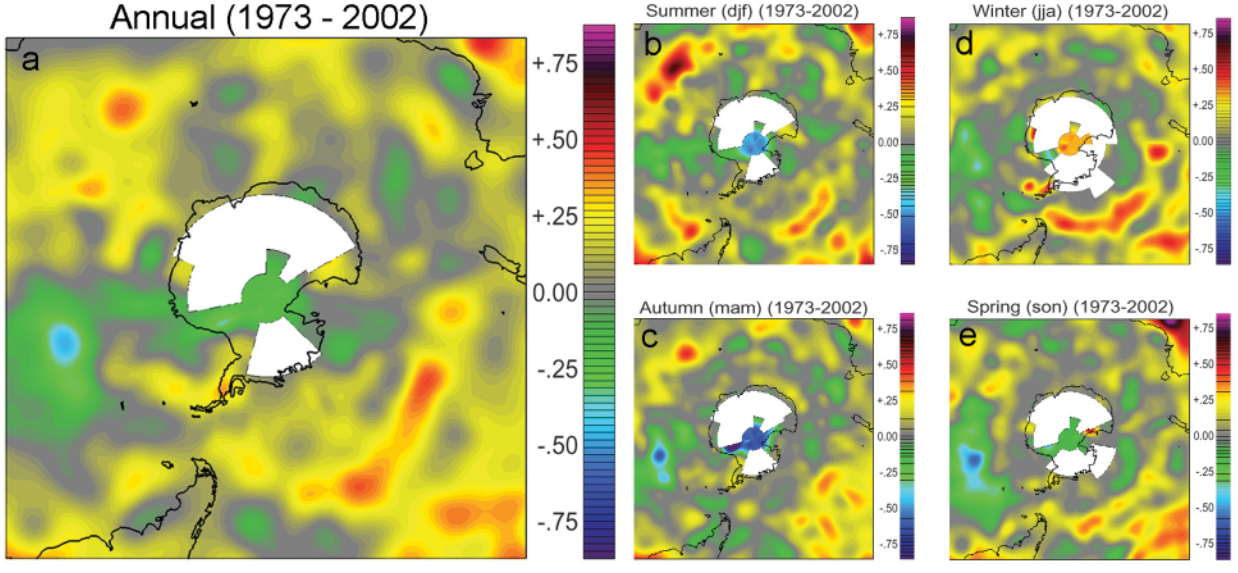

FIG. 48. Surface air temperature trends from 1973 through 2002 for Antarctica. White areas are missing data. (a) Annual, (b) summer (DJF), (c) autumn (MAM), (d) winter (JJA), and (e) spring (SON).

PALEOCLIMATE INDICATORS IN ANTARCTICA

The annual accumulation of ice layers through compaction of snow on the Antarctic continent also contains climatic information that is retrievable through the drilling of ice cores. Through various physical and chemical analyses of this ice, information about not only precipitation, but also temperature, atmospheric trace gas concentrations (e.g., carbon dioxide, methane, nitrous oxide from minute air bubbles trapped in the core), dustiness of the atmosphere, and ash layers from volcanic eruption as well as much more can be derived. Since much of the continent of Antarctica is ice covered year-round, there are numerous ice core records available; however, by far the longest and least disturbed of these is Vostok, located on the East Antarctic Ice Plateau (78° 28′S, 106° 48′E, at 3488 m above sea level). Vostok also has the advantage of being located in an area where the ice is more than 3.5 km thick and the relationship between the chemical properties of the ice and temperature at the site is relatively uncomplicated. Temperature anomalies (relative to the recent period) over all 420,000 years of ice accumulation are shown in Fig. 49 and the inset graph zooms in on the last 12,000 years. As is evident from the graph, temperature variability has been far greater over the last several hundred thousand years than during the last 10,000 (a time period known as the Holocene). The large dips in the graph illustrate the "ice ages" while the peaks are climates similar to our current interglacial. Temperatures have actually declined throughout the Holocene by approximately 1°C (Ciais et al. 1992) and as was illustrated in Fig. 48a, this decline in temperature is continuing up to 2002. This Holocene temperature trend has also been seen in ice cores from the Arctic (e.g., Bradley 1990), though in sharp contrast, the last century has shown increasing temperatures for the Arctic.

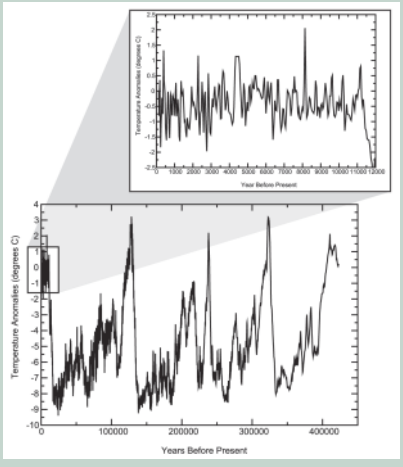

FIG. 49. Record of Antarctic temperature for the last 420,000 years reconstructed from elements of the Vostok ice core (Petit et al. 1999). Inset: last 12,000 years. See text for more details.

of Barrow, while data labeled "Tundra" is a composite of snowmelt dates determined over the open tundra, and for the past 17 years at the CMDL Barrow Observatory. It is seen that the moving mean average values in the two datasets, indicated by the fit lines, were nearly equal in the late 1950s but started to depart after that time. The cause of this departure was identified as the "urbanization" of Barrow in the immediate vicinity of the NWS station (Dutton and Endres 1991). The advancing date of snowmelt in the tundra record was not statistically significant (at 95%) until 1993.

The date of snowmelt in the vicinity of Barrow was carefully followed and analyzed in papers by Stone (1997), Foster et al. (1992), Dutton and Endres (1991), and Foster (1989). These analyses, and others over the northern Alaska region, have led to the conclusion that there is a trend toward an earlier snowmelt in large portions of the Alaskan Arctic. However, the extremely early melt date in 2002 can only partially be attributed to the observed trend. The 2002 melt date on the tundra is more than two weeks earlier than what would have been projected based on the trend analysis alone.

6. REGIONAL CLIMATE

a. North America—A. Douglas,[7] K. Gleason,[8] D. Phillips,[11] and A. M. Waple[8]

i) CANADA

Nationally, Canada had its 10th consecutive warmer than average year in 2002. Ranking 13th warmest since national records began in 1948, the year began with the

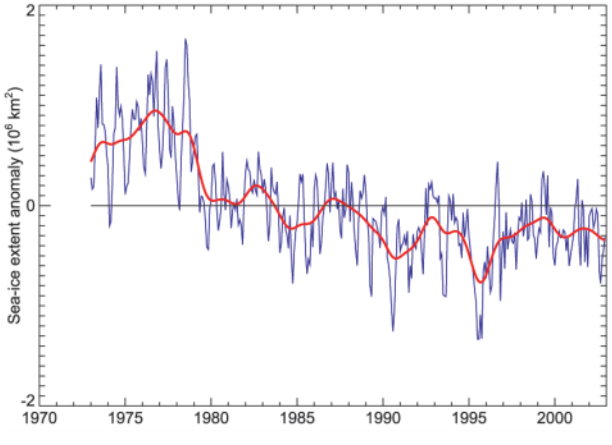

FIG. 50. Monthly sea ice extent anomalies for the Northern Hemisphere (source: Hadley Centre, Met Office; updated with help from NOAA/NCEP).

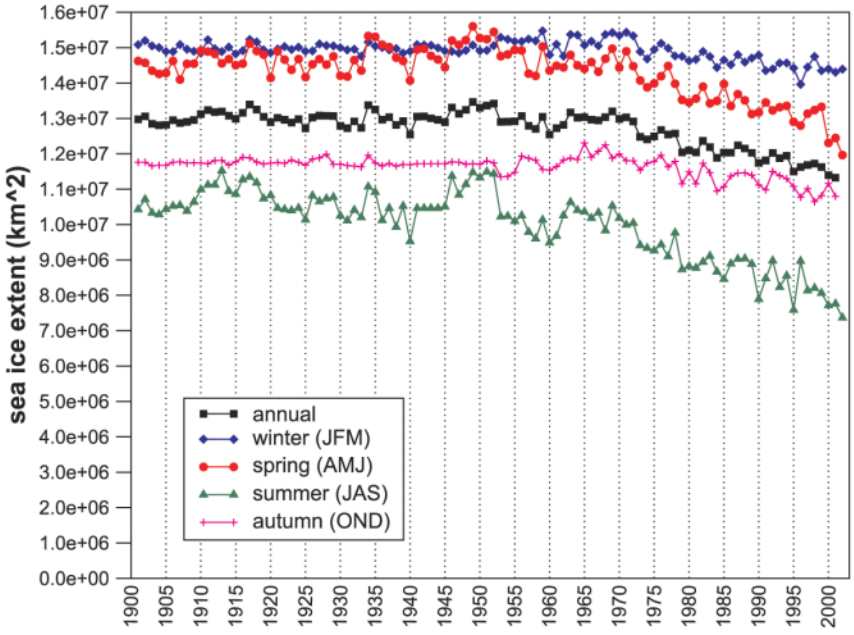

FIG. 51. Seasonal sea ice extent in millions of square kilometers for the Northern Hemisphere 1900–2002.

19th consecutive warmer than average season for Canada. Spring was the only colder than normal season in 2002 and the last 21 of 22 seasons have been warmer than average. Annual precipitation was slightly above normal though large regional and seasonal variations were observed throughout the nation. Drought affected a large portion of the prairies in 2002.

(i) Winter and spring

While winter (December 2001–February 2002) was warmer and drier than average across large parts of Canada, spring (March–May 2002) was the first colder than average season since spring 1997. The winter warmth continued a trend in recent years of warmer than average winter seasons. The last significantly colder than normal winter in Canada was in 1994. The Great Lakes/St. Lawrence regions of eastern Canada had their warmest winter ever with less than 10% of the Great Lakes achieving ice cover. The daily highs failed to rise above freezing on only 25 days in Toronto compared to an average of 55, and the average winter temperature in downtown Toronto was the warmest since record keeping began in 1840. In Montreal, for the first time since modern record-keeping began in 1941, overnight lows never dipped below –19°C; the mark of a cold day.

However, spring more than made up for the mild winter. Nationwide, Canada had its fifth coldest spring on record. In western Canada, it was the coldest spring in 120 yr of record keeping and the first day of spring was the coldest day of the year. For many cities, March was colder than January and February for the first time in recorded history. Hundreds of new minimum temperature records were set, some of which broke 100-yr-old records.

A dry spring also followed an extended period of dryness across much of the nation. At the end of 2001, many farmers needed 60% more precipitation prior to the start of the growing season just to replenish water supplies for 2002—an unprecedented amount. Instead, precipitation was 60% below average, which, in addition to unseasonably cool temperatures, prevented many farmers from planting their crops. Corn crops were planted

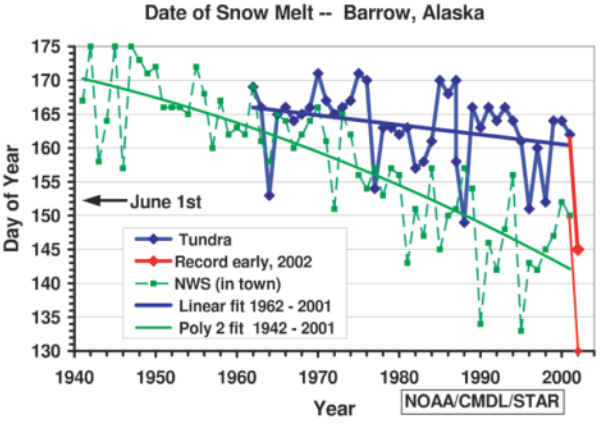

FIG. 52. Date of annual snowmelt in the urban area (green lines) of Barrow, AK, and at the remote CMDL Barrow Atmospheric Baseline Observatory (blue lines). The green dashed curve identified as "NWS" is based on the manually measured snow depth at the NWS station in Barrow. The "tundra" curve is based on several different open tundra solar albedo measurement instruments that for the past 17 yr have operated at the CMDL Barrow Observatory. The latest snowmelt-date data for 2002 is indicated in red on both curves and is the earliest melt date within each dataset. The solid "fit" curves are least squares fits to the data. The tundra data through 2001 are fit with a straight line that has a significant negative slope. The Barrow urban NWS data are best fit with a second degree polynomial and indicate an accelerated advance in the snowmelt date since the 1950s (courtesy E. Dutton and R. Stone, NOAA/CMDL).

as much as three weeks later than normal, which created further problems when midseason rains failed to arrive.

(ii) Summer

(a) Eastern Canada

Summer 2002 was notable for its lack of severe weather. There were fewer tornadoes, fewer lightning strikes and fewer cases of reported property damage due to severe weather across Canada. In Ontario, 55 severe weather events, a third of what normally occurs led to only two confirmed tornadoes and eight unconfirmed reported tornadoes.

However, the lack of severe weather also coincided with abnormally dry conditions in central Canada for the second consecutive summer. For several cities August was not only the driest August on record, but the driest of any month. August was the driest since 1937 for the Toronto Pearson station. For the Great Lakes region, five of the last six summers have been drier than normal.

As notable as the lack of rain in the east, were the record-warm temperatures. The warm season concluded in eastern Canada with the warmest September since records began, as September averaged warmer than June. It was a record-warm summer in many locations. At Toronto Pearson, the average 1 June to 30 September temperature was 21.5°C, 3.2°C degrees warmer than normal and the warmest in 63 years. The number of "hot days" (days with a temperature maximum above 32°C) and "hot nights" (nights which do not dip below 20°C) was also excessive for Toronto. The number of hot days was 23 in 2002 compared to a normal of 5. The number of hot nights was a record 19 also compared to a normal of 5. The number of cooling degree days from April to September in 2002 was 511 or 222% of normal for the city of Toronto.

Montreal also had its hottest and driest summer period (21 June–22 September) on record. The previous driest was in 2001, yet the 2002 summer had about 25% less precipitation than the previous summer. In the Maritimes, summer was slow to start but overall temperatures were close to normal, but for the fifth summer in the past six, precipitation totals were lower than normal.

(b) Western Canada

July and August were dry on the west coast as well as across the prairies. Vancouver, British Columbia, had its driest July and August in 2002, tied only with 1984; the precipitation total for the two months was 19.6 mm. Victoria had its second driest with 10 mm. However, conditions in the Prairie Provinces were far worse with one of the worst growing seasons in Canada's history. Prolonged drought, as well as deluges of rain, devastating plagues of grasshoppers and mites, and record early season freezes and snows contributed to a season of misery for prairie farmers. In 2001, the drought affected the southern areas of Alberta and Saskatchewan. In 2002, the drought moved northward affecting the larger central and northern areas of the provinces. The pasture was poor over three-quarters of Alberta and only good in 20% of Saskatchewan. Edmonton had its second warmest and record driest June and July. Maximum temperatures on seven days exceeded 30°C in the city.

In contrast to the hot dry conditions of most of June and July, western farmers encountered heavy rains and freezing temperatures in late JAS. From January 2001 to June 2002, Saskatoon received only 44% of normal precipitation, a deficit of 263 mm. The drought persisted despite a cool and wet August over much of Alberta and Saskatchewan. Soil moisture levels were still far below average at the end of the season and the drought was compounded by an early freeze. Century-old August records were shattered in many parts of Saskatchewan when the temperature dipped below freezing in early August. Snow (22 cm) fell in Edmonton and northern Alberta in late July. It was the first time since record keeping began that Edmonton has ever had snow in July.

Total wheat production was less than half of the record crop of 1990 and more than 25% below the already low yields of 2001. The 2002 crop will not only be remembered for yielding so little, with a record number of acres remaining unharvested, but also for the poor quality of the crop that was harvested.

(iii) Autumn

The national average temperature for SON, was 0.8°C, the 12th warmest fall in 55 yr, thanks to extremely mild weather in the north and warm sunny conditions in British Columbia. On the prairies however, it was a much different story. Winnipeg had its coldest October on record and the only October when the average temperature stayed below freezing. In many cities on the prairies, October was one of the three coldest ever.

Several hurricanes that developed in the Atlantic in early fall (September) also affected Canada. On 12 September, Gustav made landfall near Sydney, Nova Scotia, a day after regaining hurricane strength, after brushing the coast of North Carolina. Gustav was the first hurricane to make landfall in Nova Scotia in six years and the storm led to power outages, downed trees, and minor flooding. The greatest rainfall

(100 mm) occurred near Antigonish, Nova Scotia and the highest wind speed (122 km h^{-1}) occurred on Sable Island. Wind gusts over 100 km h^{-1} from the remains of Gustav were still being reported in Newfoundland days afterward. Fortunately, disaster was narrowly averted in Charlottetown, Prince Edward Island, as Gustav's storm surge arrived just 4–5 h before high tide. Had it hit at the tide's peak, an additional 70 cm of elevated water would have inundated the downtown core. Hurricanes Isidore and Lili also brought rain and wind to Canada after coming ashore in the United States, though damage was limited.

A parade of midlatitude storms also drenched Halifax in late fall, making it the wettest November on record. Nearly 280 mm of precipitation fell at the International Airport, compared to a normal level of 154 mm. November weather systems were frequent, slower moving, and more intense than usual. At midmonth, a huge storm system moved across the Maritimes and then stalled southeast of Halifax, dumping a record rainfall over the region. The airport got 120.3 mm of rain. The storm left flooded streets and basements across the province. On 18 November, Halifax got an additional soaking of 70 mm of rain along with some snow and freezing rain.

ii) United States

(i) U.S. temperature

Mean temperature across the contiguous United States was above average for 2002, though three of the last four years were warmer (Fig. 53). The annual average temperature in 2002 was 12.2°C, which is 0.6°C above the long-term mean (1895–2002), the 14th warmest year on record. Arizona and much of the Northeast had much above-average annual temperature. No state in the contiguous United States had significantly colder than average annual temperatures (Fig. 54) for the second consecutive year although considerable seasonal variability in temperature was evident across the country (Fig. 55). Both the 2001–02 winter (DJF) and summer (JJA) were much warmer than the long-term mean and were associated with above-normal 500-hPa heights across a large portion of the country (Fig. 56), whereas spring (MAM) and fall (SON) were near normal.

The 2001–02 winter was exceptionally warm across the Great Plains, Great Lakes, and the Northeast (Fig. 55a). Record warmth occurred in nine states across these regions and the warmest winter on record was recorded for the Northeast region (Pennsylvania, Maryland, Delaware, New Jersey, New York, Connecticut, Rhode Island, Massachusetts, Vermont, New Hampshire, and Maine). The period JJA tied with 1988 as the third warmest summer on record, behind only 1934 and 1936. Colorado, Maryland, and Delaware had their warmest summers on record in 2002 (Fig. 55c) and in the Southwest region (Utah, Colorado, Arizona, and New Mexico), summer also ranked as the warmest on record.

Many all-time temperature records were broken as a result of the intense heat during the summer months. Fort Collins, Colorado, reported its warmest June and July on record while Las Vegas, Nevada, and Salt Lake City, Utah, experienced their hottest month on record in July. Death Valley, California, tied its highest daily mean temperature on record, 45.3°C, also in July. Alaska experienced its warmest fall and year on record with average temperatures of more than 4°C and 2°C above the long-term mean (1918–2002), respectively. Every season averaged above the mean for Alaska in 2002. Persistent ridging over the state, especially during the fall was associated with the warmer than average temperatures. Additional information on Alaska is available in section 5b.

A trough plunged southward from Canada bringing significantly below average temperatures to much of North America during October [Climate Prediction Center (CPC) 2002a]. As a result, October ranked as 14th coldest on record and was the first both cooler and wetter than average month in the continental United States since November 2000.

(ii) Precipitation, drought, and wildfires

Precipitation over the contiguous United States was near-normal in 2002, with a departure from the long-term mean (1895–2002) of 11 mm. Dry conditions persisted across much of the western United States, which had suffered from an ongoing drought since 2000. The East Coast, which endured drought conditions over

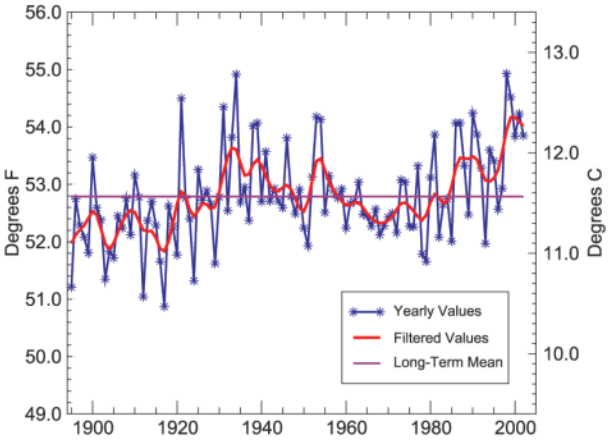

Fig. 53. Average annual temperature for the contiguous United States from 1895 through 2002 .

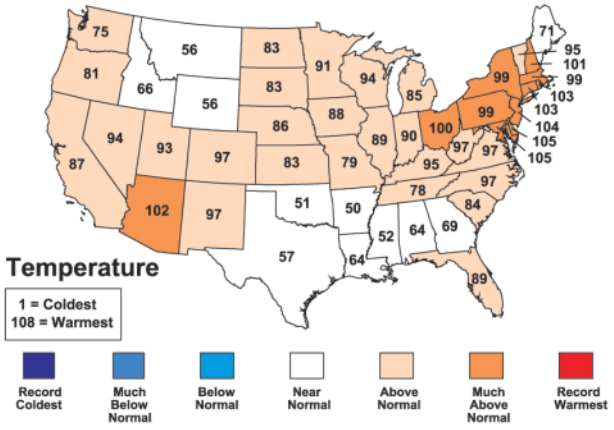

FIG. 54. Statewide temperature ranks for 2002. A rank of 108 represents the warmest year since 1895. Much above-normal temperature is defined as occurring in the top 10 warmest years (i.e., ranks 99–108). Above-normal temperature is defined as occurring in the warmest third of the recorded years. Much below temperature is likewise the coolest 10 yr and below normal is the remaining cool third of the distribution.

much of the past four to five years, received some much needed drought relief in 2002. Most of the precipitation occurred during the last four months of the year, effectively ending the long-term drought and dampening the eastern wildfire season. Louisiana had its wettest fall on record, primarily due to three tropical systems making landfall on or near the Louisiana coastline. Colorado had its driest year on record (Fig. 57), which contributed to a severe wildfire season. Parts of central and eastern Texas suffered from flooding from July through October while southern Texas endured ongoing drought conditions.

Seven tropical systems made landfall in 2002, the most since 1998, when seven systems also made landfall in the United States. Further details on these storms and other aspects of the 2002 Atlantic hurricane season are discussed in section 4b1.

Overall, the 2001–02 snow season in the United States was below average. This resulted from a combination of much above-normal temperatures and a general lack of precipitation during the winter months. But anomalously warm water temperatures in the Great Lakes provided ample moisture to lake-effect snowstorms and many locations near the lakes had record snowfalls. In the West, low snowpack from the winter contributed to the water shortages and extreme wildfire conditions experienced in 2002.

Due in part to the ongoing drought in the West, the United States wildfire season began earlier than average and became the second largest wildfire season in the past 50 years. The largest wildfire season occurred in 2000 when 3.0 million ha of land were consumed. Fires in Colorado, Arizona, and Oregon were reported as the largest in the last century for each of these states. By the end of June, nearly 1.1 million ha had burned; more than double the 10-yr average of 432,000 ha. One of the largest fires of the season was the "Hayman Fire" near Denver, which consumed 136,000 acres (55,000 ha), and was the largest single fire in Colorado's history. For the season, over 370,000 ha were consumed across the state of Colorado by over 3000 fires. In Oregon, more than 1 million acres (405,000 ha) of land were burned during the 2002 wildfire season; approximately 1.6% of the state.

The percentage of the United States in severe to extreme drought grew from 23% in January to a peak area coverage of approximately 39% by July, based on the Palmer Drought Index (Fig. 58). Most of the expansion occurred across the western United States, while drought coverage in the mid-Atlantic and southeast regions remained fairly steady. During the first half of

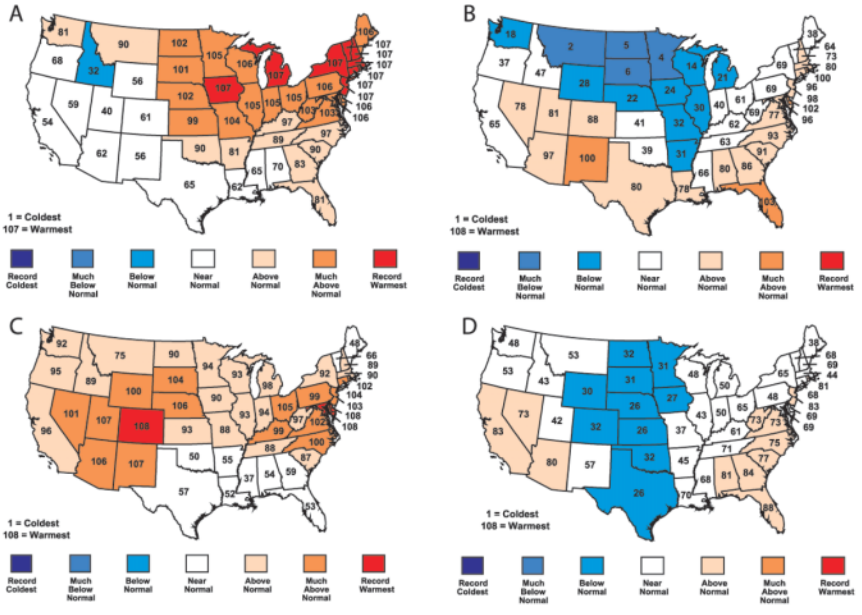

FIG. 55. 2001–2002 statewide rankings of temperature averages for (a) DJF, (b) MAM, (c) JJA, and (d) SON. See caption for Fig. 54 for further details on how the states are ranked.

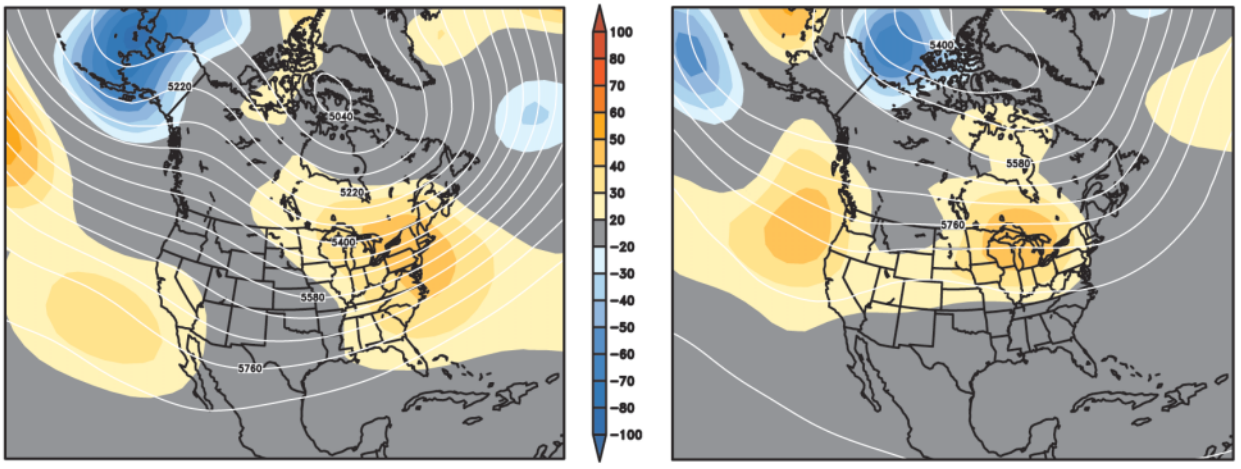

Fig. 56. 500-hPa heights and anomalies (m) for (a) 2001/02 winter (DJF) and (b) 2002 summer (June–July).

the year, drought in the Northeast diminished as a result of a wet spring period.

As the year progressed, drought conditions in the West intensified rapidly and expanded in areal extent during June and July as a result of much above-normal temperatures combined with much below-normal precipitation. The Palmer Hydrological Drought Index (PHDI) map for July illustrates the long-term drought conditions across the contiguous United States during this time (Fig. 59). By the end of the year, drought along the East Coast had all but vanished due to a very wet September–December period while drought in the West remained, resulting in an overall drop in the U.S. areal drought coverage to 22%. Conditions across the Central Plains and the Great Lakes deteriorated rapidly as the year came to an end.

At the peak of the drought in 2002, the size and extent of the drought was comparable to that of the 1988 drought, but still not as significant as the "Dust Bowl" drought of the 1930s and the severe drought of the 1950s. Figure 60 illustrates the change in the PHDI conditions from the end of 2001 through December 2002. Features to note are the wetter to much wetter conditions along the East Coast; drier conditions across the Southwest, High Plains, and the Great Lakes region; and very little change depicted throughout parts of the West.

Instrumental records of drought for the United States extend back approximately 100 years. These records capture the major twentieth century droughts, but are too short to fully assess the reoccurrence of major droughts such as those of the 1930s and 1950s and now the late 1990s–2002. Scientists have developed paleoclimatic records of drought from a variety of types of proxy data that span the past hundreds to tens of thousands of years, and longer. These records demonstrate patterns of natural drought variability and allow us to compare twentieth century droughts with those of the past. Droughts of the last four centuries are well documented in paleoclimatic proxies such as historical documents and tree rings. Spatial patterns of drought for every year since 1700 have been generated from a gridded network of tree-ring reconstructions (Fig. 61). Five years which have a similar "footprint" (or spatial pattern) of drought to the 2002 pattern, according to the tree-ring reconstructed Palmer Drought Severity Index (PDSI) are shown in Fig. 61. However, Fig. 61 illustrates that dryness in 2002 was more extensive and severe than many of the droughts in the last several hundred years.

(a) The West and Texas

In the western United States, the absence of adequate precipitation and snowpack during the winter

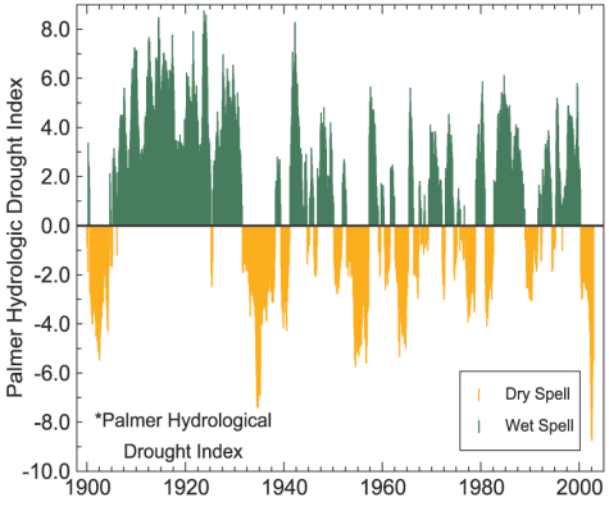

Fig. 57. Colorado statewide monthly PHDI, Jan 1900–Dec 2002.

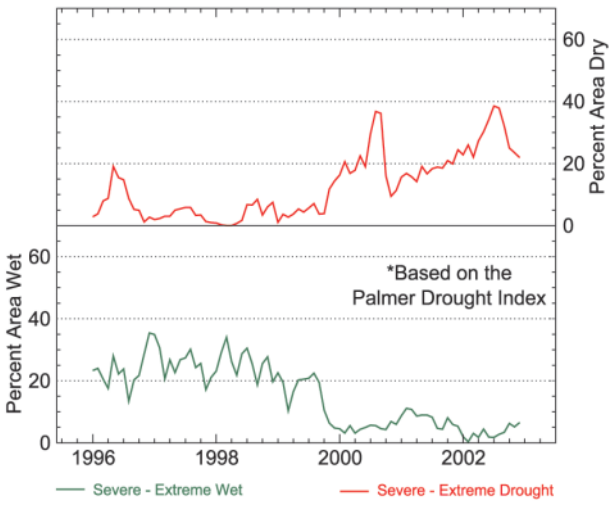

Fig. 58. Percent area of the contiguous United States that is very wet or very dry based on the PHDI, Jan 1996–Dec 2002. These percentages are computed based on the climate division dataset. Those climate divisions having the monthly average precipitation in the top 10 percentile of their historical distribution are very wet and those in the bottom 10 percentile are very dry.

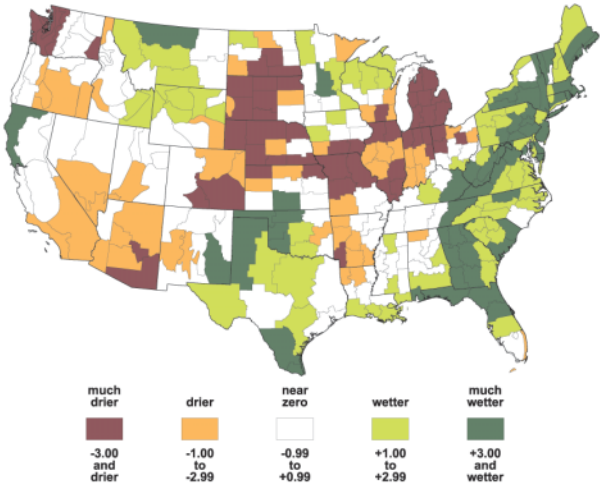

Fig. 60. The difference in the PHDI between 31 Dec 2001 and 31 Dec 2002 by climate division.

and spring seasons in combination with above-normal to near-record temperatures during the spring and summer (Figs. 55b,c) led to worsening drought conditions across much of the region. Water supplies were stressed, causing devastating impacts on agriculture while contributing to an extremely active wildfire season. Severe drought in Montana, which had persisted for more than three years in some places, forced farmers to abandon more than 20% of the winter wheat crop for the second consecutive year. In Wyoming, where dry conditions had also persisted since 1999, record-dry conditions during August 2001–July 2002, led to the driest PHDI in the last 100 years for the state.

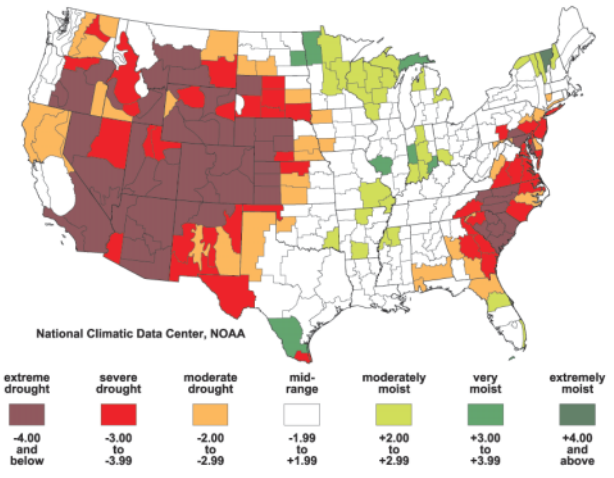

Fig. 59. PHDI for Jul 2002. Illustrates long-term hydrological conditions.

Record dryness also occurred in the intermountain basin throughout much of the year. Utah, Colorado, and Arizona each had their driest January–August period on record, (Fig. 62, see also Fig. 63) while much of the rest of the western states experienced much below-normal precipitation. The state of Colorado had its driest February, April, spring, and year-to-date periods from April through December, including the driest year on record (see Fig. 63). The previous driest year on record for Colorado occurred in 1934. The unprecedented moisture deficits in combination with extreme temperatures resulted in a statewide PHDI that rapidly reached record drought intensity by the end of the year (Fig. 57).

Flooding in central and eastern Texas was a persistent problem for several months from July 2002, when a cutoff low pressure system over Texas brought major flooding to the San Antonio and Austin regions of Texas. Accumulations of 120–380 mm were common across the region and approximately two dozen counties were declared disaster areas. Parts of south-central Texas had been suffering from drought prior to this event and the soil was incapable of absorbing such an abundance of precipitation over a short period of time. Record breaking rainfall also affected the southeastern portion of the state in mid-August. Galveston, Texas, reported 291 mm, which is the highest daily total on record in August and the greatest single-day total since 310 mm fell in October 1913. The remnants of Tropical Storm Fay brought heavy rains and severe weather to coastal and south-central Texas in September where 120–300 mm of rainfall was reported. In Oc-

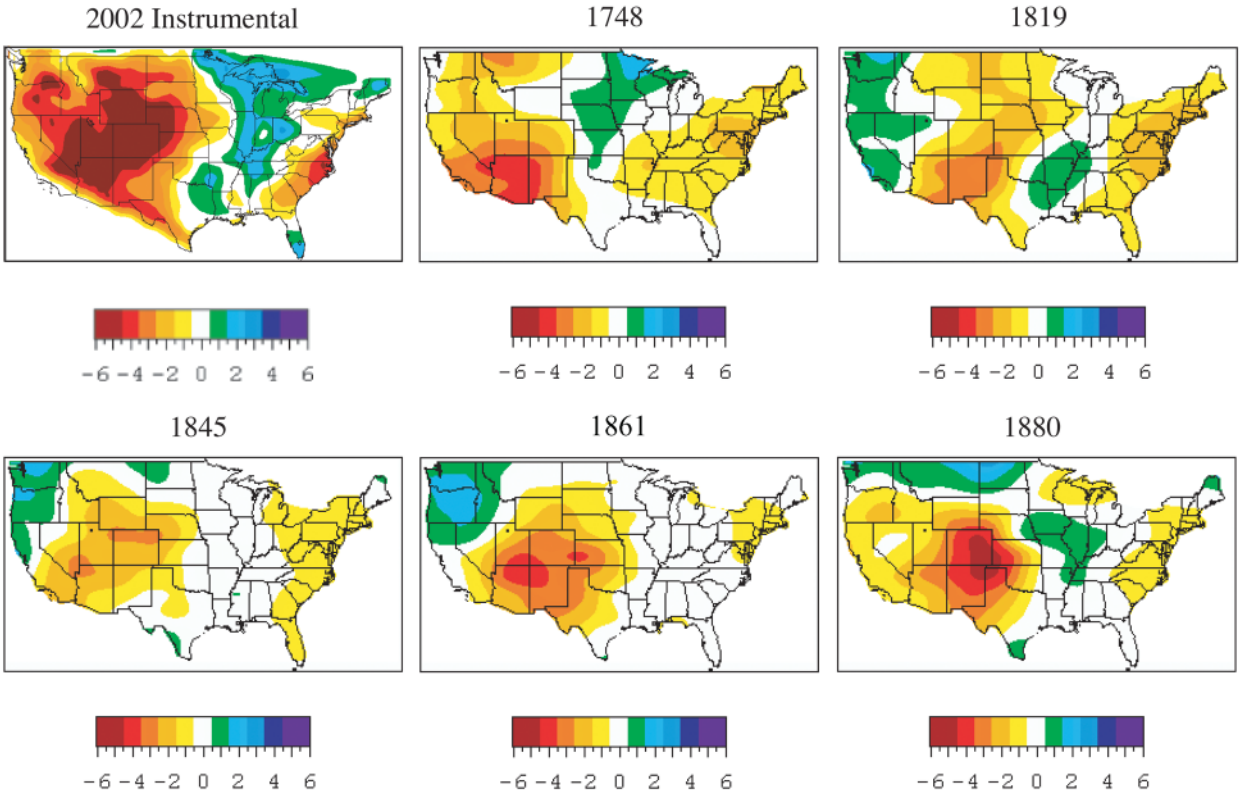

FIG. 61. Analog footprints of drought coverage (as depicted by PDSI) across the United States based on a gridded network of tree-ring reconstructions.

tober, Hurricane Lili came ashore in western Louisiana, bringing significant rainfall to eastern Texas. See section 4b1 for further details on rainfall associated with 2002 tropical storms.

Conditions in extreme south Texas were drier than normal for most years since 1990. Brownsville, Texas, had above-normal temperatures and below-normal precipitation during much of 2002. Precipitation from January through June was below to much below normal in the lower Rio Grande Valley. During SON, the region received above-normal precipitation and by the end of the year, drought conditions had diminished dramatically. Precipitation for the year was around 35 mm above the annual average due in large part to the wet last third of the year.

(b) The East Coast

While the western United States dealt with one of the largest wildfire seasons in 50 years, the wildfire season in the eastern United States, which traditionally intensifies in the fall months, was suppressed due to the wet conditions from September to December. Steady amounts of rainfall fell over the drought-stricken region, a result of tropical activity and an active storm track across the southeast. Consequently, below-average wildfire activity was reported throughout the eastern United States in 2002.

More than four years of drought had affected much of the region from Georgia to Virginia with normal to below-normal precipitation reported throughout most of the southeast through August (Fig. 62). In September, Tropical Storm Hanna made landfall near Mobile,

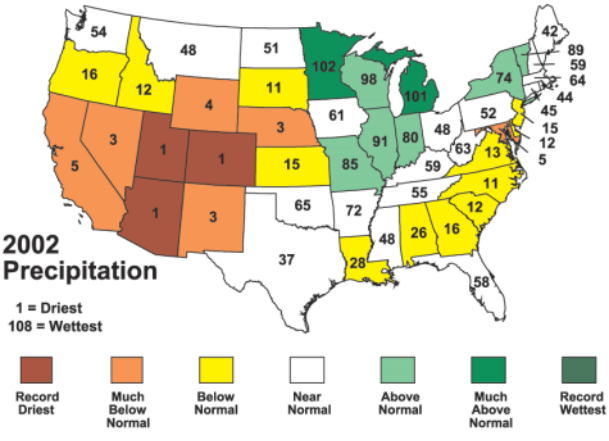

FIG. 62. Precipitation statewide ranks for Jan–Aug 2002 across the contiguous United States. For how the rankings are calculated, see caption for Fig. 54.

Alabama, and tracked northeastward bringing moderate to heavy rainfall across Alabama, Georgia, South Carolina, and North Carolina. Tropical Storm Kyle came ashore along the South Carolina coast in October bringing heavy rain to portions of Georgia, South Carolina, and North Carolina. Even with the above-average rainfall, well and reservoir levels remained low throughout much of the region at the end of the year.

From 1999 through 2002, Atlanta received only 80% of its normal precipitation, which ranks as the second driest consecutive 4-yr period on record (Fig. 64). Atlanta's precipitation total during this time was 4.07 m, which is less than the 1971–2000 4-yr normal value of 5.10 m by almost one year's average precipitation. The record driest 4-yr period occurred from 1893 through 1896 when only 3.99 m of precipitation fell. Had it not been for the precipitation received during the last four months of the year, Atlanta would have likely broken this long-standing record.

Conditions also improved across the Northeast. After the driest year on record for Maine in 2001 and extremely dry conditions throughout much of the remainder of the Northeast, at the end of 2001, conditions improved with three straight months of above-normal precipitation during the spring season of 2002. Normal to above-normal precipitation occurred across the region in all but three months of the year and drought was absent in most of the Northeast at year's end.

A significant snow- and ice storm affected parts of the eastern half of the United States during early December. An expansive shield of snow and ice covered much of the eastern United States, from the lower Ohio Valley, southern Appalachians, and into the Northeast. Snow accumulations of 10–20 cm were common along the northern edge of the precipitation shield, while a damaging accrual of ice affected much of the Carolinas. A major electric utilities provider in the Carolinas characterized the ice storm as one of the worst in the company's history as 1.2 million customers lost power. This surpassed the electrical outages caused by Hurricane Hugo as it moved across the central Carolinas in September 1989.

SYNOPTIC PERSPECTIVE OF THE COLORADO DROUGHT OF SUMMER 2002—C. Castro[12] and R. A. Pielke Sr.[12]

An analysis of precipitation for the period 1 September 2001–30 August 2002 showed that 9 of 15 stations representing the 8 climate divisions of Colorado were the driest in their period of record (http://climate.atmos.colostate.edu/droughtpresentations.shtml). This dryness was coincident with an exceptionally warm summer. Using the NCEP reanalysis, the 850–700-mb thickness values and 500-mb height over Colorado were the highest of the NCEP reanalysis period of record (Figs. 63a,b). In contrast, the actual water vapor was close to the long-term average (Fig. 63c). The warm, lower, and midtroposphere apparently inhibited thunderstorm activity. Earlier periods of exceptionally warm lower and midtropospheric temperature correspond to the mid-1950s, late 1970s, and early 1980s, and 1988 drought conditions in the state.

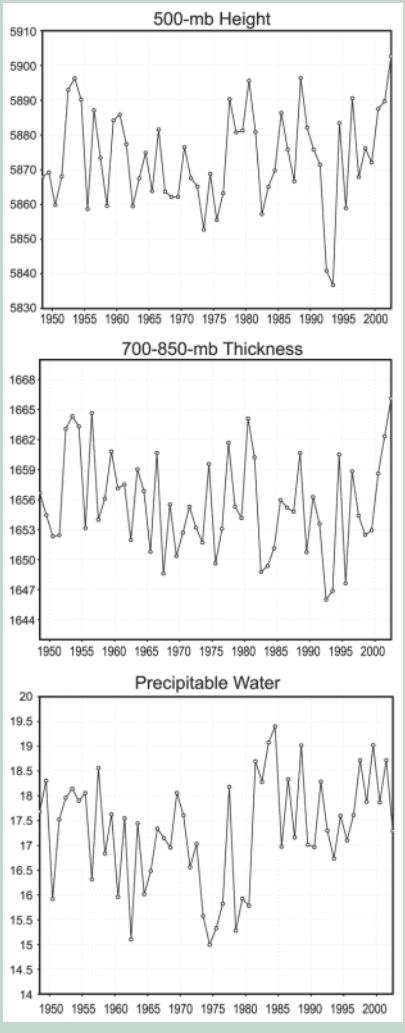

FIG. 63. NCEP reanalysis data, averaged over the state of Colorado for (a) 500-mb heights, (b) 700–850-mb heights, and (c) precipitable water.

(c) The Central Plains and Great Lakes

Heavy rain and flooding occurred across portions of the northwestern Great Lakes and north-central plains in June. Two-day rainfall totals exceeded 152 mm in a broad area of northern Minnesota. However, local totals far exceeded 305 mm in places such as Roseau, Lake of the Woods, and Koochiching counties. International Falls, Minnesota, reported its wettest June on record with 211 mm. The previous record was 208 mm in 1941. Hundreds of millions of dollars of crop losses due to flooding were reported in Minnesota and North Dakota.

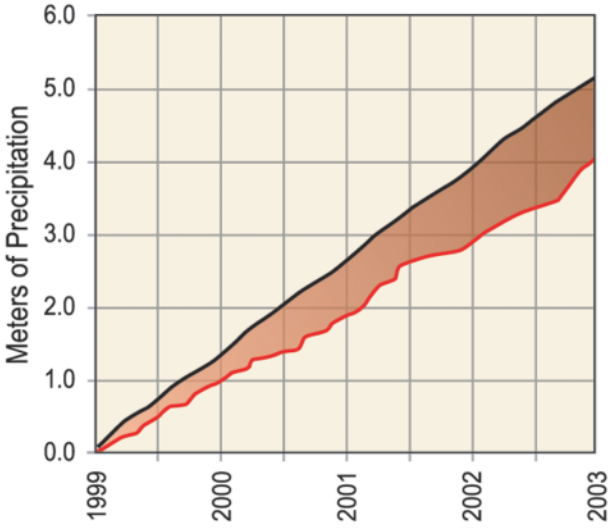

Fig. 64. Jan 1999–Dec 2002 accumulated observed precipitation (red line) and accumulated 1970–2000 mean precipitation (black line) for Atlanta, GA. Shading depicts the extent of the precipitation deficits.

Above-average winter (2001/02) temperatures across the Great Lakes kept the water temperature relatively warm, which fueled above average lake effect snowfall across the region. The monthly snowfall record for Buffalo, New York, was broken when more than 203 cm of snow fell in late December 2001. All-time record monthly snowfall was reported at Marquette, Michigan, in February when a total of 233 cm of snow fell. By the end of the season, snowfall totals for Marquette were greater than 762 cm, exceeding the previous seasonal record by 71 cm.

The western drought intensified and expanded eastward into portions of the Central Plains in 2002, where Nebraska was the epicenter for drought in the region. Precipitation was almost entirely absent over much of the state beginning in December 2001, resulting in the driest December–July in the 108-yr record (Fig. 65).

As a result of an amplified trough over the eastern United States [Climate Prediction Center (CPC) 2002b], much of the Central Plains and Great Lakes states received much below-normal to record-low precipitation during the November–December 2002 period while the Gulf and East Coast states experienced above-normal precipitation. Both South Dakota and Nebraska had their driest such periods on record; Minnesota and Iowa, their second driest.

iii) Mexico

Mexico experienced widespread drought in 2002 according to records from the Servicio Meteorological Nacional of Mexico (SMN). Nationally averaged precipitation indicates that the year ranked as the 20th driest since 1941 (739 mm versus the long-term average of 771 mm). Many dams in northern and western Mexico were at or near-historic low levels. Lake Chapala, the largest freshwater lake in Mexico was near its historic 100-yr minimum that was reported in 1957–58.

The winter of 2001/02 was dry across the north as a direct response to fading La Niña conditions and associated high pressure ridging across western North America. An amplified ridge at the end of January spread cold air into northern Mexico with Creel, Chihuahua, reporting a low of –10°C on 31 January 2002.

By the summer, El Niño conditions promoted drought through large sections of Mexico. August 2002 was the second driest August on record averaging only 99 mm of rainfall compared to a long-term average of 137 mm. Only three tropical storms tracked along the west coast from May through August compared to a normal of five storms. This decreased storm activity led to diminished rainfall along the west coast of Mexico. No tropical storms were observed in the east Pacific from 30 July to 21 August and this strongly contributed to drought conditions during August along the south coast of Mexico. Two category 5 hurricanes subsequently formed off western Mexico. Hurricane Hernan had sustained 140-kt winds and tracked away from the coast, 30 August–6 September. Hurricane Kenna had sustained 145 kt winds and recurved into the state of Nayarit during the course of its life span, 22–26 October.

Two eastern North Pacific tropical cyclones had strong impacts on Mexican weather in September and October 2002. Tropical Storm Julio (25–26 September) was short lived and relatively weak with sustained winds of only 35 kt due to strong interaction with the rugged coastline of southwest Mexico. However, Julio was

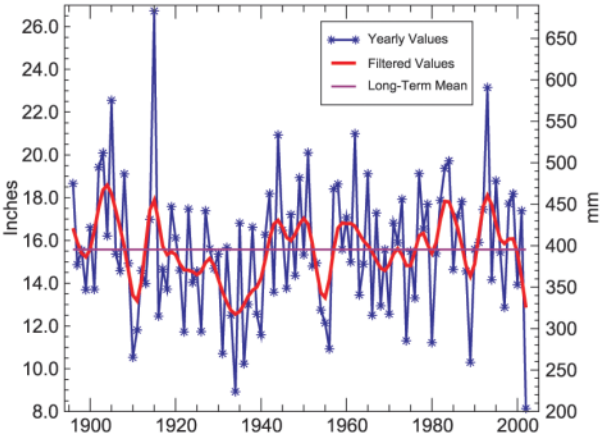

Fig. 65. Nebraska's statewide Dec–Jul precipitation for 1895–2002.

associated with a large swath of rainfall exceeding 200 mm along the coast of the state of Guerreo. Acapulco, Guerreo, received a 3-day rainfall total of 276 mm (from the 24 through 26 September) with nearby Costa Azul, Guerrero, reporting 313 mm during the same time period. As the storm moved inland, widespread 100–200-mm rains were reported across the states of southern Michoacan and Colima.

Hurricane Kenna formed on 22 October embedded in a large area of cloudiness and heavy rainfall associated with the intertropical convergence zone (ITCZ). As the storm moved northwest, heavy rainfall occurred along the south coast of Mexico with the radar site at Cuyutlan in the state of Colima reporting 397 mm of rain on 24 and 25 October. Hurricane Kenna moved into Nayarit on the late morning of 25 October. Due to the fast-forward movement of the storm, precipitation amounts were not particulary high. Just south of the landfalling hurricane, Aguamilpa reported 156 mm on 25 October and Ruiz, Nayarit, reported 106 mm. According to reports provided by the Servicio Meteorologico Nacional, there was only one indirect storm-related death.

b. Central America—B. Lyon[5]

Drought returned to portions of Central America in 2002. Although locally severe in some areas, the 2002 drought was generally not as intense as the drought that gripped the region in 2001 (Waple et al. 2002). The combination of a multiyear drought and the continued decline in coffee prices, however, had a significant impact on food security and the economy of the region, especially in Honduras, Guatemala, Nicaragua, and El Salvador.

Climatologically, rainfall is closely linked to the behavior of the easterly trade winds that flow from the tropical Atlantic across the region and into the ITCZ in the tropical Pacific. Generally speaking, the orientation of topography relative to the prevailing winds combined with the latitudinal movement of the ITCZ in the Pacific, results in a tropical wet or dry climate along the Pacific and a tropical wet climate along the Caribbean. In many locations the annual cycle of rainfall is bimodal with relative maxima during the early boreal summer and autumn seasons.

Rainfall during 2002 was erratic. Heavy rains during May and early June produced localized flooding across sections of northern Panama and Costa Rica as well as eastern and central Honduras, western Nicaragua, and El Salvador. A widespread break in rainfall developed during June with large moisture deficits emerging across sections of Guatemala southward to Nicaragua by the end of July (Fig. 66a). First-season crops became severely stressed in pockets of eastern Guatemala, southern Honduras, northeastern El Salvador, and northern Nicaragua with the UN World Food Program reporting losses of 50%–90% in some areas. Especially hard-hit were subsistence growers in marginal agricultural areas.

Below-average rainfall in Central America is common during the onset of El Niño events such as occurred in 2002. However, given the moderate strength of the 2002 event the ITCZ in the eastern Pacific was not significantly displaced from its climatological position and anomalous convection in the equatorial Pacific was confined near the international date line. Rainfall rebounded somewhat in many areas during the second half of the rainy season (Fig. 66b) and for the region as a whole more favorable harvests were anticipated for many second-season crops.

c. South America—A. M. Waple[8]

The year 2002 was anomalously warm in parts of Paraguay and Bolivia with annual temperatures between 1° and 2°C above normal for northern Paraguay. This was accompanied by a second year of serious drought conditions (Fig. 67). In October, the Paraguayan government declared a national emergency as approximately 5000 residents and farmers were affected by the drought conditions and food shortages.

In contrast, a drought that persisted in eastern Brazil throughout much of 2001 was alleviated by significant rainfall during January. Precipitation amounts were 100–200 mm above the 1979–95 average. Along the northeast coast of Brazil, nearly 200 mm was recorded at Fortaleza in January. Relatively dry weather dominated much of Brazil during March, but the increase in precipitation during January and February prompted government officials to lift electricity rationing measures that had been in place since June 2001. Many reservoirs that supply water to hydroelectric power plants had returned to more normal levels by the end of March.

Farther south across northern Argentina and Uruguay, heavy rainfall brought monthly precipitation surpluses of 100–300 mm. Artigas, Uruguay, received over 450 mm of rain during March, nearly 3 times the normal monthly amount.

Northern Brazil continued to receive above-average rainfall through April with totals in the northern Brazilian city of Vitoria, of 36 mm above normal during April. Other areas of above-average precipitation in April were the Pampas region of Argentina as well as all of Uruguay.

Flooding that began in May 2002 in Chile continued into early June, with some of the heaviest rains in

nearly 80 years affecting central Chile. The city of Concepción received 70.6 mm of rain during the first 7 days of June.

A series of winter storms affected southeast Peru and parts of southwestern Bolivia during July. In Peru, a state of emergency was declared on 13 July, where snow and freezing weather were responsible for the deaths of 59 people. Across the Bolivian department of Potosi, the cold, snowy weather resulted in four deaths with cattle losses as high as 50%. The cold and snowy weather continued into August in Argentina, Chile, and Peru. Heavy snowfall on 8 August prompted Peruvian officials to temporarily close the Inca Trail to the ancient ruins of Machu Picchu.

In Peru, flooding along the Blanco River in the Amazon jungle region killed four people on 10 November. The river brought flooding to four towns near the city of Satipo, about 280 km east of Lima.

Overall southern Brazil was dryer than average for 2002, and Uraguay was anomalously wet (Fig. 67) in part due to the development of an El Niño in midyear (see southeastern South America data in Fig. 10).

d. Europe—L. Alexander[1]

i) Temperature

Annual temperatures in 2002 were well above average across Europe especially in eastern, central, and northern regions. Annual anomalies (with respect to a 1961–90 reference period) were more than 1°C above average, although there were marked regional and seasonal variations (Fig. 68). Temperatures across most of the United Kingdom and Ireland were above the 98th percentile of the 1961–90 distribution when averaged over the whole year. With an average minimum central England temperature of 6.8°C, 2002 tied 1999 as the warmest year in a 125-yr record (Fig. 69).

Anomalous warmth was widespread in all four seasons, although cooler than normal conditions prevailed across most of Scandinavia during SON (Fig. 68d). The 2001/02 winter season (DJF) was particularly warm over Scotland, Ireland, and Portugal while Italy and the Adriatic had cooler than normal conditions (Fig. 68a). Although parts of Scandinavia started the year with below-average conditions, Sweden was warmer than average in every month from January to September. February was a particularly warm month across Europe with an average land temperature anomaly of over 5°C, the second warmest value during this month since records began in 1870.

Many stations in eastern Europe and Scandinavia had record temperatures. The town of Vidin in Bulgaria had daily temperatures of nearly 18°C above the February average. Spring temperatures (MAM) continued to be well above average over the whole continent, particularly in the north (Fig. 68b) and these anomalous conditions persisted into the summer

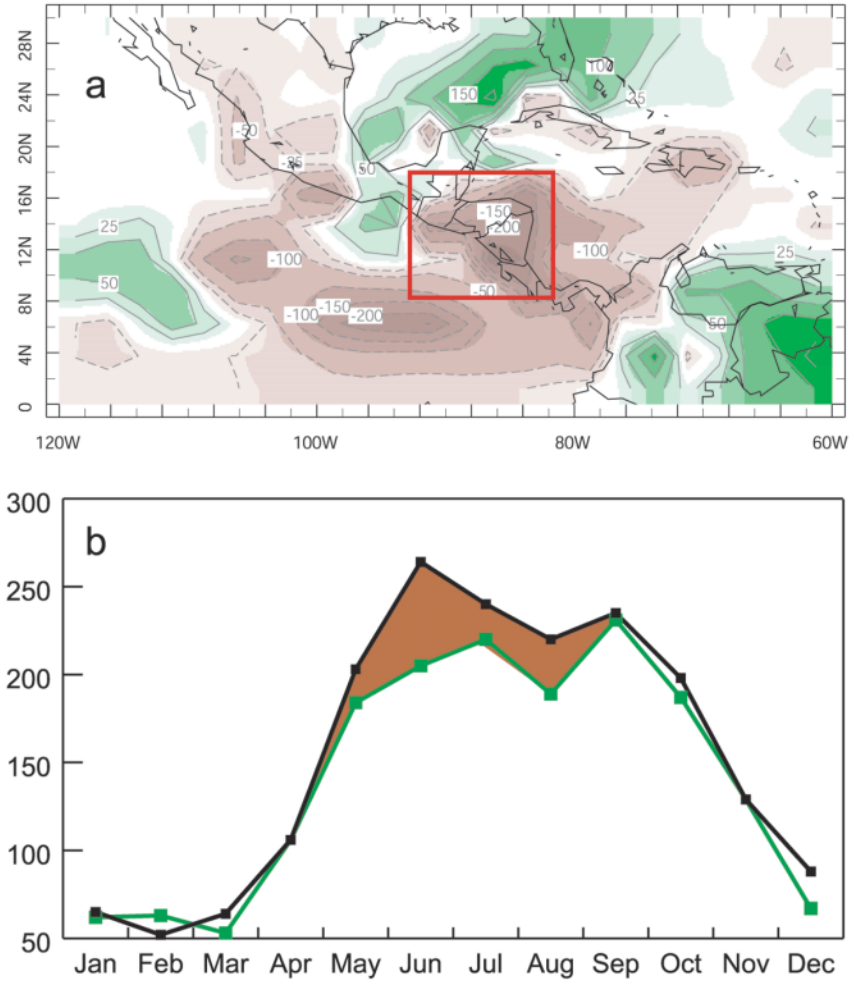

Fig. 66. (a) Monthly rainfall anomaly (mm; 1979–2002 base period) for Jun 2002 and (b) time series of observed monthly rainfall (mm; green line) and climatology (black line) averaged over red box in (a) for Jan–Dec 2002 (data from CPC, CAMS_OPI).

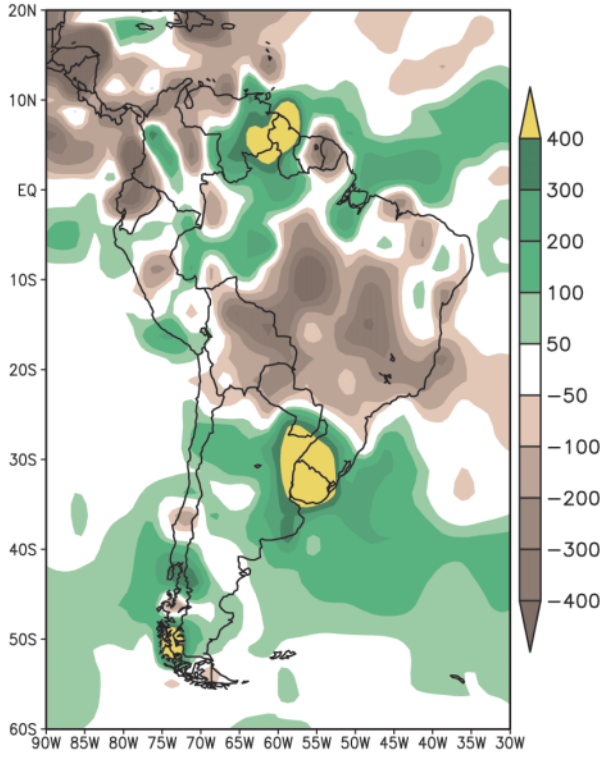

Fig. 67. Annual precipitation anomalies for 2002 for South America from CAMS combined satellite and rain gauge–derived precipitation estimates. The anomaly base period is 1979–95.

months (Fig. 68c). Southern Norway, Sweden, and the Baltic states recorded temperatures above the 98th percentile during JJA with Sweden having its warmest summer since records began in 1860. Persistent high temperatures were also observed in Switzerland during June. However, Portugal and eastern parts of the Pyrenees had below-average temperatures.

A different spatial pattern from the other seasons occurred in the SON period with a marked temperature contrast between western and northeastern regions. Temperatures in the United Kingdom, Ireland, and northern France were in the top 10th percentile while much of Scandinavia, the Baltic region, and northwestern Russia experienced temperatures in the lowest 10th percentile. The year ended with milder conditions in the west and colder conditions in the north and east, which reduced the average temperature in Europe in December to more than 4°C below the 1961–90 average.

2) Precipitation

When averaged over the year, most of Europe experienced average or below-average precipitation in 2002. However parts of Germany, eastern Europe, the United Kingdom and Iceland had more precipitation than normal. With a total of 1118 mm, it was the 10th wettest year in the 237-yr England and Wales precipitation series.

January was dry except in northern Norway, southern Sweden, and Iceland, all of which had more than twice their average total. February showed a mixed pattern with dry conditions over Spain and Portugal but wetter than average conditions over northern regions. The northwest region of England and Wales had its highest rainfall total (155 mm) in a 130-yr record in February, as a succession of deep depressions brought very unsettled conditions with frequent gales across the whole of the United Kingdom.

The spring months (MAM) had mostly drier than usual conditions. However, Iceland was very wet in April. A total of 267 mm at the eastern town of Akurnes was more than 3 times above the monthly average. Eastern parts of the Pyrenees also had well above-average precipitation. In May, northwestern Europe had above average rainfall as did eastern Spain and Switzerland.

During the summer season (JJA) there was widespread flooding across much of Europe. In August northeast England experienced its highest daily rain-

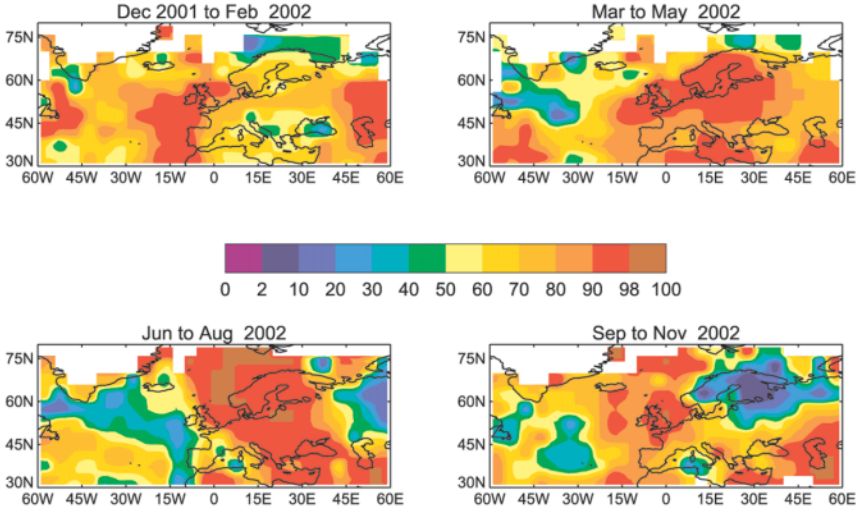

Fig. 68. European surface temperature in 2002 expressed as percentiles of 1961–90 modified two-parameter gamma distributions for 2001/02 (a) DJF, (b) MAM, (c) JJA, and (d) SON (source: Jones et al. 2001; Horton et al. 2001; Jones and Moberg 2003).

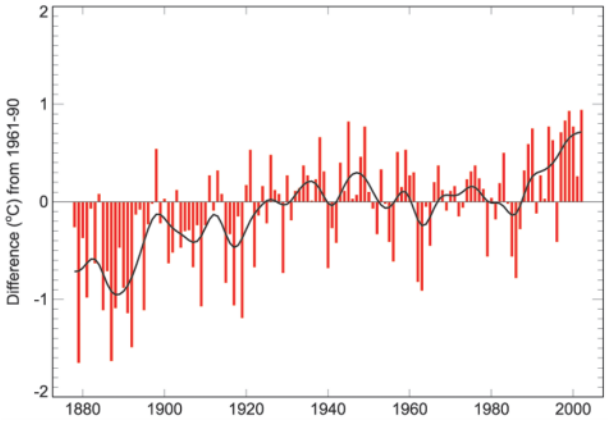

FIG. 69. Minimum Central England temperature, 1878–2002. Values are expressed relative to 1961–90. The time series is fitted with a smoothed 21-term binomial filter (Source: Parker et al. 1992).

fall total since records began in 1931, the highest daily value on record for any month in any England and Wales region (61 mm). Central Europe (including Germany, the Czech Republic, Austria, Romania, and Slovakia) suffered exceptionally heavy rain in July and August causing the Danube and Elbe Rivers to overflow in the worst flooding in over a century (see Fig. 70). At its peak, the level of the Danube was reported to be 10 m above normal. Thousands of people were forced to evacuate from low lying areas north of Budapest and from the cities of Prague and Dresden. Austria was also affected after experiencing its highest 2-day rainfall total since records began and the city of Salzburg was declared a disaster zone. More than 100 deaths were reported and the damage was estimated at 9 billion U.S. dollars in Germany alone.

Precipitation was higher than normal on the Iberian Peninsula in September and 21 people lost their lives in the Languedoc region of southern France when exceptionally heavy rainfall caused flooding. Cardet, France, recorded a rainfall total of 690 mm in just 48 h. SON remained wet in central and eastern Europe, Iceland, and Portugal while well below-average conditions prevailed in the west of Norway and northwest Scotland. There was severe local flooding in southern England in November and the latter half of December when Paris also sustained flooding. OND was the thid wettest averaged across England and Wales since 1766 (Fig. 71).

e. *Africa*—C. McBride,[10] P. Ambenje and DMCN,[2] and A. M. Waple[8]

i) West Africa

Areas of Mauritania, Senegal, and other areas of West Africa suffered from an extremely poor rainfall season during their normally wet months of July and August 2002 (see Fig. 95). The ITCZ was located south of its normal position in extreme West Africa allowing dryness to emerge in parts of Senegal, Gambia, and Guinea Bissau during July.

The dryness persisted through much of August and while westward-moving thunderstorm clusters provided some relief in August and September, they decreased in intensity during early September over Senegal, southern Mauritania, and west-northwestern Mali. Parts of western Mali recorded rainfall amounts in excess of 50 mm for the first week of September 2002 and central and southern Senegal received generally less than 30 mm, partially helping to restore some of the moisture that was depleted during the extremely dry weeks in July and August. However, September rains arrived too late to prevent substantial agricultural and hydrological problems throughout the area. Seasonal rainfall totals were the lowest in at least 50 years in much of the region.

The 2002 rainy season was the driest since at least 1950 across Senegal's Groundnut Basin, underperforming even the dry 1983 rainy season. The seasonal dryness was accompanied by extreme heat during June and July and the drought led to withered crops and resulted in livestock losses across most of Senegal, Gambia, southern Mauritania, and parts of southwestern Mali.

A strong cold front treked across Morocco during 17–18 November and produced severe flooding that resulted in at least 60 deaths. The flash flooding was characterized as the worst to strike the country in 30 years. Flood damage also ignited a fire at a large oil refinery in the industrial town of Mohammedia.

ii) East Africa

(i) The climate of the GHA in 2002

From mid-1998 to 2001, some parts of the region were affected by one of the longest and most severe droughts in the history of available records. Floods preceded the prolonged drought over many parts of the equatorial sector of the subregion. This variation from extreme floods to severe droughts was beyond the traditional coping strategies of most of the communities and governments. In some parts of the Greater Horn of Africa (GHA), the drought conditions persisted up to the year 2002 (Fig. 72) and the cumulative effects had severe socio-economic impacts in such areas. In other parts, intense rainfall during some seasons of 2002 provided relief from the prolonged drought conditions.

(a) Southern sector

This sector has a primary rainy season from November to March. During January 2002, heavy and intense rainfall lashed much of the sector.

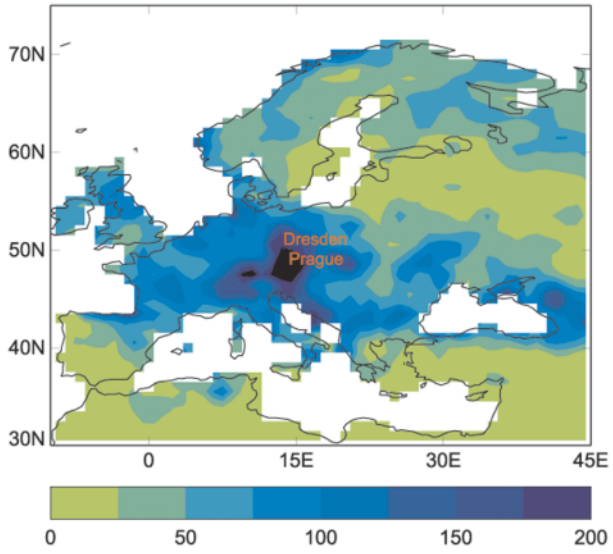

Fig. 70. Actual precipitation anomalies (in mm) with respect to 1961–90 in Aug 2002 for the European region (source: GPCC 1998; Rudolf et al. 1994).

Significant rainfall amounts were sustained over vast areas of Tanzania from February to March 2002 with near-normal to wet conditions over much of the sector. The heavy rainfall in the coastal areas in the month of March was mainly due to cyclone activity in the southwest Indian Ocean. Moderate to heavy rainfall was sustained over the sector in the month of April. However, dry conditions occurred in the southwestern and central parts of the sector while near-normal to wet conditions occurred elsewhere during the month. The coastal parts of the sector experienced their wettest April since records began in 1961.

A near-complete withdrawal of the summer rains occurred in May. Most locations had less than 40 mm of rainfall with some locations in central Tanzania experiencing their driest May on record.

(b) Equatorial sector

Rainfall in this sector has a bimodal distribution with the rainy seasons occurring in MAM (long rains) and OND (short rains). January and February are generally dry and hot while the JJAS season is dry and cool over most areas. Locations in the vicinity of Lake Victoria and parts of the coastal strip, however, experience rainfall throughout the year.

The equatorial sector was characterized by generally dry conditions in January and February 2002 except for some rainfall events in the southern areas during January. A significant increase in rainfall was observed in the sector in March with the bulk of the rainfall occurring in the first half of the month. Vast areas of the sector experienced near-normal to wet conditions with some localized areas in northwestern Tanzania experiencing their wettest conditions on record for the month since 1961. The wet conditions occurred over southern Uganda, northwestern Tanzania, and parts of western and central Kenya. Low rainfall amounts and associated dry conditions persisted over the northeastern parts of the sector. A dry spell began near the end of March and extended to early April. However, significant rainfall was recorded from the middle of April to mark the establishment of the long rains season that extended into May in most areas.

Vast areas of the sector experienced near-normal to wet conditions with some areas in central Kenya experiencing record wet conditions for the month of April. Rainfall was erratic in some areas. In other areas, the season was characterized by low rainfall totals arising from a late onset and an early withdrawal with short and heavy episodic rainfall events occurring in early March and April. In other areas, the long rains completely failed and exacerbated the cumulative impacts of the consecutive severe droughts of the previous years.

Significant rainfall was sustained in the western parts of the sector in May. This resulted in near normal to wet conditions with some locations experiencing record wet conditions for the month. However, a significant decline in rainfall leading to dry conditions occurred over the eastern parts of the sector to mark an abrupt cessation of the long rains season. Dry conditions engulfed some areas in the western parts of the sector during the JJA period.

The short rains (OND) were characterized by a poor distribution in parts of the sector. But in general, beneficial rainfall occurred over parts of the western, central, and coastal areas of the sector.

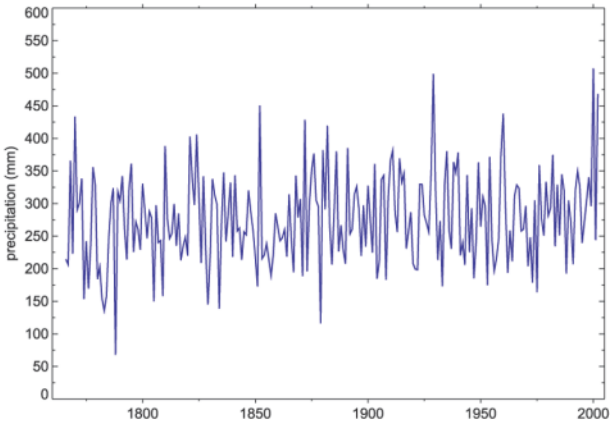

Fig. 71. Oct to Dec England and Wales precipitation totals, 1766–2002 (source: Jones and Conway 1997; Alexander and Jones 2001).

(c) Northern sector

The primary rainy season in the northern sector occurs during JJAS. The 2002 rainfall season showed signs of starting in April, however, the rainfall declined again in May with some locations experiencing record-dry conditions for the month. There was a resurgence of rainfall in June in the western parts of Sudan and Ethiopia, indicative of the proper onset of the summer rainfall season. However, dry conditions occurred in the eastern parts of Sudan and parts of central Ethiopia. In general, most locations in western Sudan and northwestern Ethiopia had adequate rainfall during JJAS. The eastern parts of Sudan were characterized by alternating near-normal to wet conditions and near-normal to dry conditions. Conversely, dry conditions persisted over parts of central Ethiopia depicting a total failure of the rainfall season (Fig. 72).

RAINFALL CLIMATOLOGY OF EASTERN AFRICA (GREATER HORN OF AFRICA)

The climate of the GHA is quite complex both spatially and temporally. For ease of description, the subregion is divided into three sectors based on periods of rainfall onsets and withdrawals. These are the southern sector (central and southern Tanzania), equatorial sector (Uganda, Rwanda, Burundi, Kenya, southern Somalia, northern Tanzania, southern Sudan, and southern Ethiopia) and the northern sector (Sudan, Ethiopia, northern Somalia, Djibouti, and Eritrea).

Peak rainfall seasons in each region are closely associated with the location of the ITCZ. December–March is the peak rainfall period for the southern sector. The rainbelt shifts from the Southern Hemisphere to lie over the equatorial region during the Northern Hemisphere spring (MAM) period and hence most of the rainfall is concentrated within the equatorial sector. Some parts of the subregion that are close to large water bodies however receive substantial rainfall almost year-round. The rainbelt then shifts northward to result in peak rainfall for the northern sector from May/June to September/October. The rainbelt migrates southward from the Northern Hemisphere during the boreal autumn to result in the second rainfall season (OND) over the equatorial sector.

Anomalies in the general circulation over the GHA that have been linked to extreme climate events such as droughts and floods have been associated with the ENSO phenomena, tropical cyclone activity in the Indian Ocean, and anomalies in monsoon wind systems among many other regional systems. ENSO events have a strong influence on the rainfall fluctuations over many parts of the GHA during all seasons. However the impacts vary significantly spatially and seasonally. The impacts also depend on the evolution phases of ENSO such as the onset, maturity, seasonal persistence, and withdrawal phases. In general, El Niño episodes are often associated with above-normal rainfall conditions over the equatorial parts of eastern Africa during the OND season and below-normal rainfall over much of the Horn of Africa during JJAS rainfall season. Conversely, La Niña events often give rise to below-normal rainfall over much of the GHA during OND and MAM periods and above-normal rainfall during the JJAS rainfall season.

iii) Southern Africa

(i) January–June 2002

Most regions received below-average rainfall totals in the summer season (DJF; Fig. 74). January was cooler for most of the country except for the north and north-eastern parts and most of KwaZulu-Natal and places in the eastern Cape.

A large part of the summer rainfall regions received anomalously high rainfall totals for the second quarter of the year (AMJ; Fig. 75.). The unprecedented wet conditions over the summer rainfall regions persisted through the winter into spring. Wet conditions during winter over the summer rainfall regions are normally associated with a higher than normal frequency of cut-off low systems penetrating farther north than usual. However, parts of the winter rainfall regions remained anomalously dry.

(ii) July–December 2002

July was cooler for much of the country. Extensive heavy snowfalls in the Eastern Cape that started on 16 July, lasted nearly a week and led to the closing of mountain passes. Elliot was at the center of the heavy snowfalls in the eastern Cape where about 3000 informal dwellings, 100 farmhouses, and 50 shops were destroyed. A state of emergency was declared in the magisterial districts of Cala, Ugie, Elliot, Indwe, and Barly East that were, for several days, cut off from the national power grid and road contact with the outside world. Many power and telephone lines throughout the Drakensberg region snapped under the weight of the snow or because trees collapsed on them.

At least 14 people were confirmed to have died, while some were still missing, after floods devastated east London and the eastern parts of the eastern Cape from the 15 August. East London recorded a 24-h rainfall total of 317 mm on 15 August. About 3000 people from informal settlements were left homeless by the

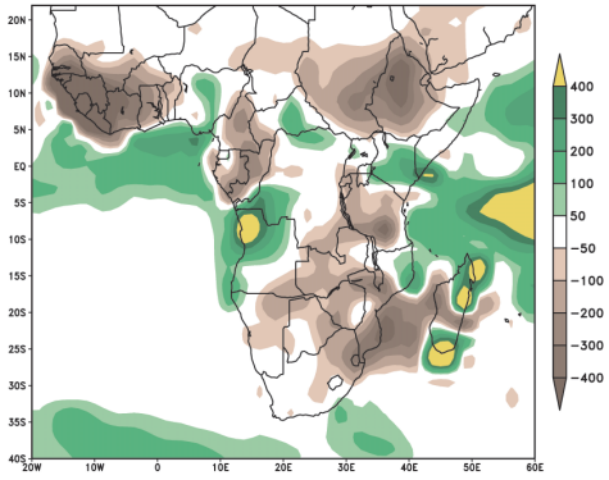

FIG. 72. Annual precipitation anomalies for 2002 for Africa from CAMS combined satellite and rain gauge–derived precipitation estimates. The anomaly base period is 1979–95.

heavy rains. Several roads in the eastern Cape were also closed to traffic.

Most of southern Africa, except for the western and southwestern coast and adjacent interior of South Africa, received below-average rainfall totals during the OND period. This rainfall deficit may have been due to the presence of El Niño and anomalously warm equatorial Indian Ocean surface temperatures. An anomalously warm equatorial Indo-Pacific enhances the probability of below-average summer rainfall totals over much of the region.

Temperatures in October were also below normal ranging from as low as 2°C to more than 38°C within a span of three weeks. This together with a lack of rain caused extensive damage to the wheat crop in the summer rainfall region. Estimated average crop damages of 35%–40% occurred due to the dry conditions and heat.

f. Asia

i) RUSSIA—O. Bulygina,[4] N. N. Korshunova,[4] and V. N. Razuvaev[4]

Weather conditions in 2002 were analyzed for the

KILIMANJARO SNOW—D. Hardy[9]

Snowfall measurements at the summit of Kilimanjaro indicated the return of a more typical precipitation regime during 2002 (Fig. 73). Long-term records from surrounding lowland stations (Tanzania and Kenya) normally exhibit a bimodal seasonality, with a primary peak in MAM (Masika or "long rains"), and a secondary peak in October–November (Vuli or "short rains")—with an enhanced Vuli during El Niño (Ropelewski and Halpert 1987; Nicholson and Kim 1997).

Through 2000 and 2001, Kilimanjaro precipitation seasonality was disrupted (Fig. 73), and the amount of precipitation appears to have been suppressed; these findings are consistent with regional drought conditions (cf. Lawrimore et al. 2001; Waple et al. 2002). The extreme snowfall recorded on Kilimanjaro during January of 2001 was coincident with record rainfall measured elsewhere in the region.

Kilimanjaro's glaciers are extremely sensitive to precipitation variability (Jäger 1931; Kaser et al. 2003, submitted to *Int. J. Climatol.*), as on an annual basis, the summit climate is thermally homogeneous, with a mean annual temperature of –7.1°C. Figure 73 illustrates the consequences of drought for mass balance at the glacier surface, where energy exchange is largely governed by surface albedo. Monthly snowfall of at least 10 cm appears generally sufficient to maintain a neutral or positive mass balance. However, when monthly snowfall is uniformly low (e.g., in 2000) or when wet season precipitation is deficient, Kilimanjaro's severe climate results in conditions favorable for rapid ablation.

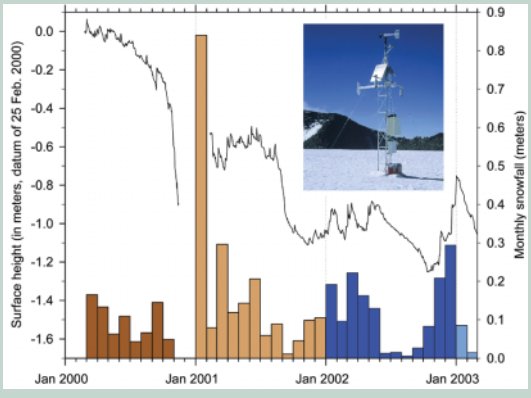

FIG. 73. Snowfall and surface height change on a glacier at Kilimanjaro's summit. Sonic distance sensors on an automated weather station (see inset image) make hourly measurements, allowing determination of surface height (solid line, left-hand scale) and monthly snowfall (bars, right-hand scale). Automated measurements were not available between mid-Nov 2000 and 10 Feb 2001; snowfall during this period was determined indirectly and attributed in the figure entirely to January, a month of extreme precipitation in the region.

Russian territory as a whole and for seven quasi-homogeneous climatic zones (I—north of European Russia and western Siberia, II—north of eastern Siberia and Yakutia, III—Chukot Peninsula and Kamchatka, IV—center and the south of European Russia, V—center and the south of western Siberia, VI—center and the south of eastern Siberia, and VII—the Far East; Fig. 78).

Overall, the year 2002 was anomalously warm in Russia. During the past 70 years, the mean annual air temperature was higher only in 1995 (Fig. 76). Annual anomalies in excess of 1.0°–2.0°C covered large portions of the eastern half of the country, though annual anomalies were small and even negative over west-central Russia (see Fig. 6).

In early 2002 (January and February), most of the Russian territory experienced large positive air temperature anomalies (Fig. 77). January was extremely warm in southern regions of Siberia, where mean monthly air temperatures were over 10°C higher than the long-term mean values. In February, mean monthly air temperatures reached record values in central and southern parts of eastern Siberia (zone VI) and in the Far East (zone VII; Figs. 77 and 78). Only eastern areas of the country and the continental areas of the Magadan region experienced an abnormally cold February with temperatures of −55° to −61°C persisting through the first five days of the month.

Precipitation totals of 2–3 times the normal monthly amount were recorded in February (Fig. 79) against a background of positive temperature anomalies over most of the European territory and Siberia. Heavy snow in the mountains of northern Caucasia (zone IV) throughout February promoted the threat of avalanches as a result of the passage of a series of fronts associated with active cyclonic systems producing storm-force winds, blizzards, wet snow, and ice.

March was very warm for the Russian territory as a whole. Only March 1990 exceeded 2002 temperatures and the mean air temperature for the European territory in March 2002 was the highest in the past 70 years.

In European Russia, late spring (May) was 2°–4°C colder than usual. Freezes of different intensity were recorded everywhere in the region throughout the month. Particularly hard freezes were recorded on 15 and 21–23 May on the Central Volga (zone IV): Air temperatures were as cold as −7°C and soil temperatures reached −9°C. For most of the Asian territory, May was warm with the mean monthly air temperature 2°–4°C above normal; however, freezes were also recorded in farming regions until late May.

During May, strong winds (up to 26 m s^{-1}) were frequently recorded in the Khakasia Republic, Krasnoyarsk Territory, and in southern parts of western Siberia. On 29 May, a 500-m-wide F1 tornado (wind speeds of 40m s^{-1}) occurred in the settlement of Kamenovka (the Kemerovo region, zone V). Large precipitation deficits in parts of European Russian, the Irkutsk, and Chita regions (zone VI) led to extreme fire danger and drought in May and June.

From 20 to 23 June, heavy rains occurred in the north Caucasian region and led to severe flooding on almost all rivers of the Kuban and Terek basin and gave rise to mud flows in mountain regions (zone IV). The disaster caused damage to the region's economy and led to over 100 deaths.

In July and August, a substantial precipitation deficit led to meteorological and hydrological droughts in most regions of the territory. Forest and peat-bog fires contributed to increased smog in the area.

Contrasting the drought in European Russia, the Krasnodar Territory, and most of the Stavropol Territory (zone IV), received much above-average precipitation (about 200% of normal). During 5–8 August prolonged hot weather and a sharp change in air masses

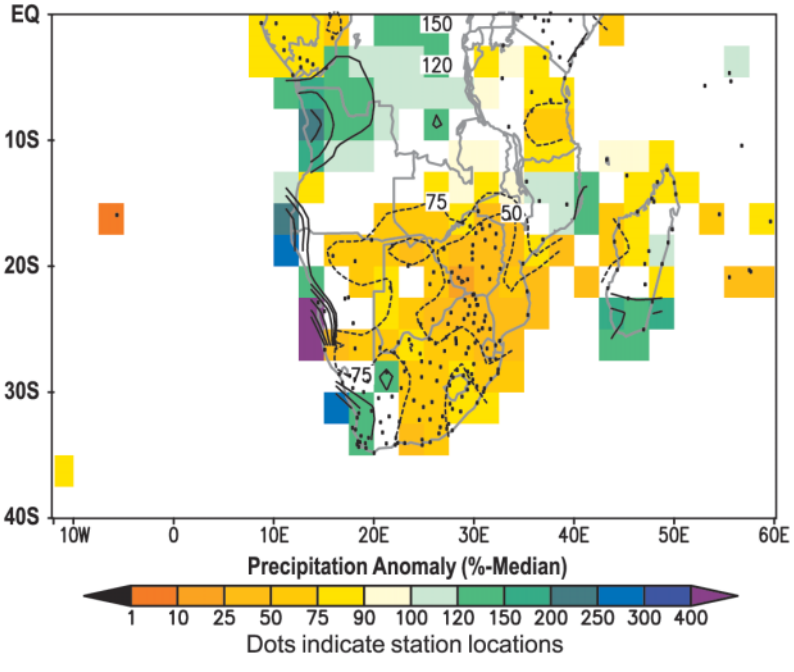

Fig. 74. Percent of median rainfall for Southern Africa for Jan to Mar 2002.

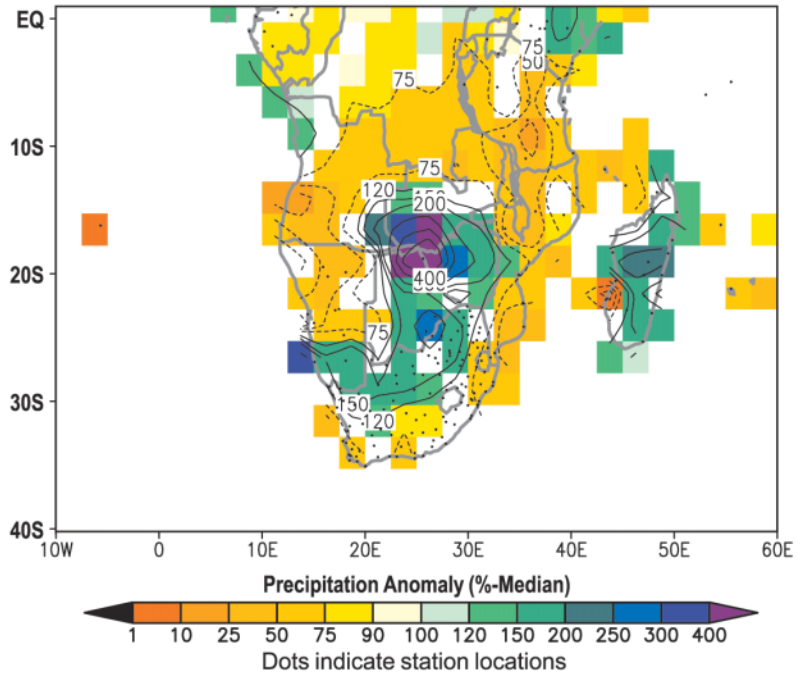

Fig. 75. Percent of median rainfall for Southern Africa for Apr to Jun 2002.

created conditions conducive to the formation of tornadoes and heavy thunderstorms on the Black Sea coast. In south Sakhalin, heavy rains caused flooding in the region's rivers. Severe floods were also caused by heavy rains in the southern Khabarovsk Territory and the Jewish Autonomous Region (zone VII).

Following prolonged summer drought in the central regions of European Russia, precipitation in September and October was 2–3 times higher than the long-term mean for these months. On 20 September, a relatively rare natural phenomenon, a glacial collapse, occurred in the Republic of Northern Osetia-Alania (zone IV) on the Kolka Glacier. The collapse triggered an avalanche of mud and debris that flowed for over 15 miles filling the Karmadon canyon, affecting small villages, and killing dozens of people. A similar collapse is believed to have occurred in 1902 killing 32 people. Glacial collapses have been predicted to occur more frequently as the climate warms in these mountain regions. In September–October, frequent precipitation was recorded in the Far East region though temperatures were near-average across Russia.

The end of 2002 was characterized by severe frosts over most of the Russian territory (Fig. 80). In the country as a whole, the mean monthly air temperature was lower only in 1941 and 1978. In the center and the south of European Russia (zone IV), the mean monthly air temperature in December proved to be the lowest for the past 70 years. In eastern Siberia, anomalies of mean monthly temperature reached –6° to –7°C. Only in the Chukot Autonomous Area (zone III), were positive temperature anomalies recorded.

iii) South Asia summer monsoon—B. Lyon,[5] A. Seth,[5] and S. J. Camargo[5]

JJAS 2002 marked the first all-India drought since 1987, ending a 14-yr run of normal monsoon rains. As reported by the India Meteorological Department, the average seasonal rainfall was 19% below normal, well below the ±10% criterion used to define a normal monsoon. Spatially the failure was widespread, with rainfall 3%–19% below normal in much of central India, 25%–45% below in peninsular India, and as much as 60%–70% below normal in the hardest hit regions of Rajasthan in the northwest. JJAS rainfall was near normal in the northeast and above normal in Kashmir.

The monsoon rains began in Kerala three days early, on 29 May, with a robust early season. By 12 June rains covered peninsular India, the northeastern region, and parts of central India as expected. By 27 June the monsoon advanced to remaining parts of Jharkhand, Bihar, Chhattisgarh, Maharashtra, Madhya Pradesh, Gujarat, Uttaranchal and parts of Himachal Pradesh, Jammu and Kashmir, East Uttar Pradesh, and south Rajasthan. The cumulative rainfall for the subcontinent was 4% above average at the end of June. The monsoon failure was the result of a widespread and persistent break during July, as can be seen in the daily rainfall totals in Fig. 81, with July 2002 all-India rainfall the lowest on record at 49% below the long-term average.

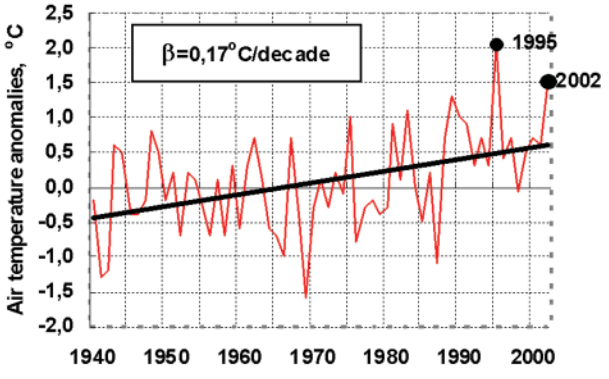

Fig. 76. Mean annual air temperature anomalies for Russia (with respect to a 1961–90 normal).

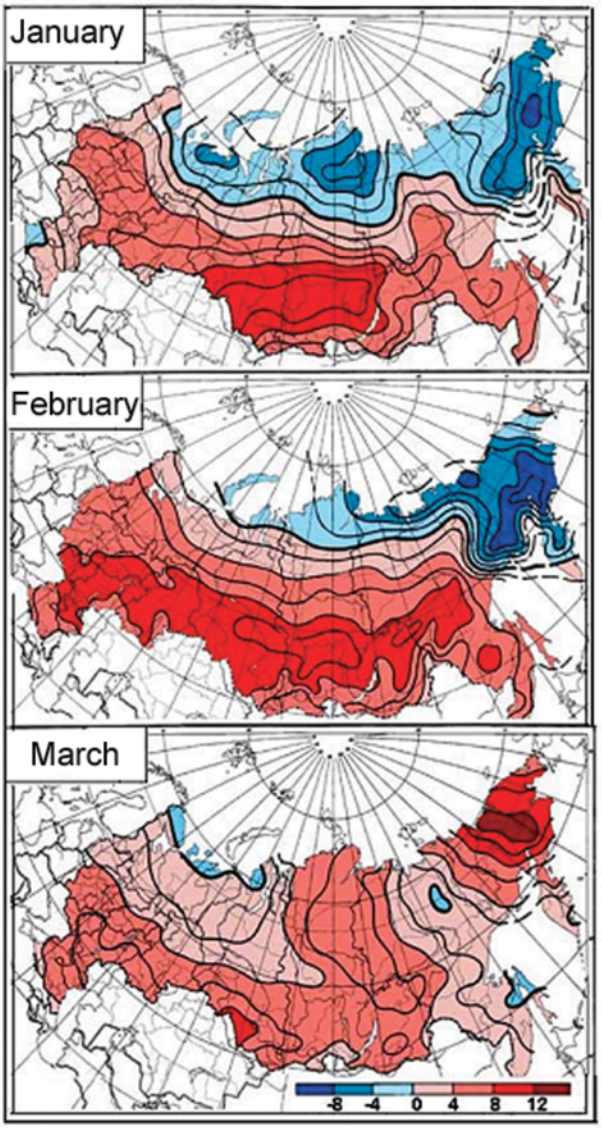

FIG. 77. Temperature anomalies (in degrees Celsius) across Russia for (a) Jan, (b) Feb, and (c) Mar.

Rainfall dropped off dramatically during the first half of July across all but northern and northeastern India. A low pressure area formed in the Bay of Bengal on 15 July and broke the dry spell in many parts of the country. However, the monsoon activity was not sustained and by the end of July virtually the entire country (except the far northeast) was facing substantial rainfall deficits (up to 76% in West Uttar Pradesh). The combined June–July deficiency for all-India (Fig. 82) was 30%, which also has few historical parallels. The monsoon did not advance fully across India until 15 August, a full month later than normal.

Unlike previous drought years, monsoon activity returned in August and September, lessening the damage in the central parts of the country. However, the northwest, a semiarid region whose monsoon season is critical because it is short, has suffered through drought in 2 of the 3 years prior to the 2002 season. The multiyear failure of monsoon rains there has exacerbated the problems of already stressed rainfed agriculture, water systems, and food security in Rajasthan and neighboring states.

In stark contrast to the developing drought conditions elsewhere, torrential July rainfall across northeast India (especially in the states of Bihar and Assam), eastern Nepal, and Bangladesh resulted in severe flooding and landslides. More than 10 million people were reported to be affected with thousands of villages and several million hectares of land inundated. Although flooding is common during the summer monsoon, the 2002 events were considered the worst observed in more than a decade.

In Southeast Asia the monsoon was also erratic. A late onset followed by spotty coverage resulted in the development of drought conditions in the Central Highlands of Vietnam and much of Cambodia by the end of July. This was the second consecutive year of drought in these areas, with drought conditions in south-central Cambodia considered the worst in two decades. The lack of sufficient rainfall reduced planting of crops by as much as 50%, stressed livestock, and resulted in food shortages in some locations.

The situation generally reversed during the second half of the season as heavy rains, first developing in mid-August across northern Thailand, Laos, and Vietnam, continued into September and October. Repeated flash flooding occurred from Myanmar eastward across Laos and northern Vietnam during this period, driving the Mekong River in Central Laos to its highest level since 1966 according to reports. Flooding occurred in the Mekong Delta for the third consecutive year, with the Dong Thap Muoi (Plain of Reeds) region of southern Vietnam and southern Cambodia the most adversely affected regions. Although the flooding in the Mekong Delta resulted in numerous fatalities and widespread damage, it was not nearly as severe as that which occurred during 2000.

iii) China floods, drought, and sandstorms—S. Lyon,[5] and S. J. Camargo[5]

During 2002, flooding in central and southern China along the Yangtze River was the most severe since the devastating floods of 1998. Areas of the country not as prone to flooding were also affected, including parts of the usually arid Xinjiang province in northwestern China and in the mountainous terrain of the Shaanxi province. Meanwhile, drought in sections of eastern China stressed agriculture and limited water supplies (Fig. 83).

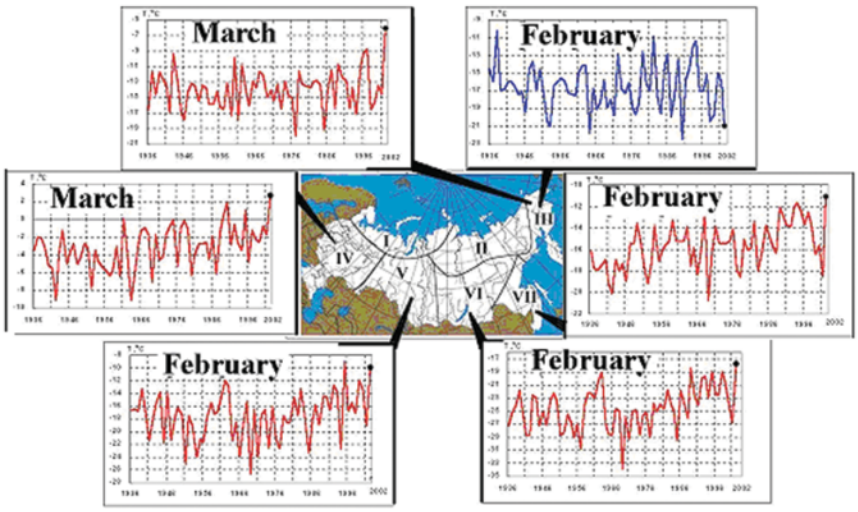

Fig. 78. Mean monthly air temperatures averaged over the zones' areas.

The summer rainy season began about a month early in many areas as unusually heavy precipitation began in mid-April in the central and eastern Yangtze River basin as well as portions of Xinjiang province in the northwest where some locations received more than 60% of their annual average precipitation by May. As heavy rains continued through June severe flooding developed in many areas of central and southern China, especially in the southern Shaanxi, Guizhou, Hunan, Jiangxi, Sichuan, and Hubei provinces, leading to hundreds of fatalities and millions of dollars in damage to infrastructure. In the Shaanxi province, south of the city of Xian, over 480 mm of rain fell in only a few days during early June with tens of thousands of homes destroyed and over 500,000 people affected. In the Hubei province to the southeast, up to 30% of the cotton crop was destroyed and replanted according to the Foreign Agricultural Service of the U.S. Department of Agriculture (USDA).

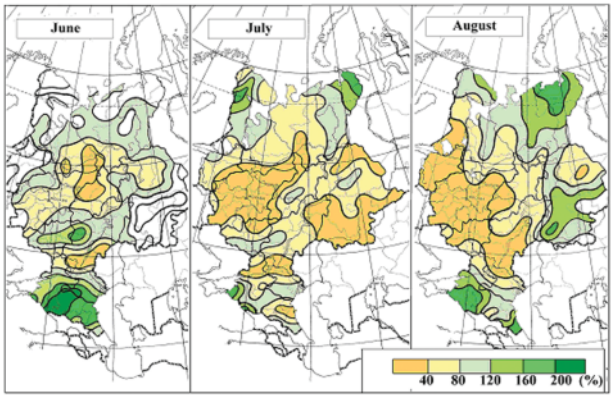

Fig. 79. Relation of monthly precipitation totals to normal over European Russia.

Although dry spells punctuated the heavy rains as the season progressed, above-average July and August precipitation totals, partially the result of tropical storm activity, caused swollen rivers to fill China's two largest freshwater lakes, Donting and Poyang, to near overflowing. The hundreds of miles of dykes that surround the lakes held, however, preventing catastrophic floods from affecting the more than 10 million people who lived in surrounding low-lying areas. According to China's Ministry of Civil Affairs, by the end of the rainy season more than 100 million people were affected by flooding with over 1500 fatalities reported and economic losses estimated at more than 4 billion U.S. dollars.

While floods gripped central and southern China, sections of the northeast saw a return of drought conditions, in some areas for the third consecutive year. Especially affected were eastern portions of the Yellow River basin in the provinces of Shandong, Hebei, and Shanxi (Fig. 83). Unusually warm and dry conditions during spring stressed winter wheat crops in the sections of the North China Plain and by the end of August some locations in the Shandong province had received only half of their average rainfall. The upper part of Nansi Lake, one of Shandong's major reservoirs, was reported to be completely dry while other water reserves dropped to below half their normal levels leaving

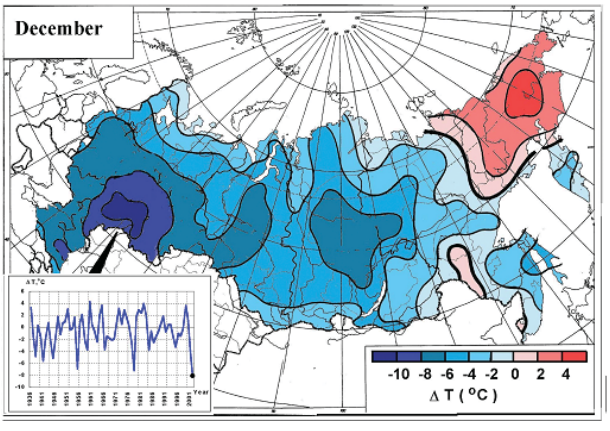

Fig. 80. Air temperature anomalies in Dec 2002. Temperature anomalies averaged over the area of zone IV (center and the south of European Russia) are at the lower left of the figure.

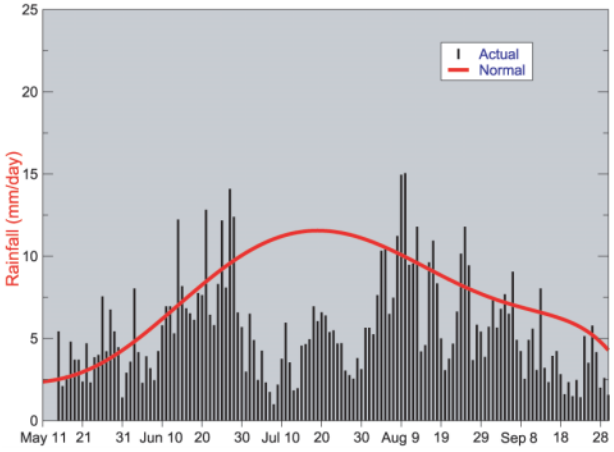

FIG. 81. The 2002 all-India daily rainfall (bars) and climatological rainfall for the period 1961–90 (red line). Source: Monsoon Online (MOL) Web site www.met.rdg.ac.uk/cag/MOL with kind permission from Dr. K. Rupa Kumar and Dr. D.B. Stephenson.

more than 1 million people facing severe water shortages. One-third of the farmland in the Hebei province faced severe water shortages by the end of August.

Land degradation and desertification are major concerns in northern and western China with a recent report from China's State Forestry Administration indicating that in the 5-yr period 1994–99 desert areas in northern China increased by over 1.5%. Fueled in part by this trend and a protracted drought in much of semiarid southern Asia, one of the worst sandstorms in more than a decade swept across northern China in March 2002. Visibility in some locations was reduced to 50 m with the 12 million residents of the city of Beijing most acutely affected. The government of China has recently pledged almost 7 billion U.S. dollars in an effort to combat the desertification problem.

iv) Central Southwest Asia drought—B. Lyon[5] and S. J. Camargo[5]

The multiyear drought, which first developed during 1998–99 in much of central Southwest Asia, eased somewhat during 2001–02 with the return of snow and rainfall in some sections (Fig. 84). The region that has been most adversely affected by the prolonged drought extends from Iraq eastward to Pakistan and northward into Tajikistan and Uzbekistan in the former Soviet Union. This area is semiarid to arid and receives the majority of its precipitation during the boreal winter season from November to April. Precipitation falls mainly in the form of snow in the mountains with rainfall typically occurring at lower elevations.

Although precipitation was improved from recent years, it remained erratic during the 2001/02 season. Satellite estimates suggested somewhat enhanced snow cover compared with the past few years in the Hindu Kush of Afghanistan, although field studies by various organizations reported amounts generally remained below their long-term climatological values. However, significant snowfall was observed in the mountainous areas of central and western Iran during December 2001 and January 2002 with heavy rains and flash flooding reported at lower elevations. The com-

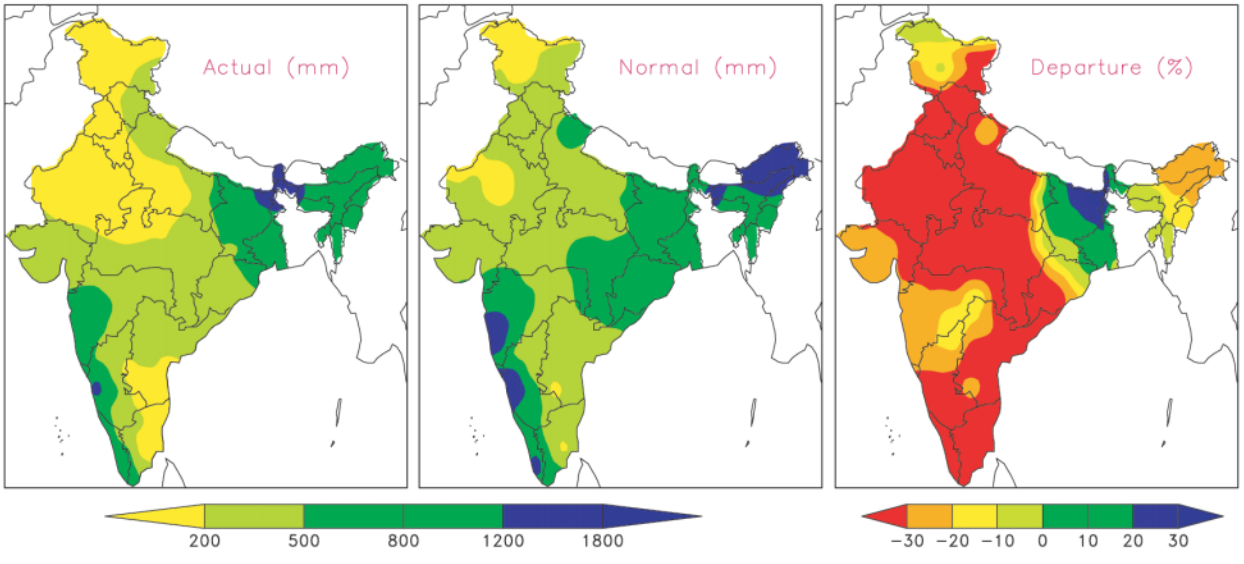

FIG. 82. Rainfall for the period 1 June–31 July: (left) observed 2002, (middle) climatological for the period 1961–90, and (right) percent departure from normal. Source: Monsoon Online (MOL) web site www.met.rdg.ac.uk/cag/MOL with kind permission from Dr. K. Rupa Kumar and Dr. D.B. Stephenson.

bination of above-average temperatures and early snowmelt, substantial rainfall, and hardened ground desiccated by prolonged drought resulted in more serious and widespread flash flooding during March and April of 2002 in parts of northern Afghanistan, Tajikistan, and central and southern Iran. With the return of rainfall in 2002, Tehran's water authority lifted its rationing program for drinking water in the capital. Thirty cities in Iran had enacted water rationing the previous summer due to the continuing drought. Crops rebounded in many areas, particularly in Uzbekistan and Iran during 2002, but drought conditions persisted from southern Pakistan westward through southern Afghanistan and into eastern Iran (Fig. 84a). The Sistan wetlands along the Iran–Afghanistan border remained nearly dry at the end of 2002 due to continuing drought conditions there. Even with the return of normal precipitation in all of the drought-affected areas, authorities expect impacts from the severe and protracted drought to continue for years to come.

g. Australasia and the South Pacific—A. Watkins[16] and J. Salinger[14]

i) Australia

The Australian climate of 2002 reflected the contrasting states of the ENSO. The ENSO state remained neutral from January through April and the Indian Ocean was warmer than normal (and remained so for most of 2002), just as it had been since early 2001. Rainfall for the period was generally near normal, with some regions of below-median rainfall in coastal and central Queensland, as well as southern South Australia, and above-average rainfall totals in the center and northern Western Australia.

As the ENSO state began approaching warm conditions in the austral autumn (May), below-normal rainfall totals began to affect much of the continent. Above-normal maximum temperatures were also observed in most locations.

As a result, Australia's winter was its seventh driest on record, as well as having its highest mean maximum temperature, and its largest diurnal temperature range on record (high-quality temperature records date back to 1950; high quality rainfall records date to 1900). Likewise, both spring and autumn also experienced record all-Australia mean maximum temperatures by considerable margins. During the eight months from March to October, which includes Australia's main crop growing season, 71% of Australia had rainfall below the 10th percentile (Fig. 85). In all, 98.7% of the continent received below-median rainfall for this period, with dry conditions exacerbated by high temperatures.

Annual rainfall values showed 2002 was Australia's fourth driest on record. Maximum temperatures, Australia-wide, were the warmest on record, while minimum temperatures were just below normal.

Australia's annual mean maximum temperature was 1.22°C above normal, compared with the previous highest anomaly of +0.91°C in 1980. Reduced cloudiness resulted in overnight temperatures being close to average with the Australian mean minimum temperature only 0.01°C below normal. Consequently, the overall Australian annual mean temperature was 0.61°C above the 1961–90 normal (Fig. 86), making 2002 Australia's fifth warmest year on record since 1910 (the period for which all-Australian averages are sufficiently reliable for use as a basis for comparison).

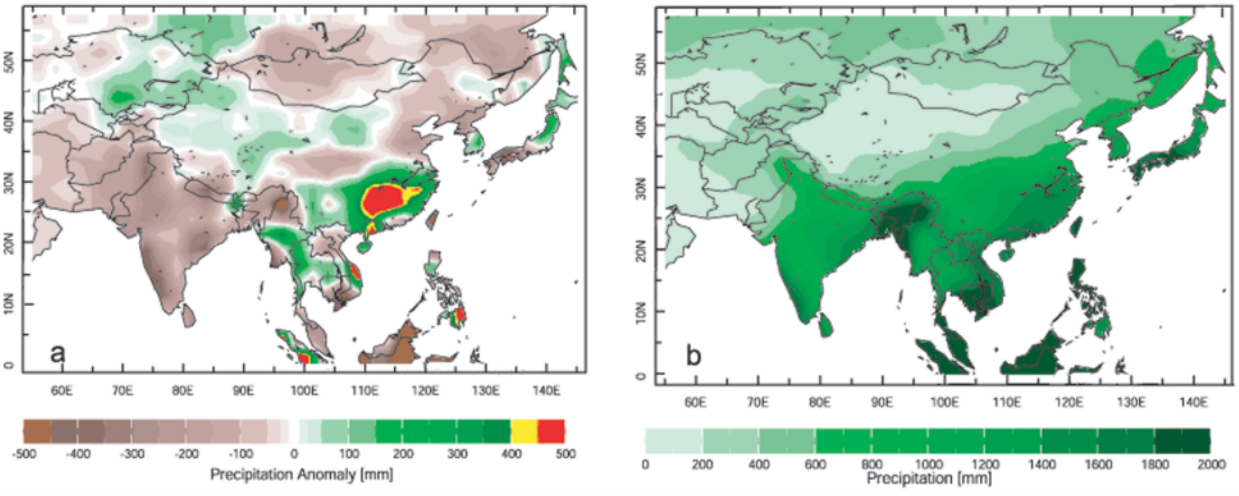

Fig. 83. (a) Annual precipitation anomaly (mm) for 2002, and (b) climatological precipitation (mm). Base period 1979–2002. Data from CPC, CAMS_OPI.

(i) January–March: A varied start to 2002

Rainfall totals were above average over much of the country during the first two months of the year. The exceptions were southeastern Queensland, South Australia near the Flinders Ranges, and parts of the Gascoyne region of Western Australia. In parts of central Western Australia, the highest rainfall totals on record were brought by Tropical Cyclone Chris, which briefly reached category-5 intensity. Heavy monsoonal rains over northern Queensland through to northwestern Australia brought as much as 400–500 mm within a week during mid-February. The Fitzroy River in northwestern Australia was said to have reached its highest-ever recorded water level early in the 4th week of February. March, however, saw average to dry conditions for most of the continent.

For parts of New South Wales, rains in February followed an exceptional period of bushfire activity which started in late December 2001 and continued until the second week of January. The "Black Christmas" fires burned over half a million hectares, with significant property (170 homes lost) and livestock losses resulting in damages costing nearly 45 million U.S. dollars. This is on top of the $40 million dollars spent in fighting the fires.

The bushfire period was heightened by unusually warm conditions over the northern half of New South Wales and Queensland in January and February, with maximum temperature anomalies reaching +2° to +3°C in places. In contrast, unusually cool conditions over south-central Australia saw maxima 2°–3°C below average over southwestern Victoria during January, and reaching 5°–6°C below average over inland Western Australia in February. These temperature anomalies were consistent with the persistent mean sea level pressure pattern for the first two months, which saw a center of high pressure located to the southwest of Western Australia directing cool onshore westerlies into the southern states, and hot dry westerlies into New South Wales and Queensland.

This synoptic pattern broke down in March with anomalously high pressure over the western half of the continent. As a result, minimum temperatures remained below average over most of the country, whereas maximum temperatures were slightly above average in most areas, reflecting to some degree the drier conditions for central and northeastern Australia.

(ii) April–December: Dry and warm conditions for the crop and pasture growing season

The dry conditions of March continued into April and May, the start of the Australian winter crop growing season, resulting in well below-average autumn (MAM) rainfall. In Tasmania, autumn 2002 was one of the driest on record, with record-low totals in parts of northwestern Tasmania. The dry conditions during autumn were associated with the tendency for large anticyclones to remain near their summertime location (latitudes 36°–40°S) rather than over the continent itself. Hence westerlies that would normally bring rainfall and cooler conditions to the southern states in the latter part of autumn had a reduced impact. This was particularly noticeable in southern Western Australia, where Perth reached 34.3°C on 1 May—their warmest May day on record (previous record, 32.4°C on 2 May 1907).

In contrast to the preceding months, April and May were exceptionally warm over most of the country. Maximum temperature anomalies from +3° to +5°C occurred over central Australia in April, and over

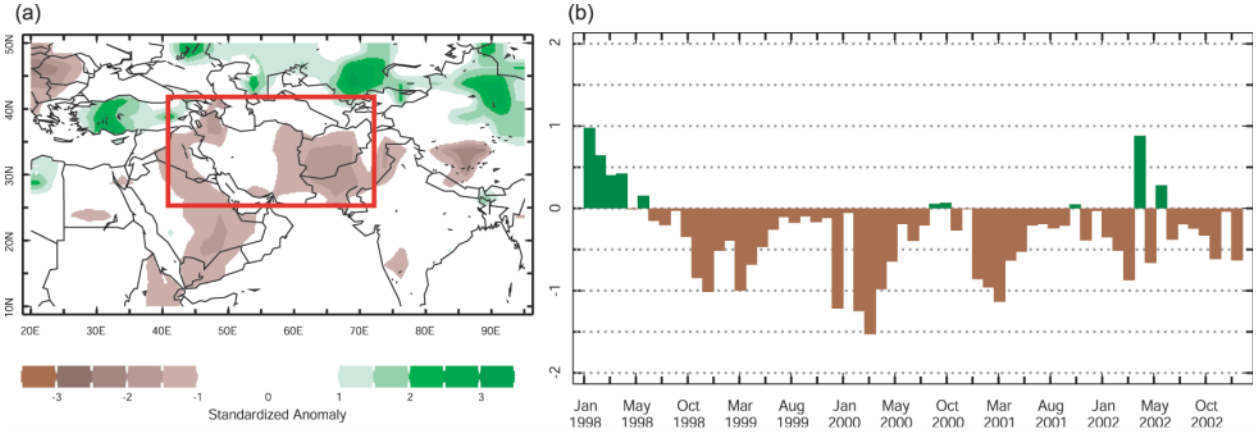

FIG. 84. (a) Average of monthly standardized precipitation anomalies for 2002 and (b) monthly time series of standardized precipitation anomalies for Jan 1999–Dec 2002 averaged over the region within red box in (a). Base period 1979–2002. Data from CPC, CAMS_OPI.

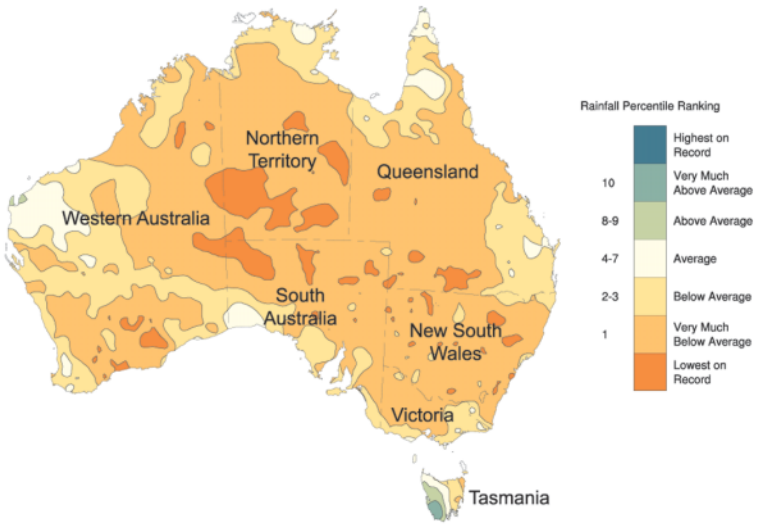

Fig. 85. Australian rainfall deciles for Mar to Oct 2002.

Western and central Australia in May. Many locations in central Australia, some with more than 60 yr of record, experienced record warmth in one or both of these months. For instance, Alice Springs Airport registered a mean April maximum of 33.3°, nearly 2°C more than the previous record in 1914, followed by a near-record mean maximum of 26.9°C in May.

By mid-June, most indicators suggested an El Niño was well established in the equatorial Pacific (see also section 4a). Over Australia, dry conditions persisted, with below average rainfall for the month experienced for the majority of New South Wales, Queensland, Northern Territory, South Australia, and Western Australia.

The dry conditions of autumn and early winter continued from July to October, with exceptionally low rainfall totals over much of southeastern Australia and practically all of inland Western Australia. For the 7-month period from April to October, (Australia's winter crop and pasture growing season), rainfall below the 10th percentile was recorded over 69% of the continent (Table 2). This is the greatest areal extent of such deficiencies for any 7-month period on record, and is followed by April–October 1946 (61.9%) and November–May 1902 (56.4%). The mean percentile value for Australia for April to October 2002 was 10, also the lowest on record for this period. In total, 98.1% of the continent had experienced below-median rainfall during the period.

For the total dry period for 2002 (March–December), 97.3% of the Australian continent experienced below-median rainfall, with 61% of the country in the lowest 10% of recorded totals (i.e., decile 1; Tables 2 and 3). This was the second largest area of decile-1 rainfall for any 10-month period on record, only marginally less than the area of the 1901/02 "Federation Drought" at its peak (Table 3). The mean percentile for the total dry period was 11.

Extremely hot conditions became established over northern Western Australia between 19 and 24 October, with some regions experiencing temperatures above 45°C on several successive days. On 21 October, Mandora in the state's northwest reached the highest October temperature ever recorded in Australia, with 46.7°C. This record was short-lived, however, with Port Hedland registering 46.9°C on the following day.

Overall, minimum temperatures were as much as 2°–4°C below average in each month from May to August, while maximum temperatures were 2°–3°C above average over a broad area of central and inland eastern Australia. This contrast reflected the clear skies over most of the country, and the unusually dry conditions over the interior.

These extremes translated to record Australia-wide temperature anomalies. In autumn the all-Australia maximum temperature anomaly was +1.83°C, the highest on record and eclipsing the previous record by +0.44°C (high-quality all-Australia seasonal temperature records commence 1950). Likewise, winter all-Australia maximum temperatures were 1.41°C warmer than normal, again the highest on record. This record was 0.45°C higher than the second ranked value (1996), with ranks 2–4 being separated by only 0.06°C.

The nine months from March to November had an all-Australia maximum temperature anomaly of +1.65°C, the warmest on record for this three-season period, eclipsing the previous record by an incredible +0.63°C (Fig. 87). Although minimum temperature anomalies were close to normal for the period (+0.07), they still exceeded the previous El Niño years with widespread Australian drought (1982 and 1994). The record value for the March–November all-Australian maximum temperature is consistent with the warming trend observed in annual data since 1910.

(iii) Wider impacts

The impact of the dry and warm conditions upon Australia's total winter crop (wheat, barley, canola, winter pulses) was large. The Australian Bureau of Agricultural and Resource Economics estimated only 16.2 million tons would be harvested, 21 million tons less than the previous years crop, the smallest harvest

Table 2. Australia-wide rainfall statistics. Data from 1900 to 2002 inclusive.

Averaging period	Area in decile 1	Mean percentile	Area below median
April–October	69%	10	98.1%
March–October	71%	9	98.7%
March–November	62%	11	98.4%
March–December	61%	12	97.3%
Jan–Dec (annual)	36%	26	81.7%

since 1994–95 (13 million tons). The area sown to summer crops was estimated to drop by 41% in 2002–03, with grains production forecast to be down 59% to 2 million tons. Such an outcome would make it the smallest summer crop since the drought of 1982–83.

The dry, warm conditions, accompanied by strong, gusty winds in late SON led to unusually early and severe outbreaks of bushfires in eastern New South Wales and northern Victoria. A bushfire in early October reached the southern suburbs of Sydney, and 100 fires were burning during the second week of November in New South Wales. In Victoria, the total number of fires to November was around 250, well above the 20-yr mean value of 80.

These early bushfires were but a precursor to severe bushfires that occurred in New South Wales from 4 to 9 December. Major fires near Sydney, the Blue Mountains, Shoalhaven, Taree, Cessnock, Gosford, and Eurobodella, totaled nearly 58 individual fires in all and were fanned by strong and hot westerly winds from the country's interior. Over 100,000 ha were burned but only 48 houses were destroyed. The fires were largely contained after rains fell in New South Wales on 10 December.

As observed in previous severely rainfall-deficient times (e.g., 1982), dust-storms became prominent over the interior, occurring on several days associated with the strong winds accompanying mainly dry cold fronts. This dust reached the coastal cities of Sydney and Brisbane on 23 October in a massive dust storm of over 1500 km in length, 400 km in width, and up to 2500 m deep (Fig. 88). A similar large duststorm affected Griffith, and to a lesser extent Sydney, on 13 November. Another large duststorm struck Griffith on 29 November.

ii) Southwest Pacific

As observed for Australia, the climate of the Southwest Pacific reflected to a large degree the state of the ENSO. Between January and May, the South Pacific convergence zone (SPCZ) was active and south of its climatological position, particularly in the west. Despite the neutral ENSO state, this is a situation somewhat more typical of La Niña events. Correspondingly, the rainfall in the northern Southwest Pacific nations was normal to dry during these times, and regions in the southwestern Southwest Pacific were normal to wet.

With the onset of warmer SSTs in the central equatorial Pacific in May, and the weakening of near-equatorial trade winds in June, the transition to a warm ENSO state was soon reflected in the rainfall patterns of the Southwest Pacific. Regions in the north rapidly shifted to well above average rainfall. In September, parts of Kiribati received over 1200% of their normal monthly rains. Conversely, the southern Southwest Pacific region became dry, with parts of New Caledonia and the southern Cook Islands receiving below 50% of their monthly rainfall during several of the post-May months. The climate pattern changed from a dry northern Southwest Pacific in the early months of 2002, to a wet northern Southwest Pacific and a dry western and southern Southwest Pacific later in the year, which reflected the change from neutral to warm ENSO conditions in the equatorial Pacific.

Table 3. Comparison of all 10-month rainfall periods for the total Australian area in decile 1. Area of Australia: 7.8 million km^2.

Start year	Start month	End month	Area in decile 1
1901	11	8	61.2%
2002	3	12	60.8%
1982	5	2	60.3%
1901	10	7	60.2%
1901	9	6	58.2%
1901	12	9	57.0%
1982	4	1	54.1%
1902	2	11	54.0%
1902	1	10	53.0%
1901	8	5	51.6%

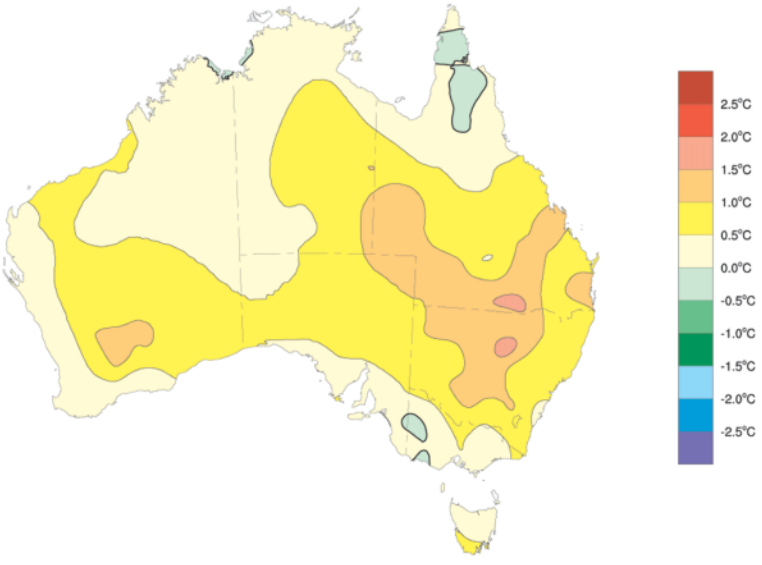

Fig. 86. Australian mean temperature anomaly for 2002.

As with the previous Southwest Pacific tropical cyclone (TC) season, the 2001/02 season was relatively inactive. Only five TCs occurred, beginning at the end of November and lasting only until early March. This is about half of the normal frequency. However, the year began with Tropical Cyclone Waka devastating the Vava'u Island group in northern Tonga on New Year's Day 2002. Sustained winds were estimated at 100 kt with gusts of up to 140 kt. An estimated 60% of all buildings were damaged, with total damages estimated to be in excess of $50 million (U.S.). The Southern Hemisphere's strongest TC of the year, and arguably the strongest cyclone ever recorded in the Southwest Pacific region (Hall and Callaghan 2003), category-5 Tropical Cyclone Zoe (Fig. 89), passed through the islands of Tikopia, Fataka, and Anuta, located 1000 km southeast of the Solomon Islands capital, Honiara, on 28 December. At its peak, winds were estimated to average 290 km h^{-1} with maximum gusts to 350 km h^{-1}, seas to 11 m and accompanying large storm surge. Although crops and some housing were destroyed, no human casualties were reported, largely due to traditional knowledge of how to survive such strong storms. Heavy rains over the mountainous regions of Java and Sumatra, Indonesia during the last week of December resulted in flash flooding and mudslides. At least 13 people died and an estimated 365,000 inhabitants were displaced from their homes.

(i) January–May: Near-normal conditions

The year 2002 began with dry conditions over much of the Southwest Pacific, with below-normal January rainfall in most regions except for those lying beneath the southward-shifted SPCZ (i.e., Fiji and New Caledonia). Driest conditions occurred in Kiribati and most nations east of the date line. The dry conditions in the east, coupled with warmer than normal local SSTs, led to some record maximum temperatures in French Polynesia during February.

In February, the SPCZ returned to near its normal location west of Rotuma (far northern Fiji), but remained south of its climatological position west of Rotuma, leading to higher than normal rainfall in a line from Tuvalu through Fiji to Tonga. Increased convection along the equator also brought increased rainfall totals for Indonesia, Papua New Guinea, and parts of Kiribati. Late January and early February brought the most active MJO phase of the season to Indonesia. The resulting heavy rains in Java (including the capital Jakarta), west Kalimantan and northern Bali flooded thousands of homes, killed at least 125 people, and left more than 330,000 homeless.

In contrast, lower than normal rainfall was observed in the northern Cook Islands and much of French

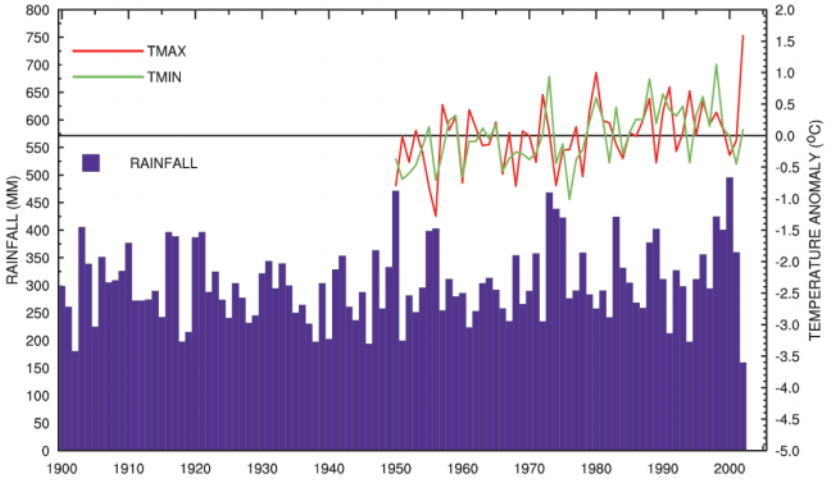

Fig. 87. All-Australia rainfall and temperature time series for the 9-month period Mar to Nov 1900–2002.

Polynesia, locations ordinarily under the mean axis of the SPCZ.

The southward shift of the SPCZ persisted into March and April. As a result, above-normal rainfall occurred in parts of New Caledonia and southern French Polynesia, and low rainfall from Tuvalu to northern French Polynesia, during March. In March a trough of low pressure over Fiji caused high winds and heavy rain that led to flooding and crop damage in northwestern Vanua Levu and western Viti Levu. A record-high rainfall total in New Caledonia (Koumac) was reported during April (341 mm, 488% of normal monthly rainfall).

Warmer than normal SSTs in April (anomalies above +1°C) in a band from the Solomon Islands to the Southern Cook Islands, coupled with enhanced convection, led to well-above-normal mean air temperatures for Fiji and central French Polynesia. The positive SST anomalies in the vicinity of Fiji remained in place until late July, resulting in near-record-high mean temperatures (Fig. 90). In May, the SPCZ remained south of its normal location west of the date line, but north of normal to its east. Maximum temperature records were set in Fiji at Rotuma and Tokotoko (33.3° and 31.7°C, on 9 and 11 May, respectively), while cloud amounts remained low over western Kiribati. In the northern Southwest Pacific, rainfall for western Kiribati and Tuvalu remained below normal. New Caledonia also experienced dry conditions, while significant flooding was observed in the western parts of Vanua Levu (Fiji).

(ii) June–December: El Niño climate patterns dominate

With the passing of an exceptionally strong westerly wind burst in mid May, the near-equatorial trade winds weakened considerably in June. A farther westerly wind burst impacted upon Fiji and western Kiribati at the end of June. By July, the SPCZ, although remaining marginally south of its climatological position, was weak and extended little farther east than Samoa. However, above-normal rainfall was observed for Fiji, Samoa, and Tonga, which all had individual locations with over 200% of their normal rainfall for the month.

In July, SSTs in the vicinity of Kiribati (and the central equatorial Pacific in general) rose to over 1.5°–2.0°C above normal, and remained that way through the August–October period. Correspondingly, the SPCZ started shifting northward, becoming slightly north of its climatological position by September.

As a result, convection occurred from August to October in the equatorial region from Nauru through to Kiribati, resulting in well-above-normal rainfall totals in the northern South Pacific. Kiritimati and Kanton Island had 1488% and 1220% of their normal September rainfall (mean September rainfall, 36 and 27 mm, respectively), a record high in both locations.

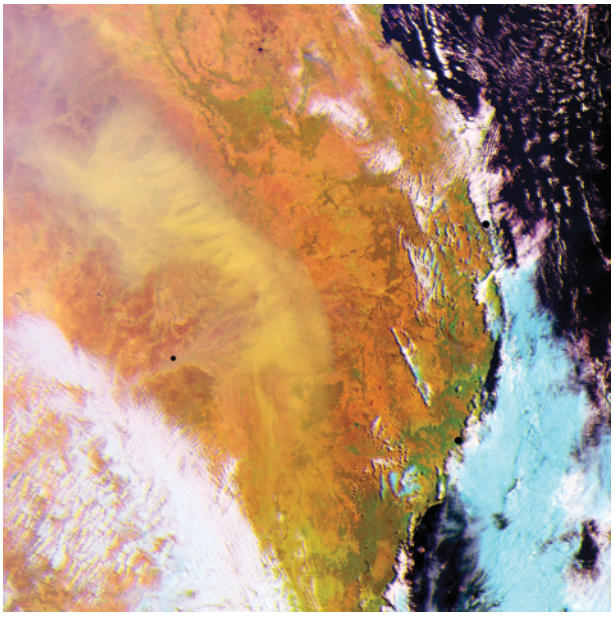

Fig. 88. The east Australian dust storm of 23 Oct 2002. Image produced by the Bureau of Meteorology from data collected by the Chinese weather satellite FY-1D.

In stark contrast to the pattern of extremely wet conditions in the northern Southwest Pacific from August to October, the western and southern Southwest Pacific was drier than normal during the same period. Below-average rainfall was recorded in Indonesia, Papua New Guinea, New Caledonia, Tonga, Niue, and the Southern Cook Islands. In the western Coral Sea, Willis Island recorded 15 consecutive months through October with rainfall below 75% of the monthly average. Fiji reported very dry conditions in its southern and western regions during October, despite the continuation of strong southeasterly winds that had affected the nation since June. Fiji typically experiences a lagged impact from El Niño events, and 2002 appeared to be no exception. In New Caledonia, rainfall was well below average for the period from June to December. Rainfall for the period from SON was only 29% of normal. Farmers were forced to feed hay to cattle as grass became unavailable, and bushfires occurred in most parts of the islands. The dry conditions also brought wildfires to Indonesia, with thick smoke haze covering Sumatra and the Malaysian peninsula during October.

Overall, the pattern of a wet northern, equatorial Southwest Pacific and a dry southern and western Southwest Pacific is typical of that experienced during a warm ENSO phase.

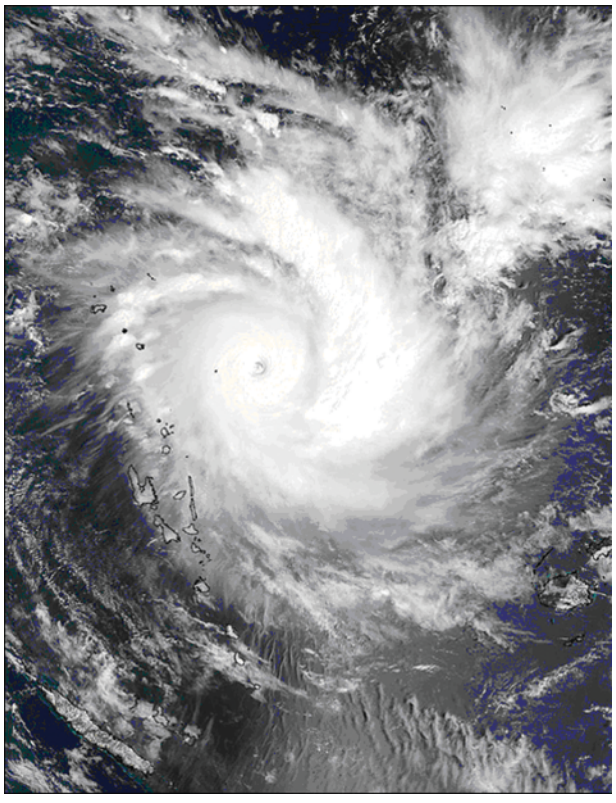

Fig. 89. Category 5 Tropical Cyclone Zoe, northeast of Vanuatu, 27 December 2002. Ten-minute average winds at this time were 125 kt. Image courtesy Jeffrey Schmaltz, MODIS Land Rapid Response Team at NASA GSFC, available from: http://earthobservatory.nasa.gov/NaturalHazards/.

iii) New Zealand

More depressions than normal formed between the Chatham Islands and New Zealand giving many areas in New Zealand a variable and windy year with many climate extremes. Seas around New Zealand remained warmer than normal from January to April and this period was dominated by below average pressures over the North Island and northern South Island. Above-average pressures prevailed over the Southern Ocean often centered south of Tasmania. The period from May to December was largely influenced by El Niño. Well-below-average pressures were dominant east of the Chatham Islands and slightly above-average pressures occurred in the north Tasman Sea resulting in windier conditions with persistent westerly and southwesterly winds predominant over New Zealand.

Rainfall in 2002 was well below normal in the northeast with the Bay of Plenty receiving less than 70% of the annual average precipitation. Rainfall was also below average in eastern Northland, Waikato, southern Waiarapa, Nelson, and Marlborough. Significant soil moisture deficits had developed in Northland, Bay of Plenty, eastern Marlborough, south Canterbury, and North Otago by the end of the year. It was wetter than average in Wanganui, coastal Southland, Fiordland, and the area near and about Christchurch.

The 2002 national average temperature was 12.5°C, which is similar to the 1961–90 average. For New Zealand as a whole, there were five warmer than average months (May, June, August, September, and December), of which June was exceptionally mild for early winter and contrasted three cooler than average months (February, October, and November). February and October were much cooler than usual.

One of the most notable severe weather events in New Zealand was the largest snowfall for many years in mid-Canterbury and inland Otago during June, leaving hundreds of travellers stranded, and thousands of homes without power. A few days later, the system brought high winds, intense rainfall, and flooding to many northern and western areas. In July, the Waikato River overflowed at Mercer flooding many nearby farms already saturated by weeks of wet weather. For the year, there were at least a dozen heavy rainfall and flood-producing events. There were also three periods with snow at low levels in parts of the South Island in late autumn and winter, followed by damaging spring frosts in some eastern areas. At least five severe hailstorms, two with hailstones the size of golf balls, damaged fruit crops, and significant soil moisture deficits had developed by the end of the year in the east of the South Island.

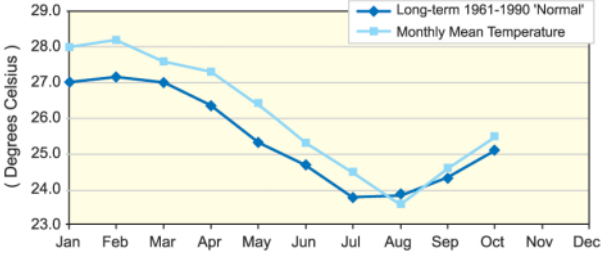

Fig. 90. Monthly average daily mean Fiji temperature for 2002.

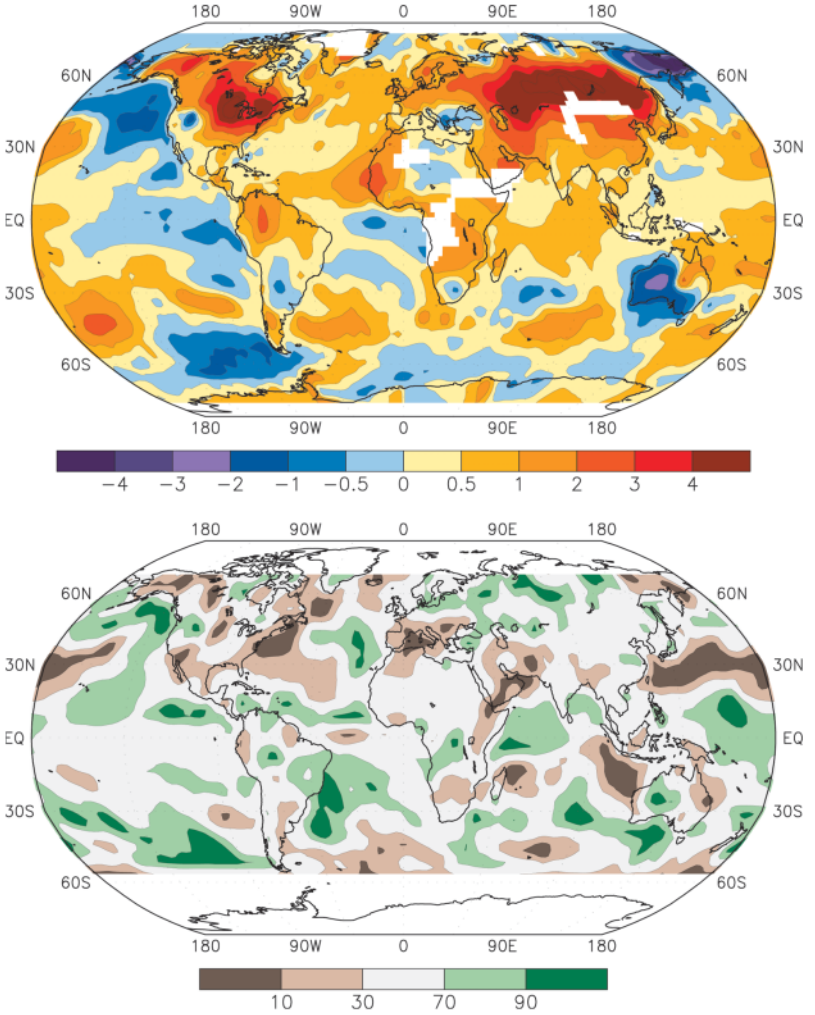

FIG. 91. Dec 2001–Feb 2002 (top, °C) surface temperature anomalies and (bottom) precipitation percentiles based on a gamma distribution fit to the 1979–2000 base period. Temperature anomalies (1971–2000 base period) are based on station data over land and sea surface temperature over water. Precipitation data are obtained from a merge of rain gauge observations and satellite-derived precipitation estimates (Janowiak and Xie 1999). The analysis is omitted in data-sparse regions (white areas).

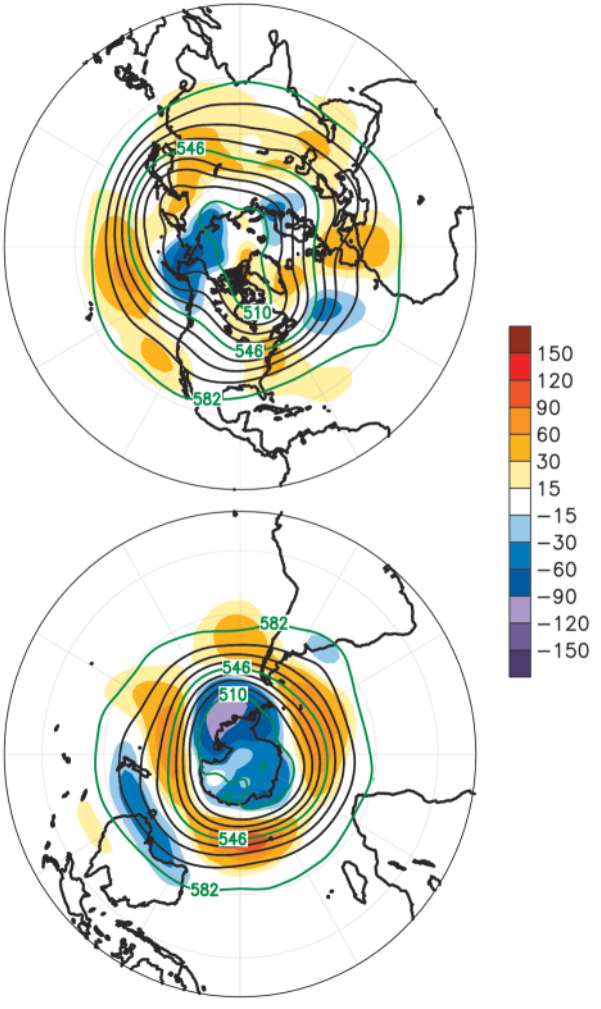

FIG. 92. Dec 2001–Feb 2002 (top) Northern Hemisphere and (bottom) Southern Hemisphere 500-hPa geopotential heights (contour interval is 9 dam) and anomalies (shading). Anomalies are departures from the 1979–2000 base period means.

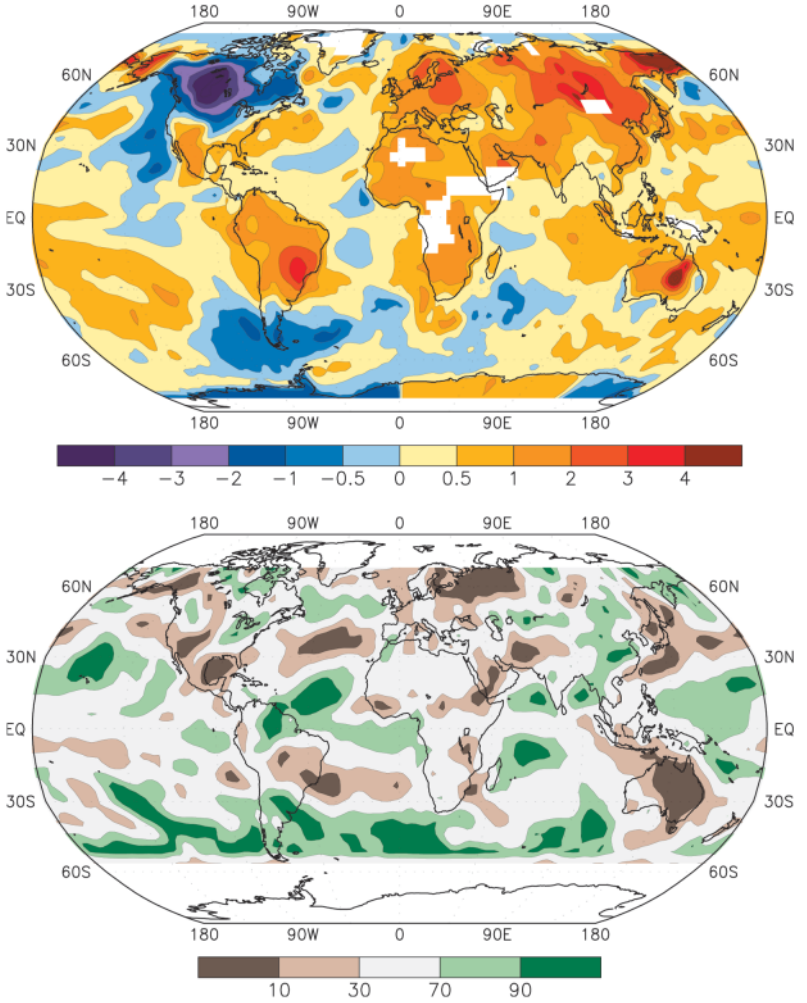

Fig. 93. Mar–May 2002 (top, °C) surface temperature anomalies and (bottom) precipitation percentiles based on a gamma distribution fit to the 1979–2000 base period. Temperature anomalies (1971–2000 base period) are based on station data over land and sea surface temperature over water. Precipitation data are obtained from a merge of rain gauge observations and satellite-derived precipitation estimates (Janowiak and Xie 1999). The analysis is omitted in data-sparse regions (white areas).

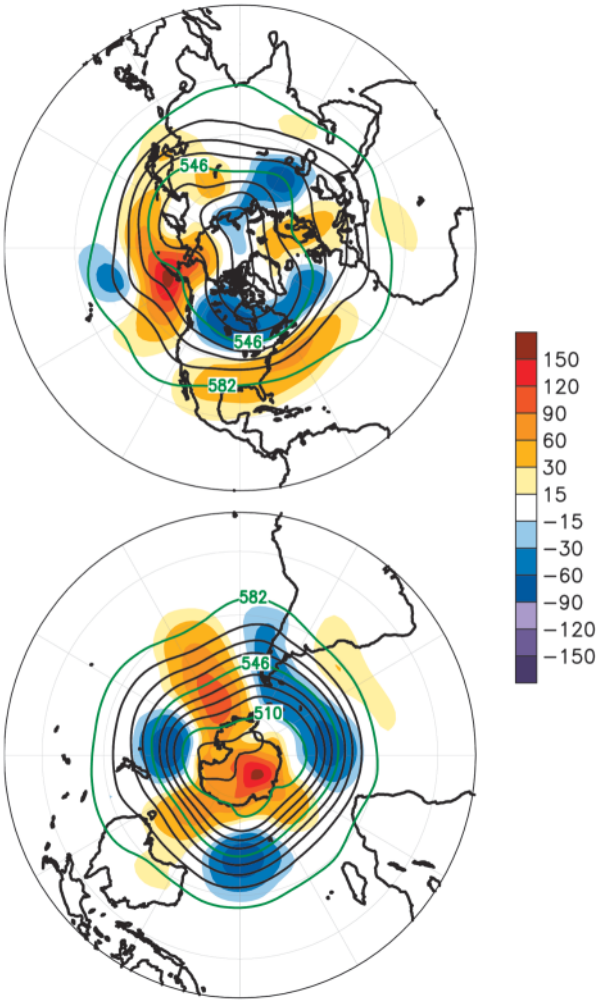

Fig. 94. Mar–May 2002 (top) Northern Hemisphere and (bottom) Southern Hemisphere 500-hPa geopotential heights (contour interval is 9 dam) and anomalies (shading). Anomalies are departures from the 1979–2000 base period means.

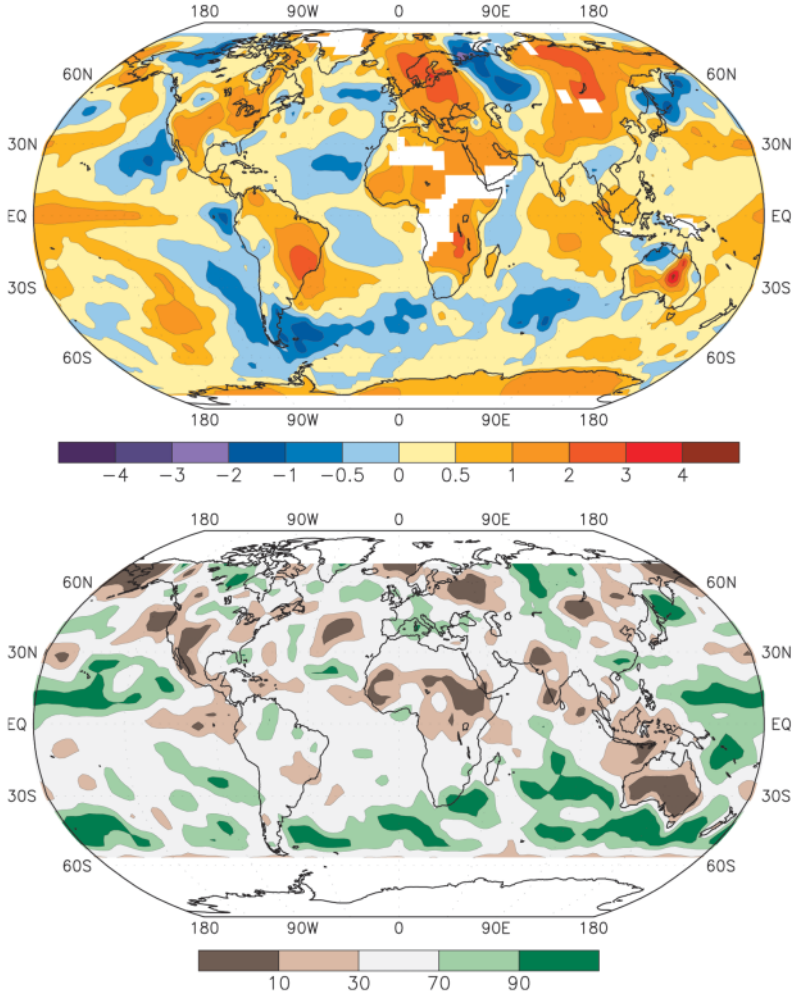

FIG. 95. Jun–Aug 2002 (top, °C) surface temperature anomalies and (bottom) precipitation percentiles based on a gamma distribution fit to the 1979–2000 base period. Temperature anomalies (1971–2000 base period) are based on station data over land and sea surface temperature over water. Precipitation data are obtained from a merge of rain gauge observations and satellite-derived precipitation estimates (Janowiak and Xie 1999). The analysis is omitted in data-sparse regions (white areas).

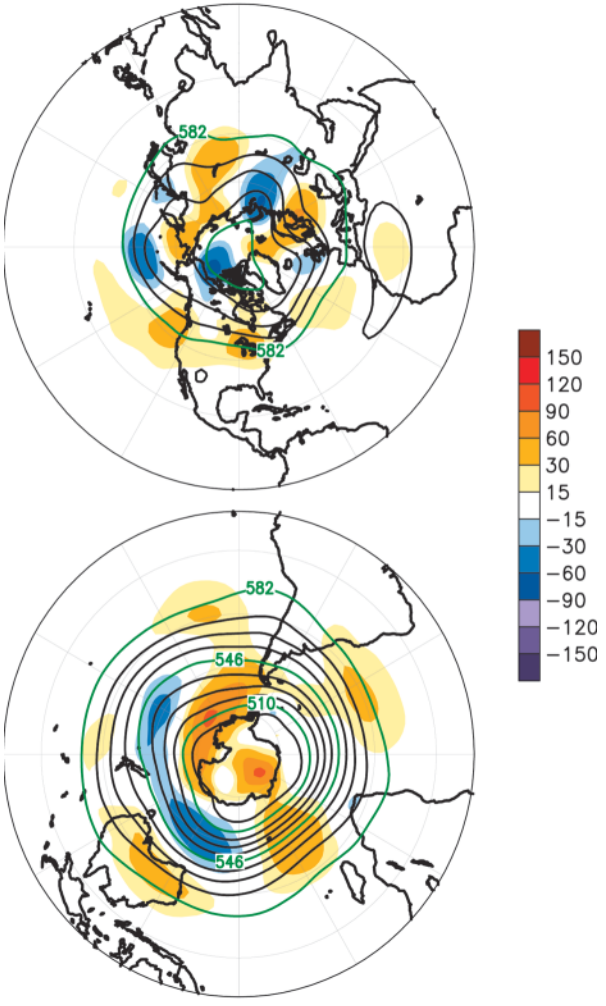

FIG. 96. Jun–Aug 2002 (top) Northern Hemisphere and (bottom) Southern Hemisphere 500-hPa geopotential heights (contour interval is 9 dam) and anomalies (shading). Anomalies are departures from the 1979–2000 base period means.

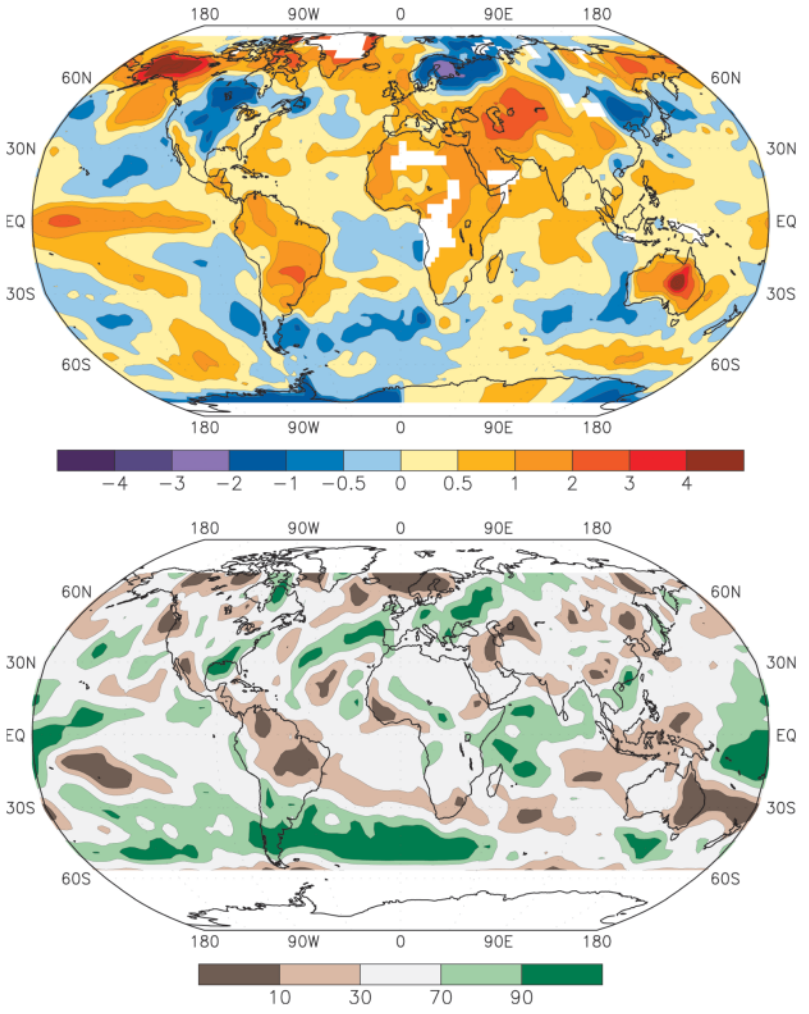

Fig. 97. Sep–Nov 2002 (top, °C) surface temperature anomalies and (bottom) precipitation percentiles based on a gamma distribution fit to the 1979–2000 base period. Temperature anomalies (1971–2000 base period) are based on station data over land and sea surface temperature over water. Precipitation data are obtained from a merge of rain gauge observations and satellite-derived precipitation estimates (Janowiak and Xie 1999). The analysis is omitted in data-sparse regions (white areas).

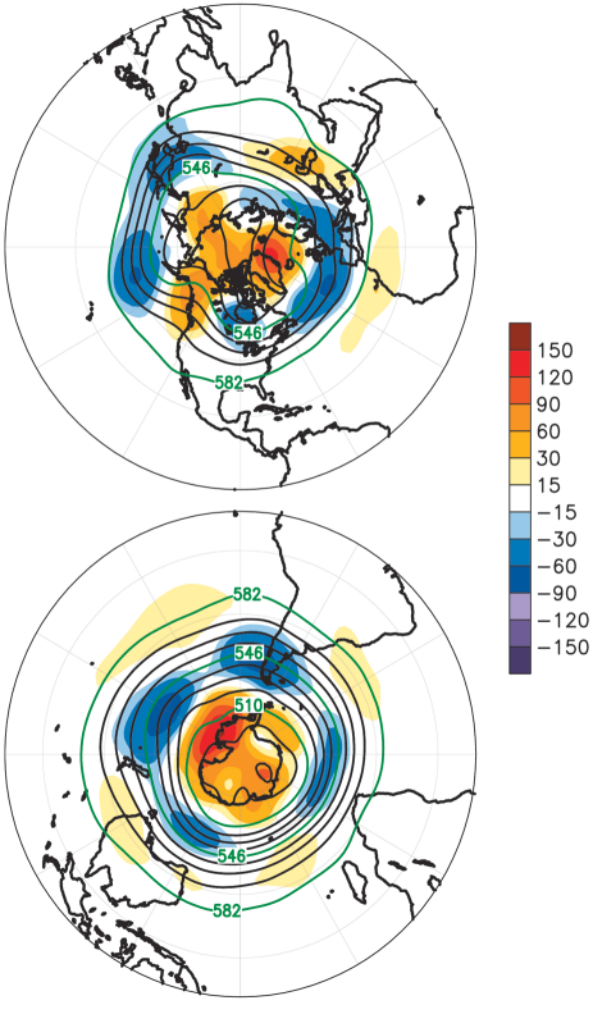

Fig. 98. Sep–Nov 2002 (top) Northern Hemisphere and (bottom) Southern Hemisphere 500-hPa geopotential heights (contour interval is 9 dam) and anomalies (shading). Anomalies are departures from the 1979–2000 base period means.

ACKNOWLEDGMENTS. This assessment would not have been possible without assistance and contributions from many scientists around the world. These scientists are named in the appendix and include a broad cross-section of expertise from within the NOAA community, from other federal laboratories, from universities and from other institutions across the globe. We would like to thank them all for their timely and valuable input. We would also like to thank the anonymous reviewers whose comments and suggestions improved this article. Special acknowledgement must also be given to Sara Veasey at the NCDC for her time and graphical expertise used in preparing this document. This assessment was supported by a grant from the NOAA Office of Global Program's Climate Change Data and Detection Program.

APPENDIX: CONTRIBUTORS

National Climatic Data Center
- Scott Stephens
- Tom Peterson
- Trevor Wallis
- Richard Heim

Hadley Centre for Climate Prediction and Research
- Nick Rayner

University of Illinois, Urbana-Champaign
- Bill Chapman
- John Walsh

NOAA/Climate Monitoring and Diagnostics Laboratory/OAR
- S. Oltmans
- H. Vomel
- Z. Sherman
- S. Montzka
- J.H Butler
- T, Thompson
- D. Mondeel
- J. Elkins
- T. Conway
- P. Novelli
- D. Dlugokencky
- E. Dutton
- B. Johnson
- R. Stone

Rutgers University
- Thomas Estilow

NOAA Paleoclimatology Program
- Connie Woodhouse
- Mark Eakin
- Bruce Bauer
- Edward Gille

REFERENCES

ABARE, cited 2003: Australian Bureau of Agricultural and Resource Economics commodity estimates. [Available online at www.abare.gov.au.]

Alexander, L. V., and P. D. Jones, 2001: Updated precipitation series for the U.K. and discussion of recent extremes. *Atmos. Sci. Lett.,* doi:10.1006/asle.2001.0025.

Behringer, D. W., M. Ji, and A. Leetmaa, 1998: An improved coupled model for ENSO prediction and implications for ocean initialization. Part I: The ocean data assimilation system. *Mon. Wea. Rev.,* **126,** 1013–1021.

Bell, G. D., and Coauthors, 2000: Climate assessment for 1999. *Bull. Amer. Meteor. Soc*., **81** (May), S1–S50.

Bradley, R. S., 1990: Holocene paleoclimatology of the Queen Elizabeth Islands, Canadian High Arctic. *Quat. Sci. Rev*., **9**, 365–384.

Bruhwiler, L. M., E. S. Kasischke, E. J. Dlugokencky, and P. Tans, 2000: Boreal biomass burning during 1998 and anomalous northern hemispheric CO. *Eos, Trans. Amer. Geophys. Union*, **81**, 260.

Bureau of Meteorology, cited 2003: Australian Bureau of Meteorology Annual Australian Climate Summary Media Release. [Available online at www.bom.gov.au/announcements/media_releases/climate/change/20030106.shtml.]

Chan, J. C. L., 1985: Tropical cyclones activity in the Northwest Pacific in relation to El Niño/Southern Oscillation phenomenon. *Mon. Wea. Rev.,* **113**, 599–605.

Chia, H. H., and C. F. Ropelewski, 2002: The interannual variability in the genesis location of tropical cyclones in the northwest Pacific. *J. Climate,* **15**, 2934–2944.

Christy, J. R., R. W. Spencer, and W. D. Braswell, 2000: MSU Tropospheric temperatures: Dataset construction and radiosonde comparisons. *J. Atmos. Oceanic Tech.,* **17**, 1153–1170.

——, ——, W.B. Norris, W.D. Braswell, and D.E. Parker, 2003: Error estimates of Version 5.0 of MSU–AMSU bulk atmospheric temperatures. *J. Atmos. Oceanic Technol.,* **20,** 613–629.

Chu, P.-S., and J.Wang, 1997: Tropical cyclone occurences in the vicinity of Hawaii: Are the differences between El Niño and non–El Niño years significant? *J. Climate,* **10**, 2683–2689.

Ciais, P., J. R. Petit, J. Jouzel, C. Lorius, N. I. Barkov, V. Lipenkov, and V. Nicolaiev, 1992: Evidence for an early holocene climatic optimum the Antarctic deep ice core record. *Climate Dyn.*, **6,** 169–177.

——, P. P. Tans, and M. Trolier, 1995: A large northern-hemisphere terrestrial CO_2 sink indicated by the 13C/12C ratio of atmospheric CO_2. *Science*, **269**, 1098–1102.

Clark, J. D., and P. Chu, 2002: Interannual variation of tropical cyclone activity over the Central North Pacific. *J. Meteor. Soc. Japan,* **80,** 403–418.

Climate Prediction Center (CPC), 2002a: *Climate Diagnostics Bulletin.* V. E. Kousky and G. D. Bell, Eds., Vol. 02, No. 10, 61 pp.

——, 2002b: *Climate Diagnostics Bulletin.* V. E. Kousky and G. D. Bell, Eds., Vol. 02, No. 12, 61 pp.

Conway, T. J., P. P. Tans, L. S. Waterman, K.W. Thoning, D. R. Kitzis, K. A. Masarie, and N. Zhang, 1994: Evidence for interannual variability of the carbon cycle from the NOAA CMDL global air sampling network. *J. Geophys. Res*., **99,** 22 831–22 855.

Cunnold, D. M., and Coauthors, 2002: In situ measurements of atmospheric methane at GAGE/AGAGE sites during 1985–2000 and resulting source inferences. *J. Geophys. Res.*, **107**(D14), 4225, doi:10.1029/2002 JD001226.

Daniel, J. S., and S. Solomon, 1998: On the climate forcing of carbon monoxide. *J. Geophys. Res*., **103**, 13 249–13 260.

Dlugokencky, E. J., E. G. Dutton, P. C. Novelli, P. P. Tans, K. A. Masarie, K. O. Lantz, and S. Madronich, 1996: Changes in CH_4 and CO growth rates after the eruption of Mt. Pinatubo and their link with changes in tropical tropospheric UV flux. *Geophys. Res. Lett.*, **23,** 2761–2764.

——, B. P. Walter, K. A. Masarie, P. M. Lang, and E. S. Kasischke, 2001: Measurements of an anomalous global methane increase during 1998. *Geophys. Res. Lett*., **28,** 499–502.

Dutton, E. G., and J. Endres, 1991: Date of snowmelt at Barrow, Alaska, U.S.A. *Arct. Alp. Res.*, **23,** 115–119.

——, and B. A. Bodhaine, 2001: Solar irradiance anomalies caused by clear-sky transmission variations above Mauna Loa 1957–1999. *J. Climate,* **14,** 3255–3262.

Folland, C. K., amd Coauthors, 2001: Observed climate variability and change. *Climate Change 2001: The Scientific Basis,* J. T. Houghton et al., Eds. Cambridge University Press, 99–181.

Forster, P. M. de F., and K. P. Shine, 2002: Assessing the climate impact of stratospheric water vapor. *Geophys. Res. Lett*., **29,** 1086, doi:10.1029/2001GL013909.

Foster, J. L., 1989: The significance of the date of snow melt at Barrow, Alaska, USA. *Arct. Alp. Res.*, **21,** 60–70.

——, J. W. Winchester, and E. G. Dutton, 1992: The date of snow disappearance on the Arctic tundra as determined from satellite, meteorological station and radiometric in-situ observations. *IEEE Trans. Geosci. Remote Sens*., **30,** 793–798.

Gadgil, S. J., P. V. Joseph, and N. V. Joshi, 1984: Ocean-atmosphere coupling over monsoon regions. *Nature,* **312,** 141–143.

Gaffen, D. J., B. D. Santer, J. S. Boyle, J. R. Christy, N. E. Graham, and R. J. Ross, 2000: Multi-decadal changes in the vertical temperature structure of the tropical troposphere. *Science*, **287,** 1239–1241.

Goldenberg, S. B., and L. J. Shapiro, 1996: Physical mechanisms for the association of El Niño and West African rainfall with Atlantic major hurricanes. *J. Climate,* **9,** 1169–1187.

——, C. W. Landsea, A. M. Mestas-Nuñez, and W. M. Gray, 2001: The recent increase in Atlantic hurricane activity: Causes and implications. *Science,* **293,** 474–479.

GPCC, cited 1998: The Global Precipitation Climatology Centre. [Available online at http://www.dwd.de/research/gpcc.]

Gray, W. M., 1984: Atlantic seasonal hurricane frequency: Part I: El Niño and 30-mb quasi-bienniel oscillation influences. *Mon. Wea. Rev.,* **112,** 1649–1668.

Hall, J., and J. Callaghan, 2003: Tropical Cyclone Zoe—The most intense Tropical Cyclone observed in the Australia/South Pacific region? *Bull. Aust. Meteor. Ocean. Soc.,* **16,** 31–36.

Hastenrath, S., 1990: Decadal-scale changes of the circulation in the tropical Atlantic sector associated with Sahel drought. *Int. J. Climatol.,* **10,** 459–472.

Higgins, R. W., J. K. Schemm, W. Shi, and A. Leetmaa, 2000: Extreme precipitation events in the western United States related to tropical forcing. *J. Climate,* **13,** 793–820.

Horton, E. B., C. K. Folland, and D. E. Parker, 2001: The changing incidence of extremes in worldwide and central England temperatures to the end of the twentieth century. *Climatic Change*, **50,** 267–295.

Houghton, J. T., Y. Ding, D. J. Griggs, M. Noguer, P. J. vander Linden, X. Dai, K. Maskell, and C. J. Johnson, Eds., 2001: *Climate Change 2001: The Scientific Basis.* Cambridge University Press, 881 pp.

Hurrell, J., S. J. Brown, K. E. Trenberth, and J. R. Christy, 2000: Comparison of tropospheric temperatures from radiosondes and satellites: 1979–1998. *Bull. Amer. Meteor. Soc.*, **81,** 2165–2177.

Jacka, T. H., and W. F. Budd, 1998: Detection of temperature and sea ice extent changes in the Antarctic and Southern Ocean. *Ann. Glaciol.,* **27,** 553–559

Jäger, F., 1931: Veränderungen der Kilimanjaro-Gletscher (in German). *Z. Gletscherkd.,* **19,** 285–299.

Janowiak, J. E., and P. Xie, 1999: CAMS-OPI: A global satellite–rain gauge merged product for real-time precipitation monitoring applications. *J. Climate,* **12,** 3335–3342

Jones, D. A., 2002: The 2002 El Niño and its impacts on Australia. *Bull. Aust. Meteor. Oceanogr. Soc.*, **15**, 91–95.

Jones, P. D., and D. Conway, 1997: Precipitation in the British Isles: An analysis of area-average data updated to 1995. *Int. J. Climatol.,* **17,** 427–438.

——, and A. Moberg, 2003: Hemispheric and large-scale surface air temperature variations: An extensive revision and an update to 2001. *J. Climate,* **16**, 206–223.

——, M. New, D. E. Parker, S. Martin, and I. G. Rigor, 1999: Surface air temperature and its changes over the last 150 years. *Rev. Geophys*., **37,** 173–199.

——, T. J. Osborn, K. R. Briffa, C. K. Folland, E. B. Horton, L. V. Alexander, D. E. Parker, and N. A. Rayner, 2001: Adjusting for sampling density in grid-box land and ocean surface temperature time series. *J. Geophys. Res.,* **106,** 3371–3380.

Kalnay, E., and Coauthors, 1996: The NCEP/NCAR 40-Year Reanalysis Project. *Bull. Amer. Meteor. Soc.,* **77,** 473–471.

Karlsdóttir, S., and I. S. A. Isaksen, 2000: Changing methane lifetime: Possible cause for reduced growth. *Geophys. Res. Lett.*, **27,** 93–96.

Kasischke, E. S., and Coauthors, 2000: Contributions of 1998 fires in the boreal forest to atmospheric concentrations of carbon monoxide and methane. *Eos, Trans. Amer. Geophys. Res.*, **81,** 260.

Keeling, C. D., T. P. Whorf, M. Wahlen, and J. Vanderplicht, 1995: Interannual extremes in the rate of rise of atmospheric carbon dioxide since 1980. *Nature*, **375,** 666–670.

Krol, M. P., P. J. van Leeuwen, and J. Lelieveld, 1998: Global OH trend inferred from methyl chloroform measurements. *J. Geophys. Res*., **103,** 10 697–10 711.

Kousky, V. E., and M. T. Kayano, 1994: Principal modes of outgoing longwave radiation and 250-mb circulation for the South American sector. *J Climate,* **7,** 1131–1143.

Lander, M. A., 1994: An exploratory analysis of the relationship between tropical storm formation in the western North Pacific and ENSO. *Mon. Wea. Rev.,* **122,** 636–651.

Landsea, C. W., 1993: The climatology of intense (or major) Atlantic hurricanes. *Mon. Wea. Rev*., **121,** 1703–1713.

——, and W. M. Gray, 1992: The strong association between Western Sahel monsoon rainfall and intense Atlantic hurricanes. *J. Climate*, **5,** 435–453.

——, R. A. Pielke, A. M. Mestas-Nuñez, and J. A. Knaff, 1999: Atlantic Basin hurricanes: Indices of climate changes. *Climate Change*, **42,** 89–129.

Langenfelds, R. L., R. J. Francey, B. C. Pak, L. P. Steele, J. Lloyd, C. M. Trudinger, and C. E. Allison, 2002: Interannual growth rate variations of atmospheric CO_2 and its $\delta_{13}C$,H_2, CH_4, and CO between 1992 and 1999 linked to biomass burning. *Global Biogeochem. Cycl.*, **16,** 1048, doi:10.1029/2001GB001466.

Madden, R. A., and P. R. Julian, 1971: Detection of a 40–50 day oscillation in the zonal wind in the tropical Pacific. *J. Atmos. Sci.,* **28,** 702–708.

——, and ——, 1972: Description of global-scale circulation cells in the tropics with 40–50 day period. *J. Atmos. Sci*., **29,** 1109–1123.

——, and ——, 1994: Observations of the 40–50 day tropical oscillation—A review. *Mon. Wea. Rev*., **122,** 814–837.

Maloney, E. D., and D. L. Hartmann, 2000: Modulation of hurricane activity in the Gulf of Mexico by the Madden–Julian Oscillation. *Science*, **287,** 2002–2004.

Mestas-Nuñez, A. M., and D. B. Enfield, 1999: Rotated global modes of non-ENSO sea surface temperature variability. *J. Climate,* **12,** 2734–2746.

Mo, K. C., 2000: The association between intraseasonal oscillations and tropical storms in the Atlantic Basin. *Mon. Wea. Rev.,* **128,** 4097–4107.

——, and V. E. Kousky, 1993: Further analysis of the relationship between circulation anomaly patterns and tropical convection. *J. Geophys. Res.,* **98,** 5103–5113.

——, G. D. Bell, and W. Thaiw, 2001: Impact of sea surface temperature anomalies on the Atlantic tropical storm activity and West African rainfall. *J. Atmos. Sci.,* **58,** 3477–3496.

Montzka, S. A., J. H. Butler, J. W. Elkins, T. M. Thompson, A. D. Clarke, and L. T. Locke, 1999: Present and future trends in the atmospheric burden of ozone-depleting halogens. *Nature,* **398,** 690–694.

Nicholson, S. E., and J. Kim, 1997: The relationship of the El-Niño Southern Oscillation to African rainfall. *Int. J. Climatol.,* **17,** 117–135.

Novelli, P. C., K. A. Masarie, P. M. Lang, B. D. Hall, R. C. Myers, and J. C. Elkins, 2003: Reanalysis of tropospheric CO trends: Effects of the 1997–1998 wildfires. *J. Geophys. Res*., in press.

Parker, D. E., T. P. Legg, and C. K. Folland, 1992: A new daily Central England Temperature series, 1772–1991. *Int. J. Climatol.*, **12,** 317–342.

——, C. K. Folland, and M. Jackson, 1995: Marine surface temperature: Observed variations and data requirements. *Climatic Change*, **31**, 559–600.

——, M. Gordon, D. P. N. Cullum, D. M. H. Sexton, C. K. Folland, and N. Rayner, 1997: A new global gridded radiosonde temperature data base and recent temperature trends. *Geophys. Res. Lett.*, **24**, 1499–1502.

Peterson, T. C., and R. S. Vose, 1997: An overview of the Global Historical Climatology Network temperature database. *Bull. Amer. Meteor. Soc.,* **78,** 2837–2849.

Petit, J. R., and Coauthors, 1999, Climate and atmospheric history of the past 420,000 years from the Vostok Ice Core, Antarctica. *Nature*, **399,** 429–436.

Prather, M. J., 1996: Natural modes and time scales in atmospheric chemistry: Theory GWPs for CH_4 and CO, and runaway growth. *Geophys. Res. Lett.*, **23,** 2597–2600.

Prinn, R. G., and Coauthors, 2001: Evidence for substantial variations of atmospheric hydroxyl radicals in the past two decades. *Science*, **292,** 1882–1888.

Ropelewski, C. F., and M. S. Halpert, 1987: Global and regional scale precipitation patterns associated with the El Niño/Southern Oscillation. *Mon. Wea. Rev.*, **115,** 1606–1626.

Rudolf, B., H. Hauschild, W. Rueth, and U. Schneider 1994: Terrestrial precipitation analysis: Operational method and required density of point measurements. *Global Precipitations and Climate Change,* M. Desbois and F. Desalmond, Eds., NATO ASI Series I, Vol. 26, Springer-Verlag, 173–186.

Simpson, I. J., D. R. Blake, F. S. Rowland, and T.-Y. Chen, 2002: Implications of the recent fluctuations in the growth rate of tropospheric methane. *Geophys. Res. Lett.,* **29**, 1479, 10.1029/2001GL014521.

Smith, T. M., and R. W. Reynolds, 1998: A high-resolution global sea surface temperature climatology for the 1961–90 base period. *J. Climate,* **11,** 3320–3323.

Stendel, M., J. R. Christy, and L. Bengtsson, 2000: Assessing levels of uncertainty in recent temperature time series. *Climate Dyn.*, **16,** 587–601.

Stone, R., 1997: Variations in western Arctic temperatures in response to cloud radiative and synoptic-scale influences. *J. Geophys. Res.*, **102** (D18), 21 769–21 776.

——, E. G. Dutton, J. M. Harris, and D. Longenecker, 2002: Earlier spring snowmelt in northern Alaska as an indicator of climate change. *J. Geophys. Res.,* **107** (D10), 4089, 10.1029/2000JD000286.

Wang, B., and J. C. L. Chang, 2002: How strong ENSO events affect tropical storm activity over the western North Pacific. *J. Climate,* **15,** 1643–1658.

Waple, A. M., and Coauthors, 2002: Climate Assessment for 2001. *Bull. Amer. Meteor. Soc.,* **83** (May), S1–S62.

Watkins, A. B., 2002: '2002 Australian climate summary: Dry and warm conditions dominate'. *Bull. Aust. Meteor. Oceanogr. Soc.*, **15**, 109–114.

Zhang, C., H. Hendon, W. Kessler, and A. Rosati, 2001: A workshop on the MJO and ENSO. *Bull. Amer. Meteor. Soc.,* **82,** 971–976.